Project funded by EUROPEAN UNION

PONTOS

Black Sea CROSS BORDER COOPERATION

Copernicus assisted environmental monitoring across the Black Sea Basin – PONTOS

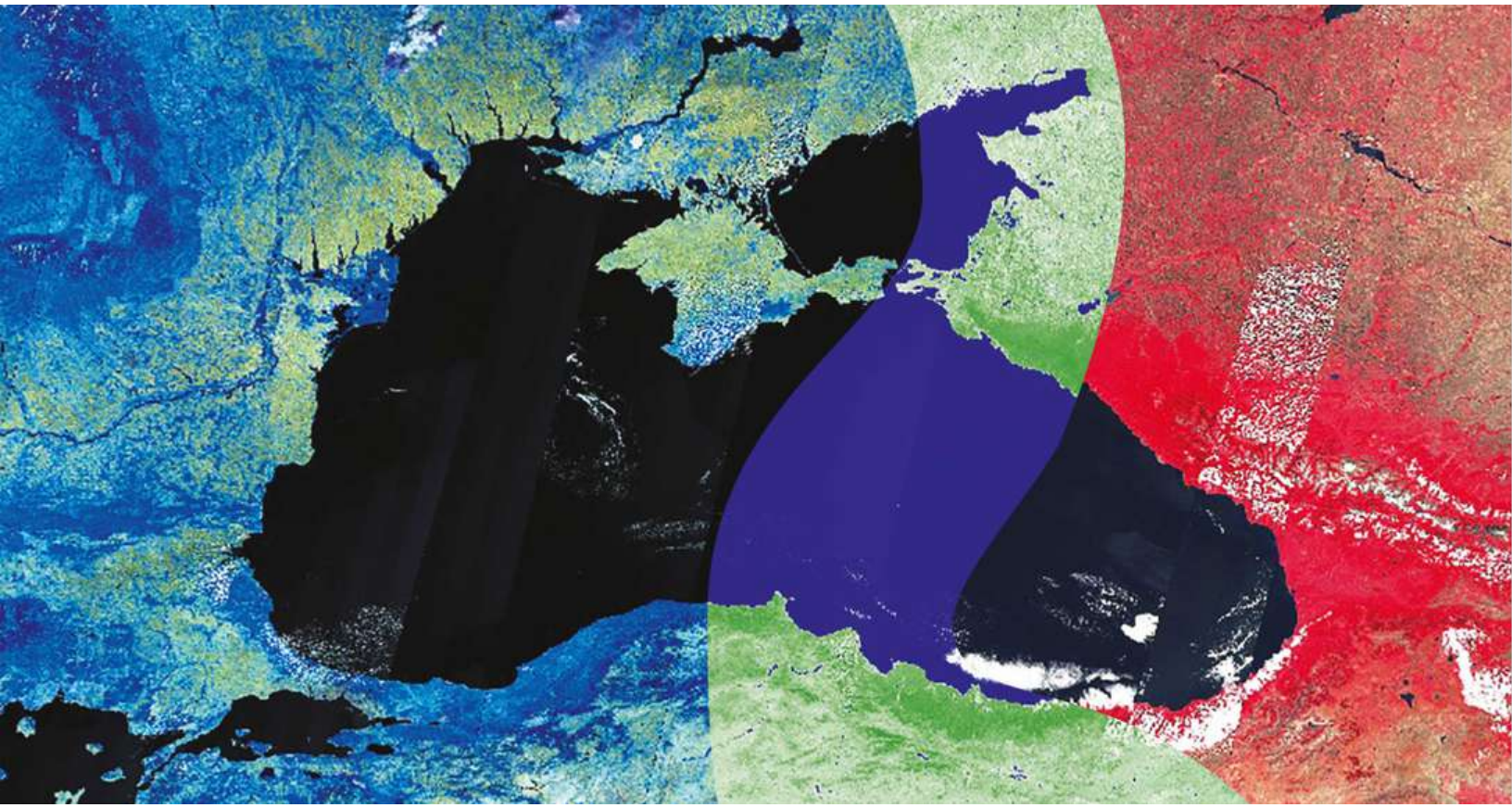

Integrated assessment on chlorophyll concentration and eutrophication dynamics

Deliverable D.T1.2.5

PONTOS-AM (Armenia)

Sevan Lake and its catchment area

Garabet Kazanjian

American University of Armenia (AUA)
Acopian Center for the Environment

2022

Executive Summary

Lake Sevan is the largest freshwater body in Armenia and the Southern Caucasus with a surface area of 1279 km^2 and a volume of about 34.0 × 109 m^3. It is one of the largest alpine lakes worldwide, situated at an altitude of about 1900 m. There are 28 rivers flowing into Lake Sevan, but it has one major outflow, the Hrazdan River. It is vitally important to Armenia as a source of irrigation, ecotourism, and the generation of hydroelectric power (HP). It is also a food source, producing the majority of Armenia's fish and crayfish catches. Furthermore, Lake Sevan and its peripheral marshlands are considered a biodiversity hotspot, hosting many endemic species, including no less than 167 endemic and migratory birds, the endemic Sevan trout (*Salmo ischchan*) with its four subspecies and the Khrami carp (*Varicorhinus capoeta sevangi*). The lake has been a protected site as part of the Sevan National Park and according to the Ramsar convention.

Throughout the past century (Between 1933–2002), excessive demands on the water resources of Lake Sevan, brought about by HP generation and abstraction for irrigation and aquaculture, coupled with incorrect policies for the management of Lake Sevan water resources, had resulted in a water-level reduction of about 20 m. This led to significant changes that ultimately induced eutrophication of the system. The eutrophication of Lake Sevan is exacerbated by increased pollution of its tributaries from industrial, agricultural, and domestic sources. Furthermore, during the last few years, new harmful cyanobacteria blooms have appeared on the lake's shores, initiating widespread local and regional concern.

Contemporary global issues, such as climate change, are expected to make matters worse by reducing precipitation rates in the Lake Sevan Basin and promoting the spread of harmful algal blooms, as cyanobacteria generally grow better at higher temperatures. The correct measures and policies need to be established in the basin to mitigate the spread of such harmful algal blooms. That entails a better understanding of eutrophication dynamics in the lake and its underlying geochemical drivers. However, frequent sampling and chemical analyses to capture both the temporal and spatial heterogeneity in such a large lake is both a costly and a time-consuming process. Thus, we find Chlorophyll- *a* (chl-*a*) data, which can be used as a proxy-measurement for algal biomass, is limited to only a few measurements per year and suffers from large data gaps due to funding and capacity limitations. This makes analyzing temporal trends in blooms extremely difficult, if not impossible.

This assessment aims to complement the *in-situ* measurements with remote sensing tools to better capture and understand the developments in the lake. We downloaded freely-available Sentinel-2 and Landsat-8 images corresponding to the period between 2013-2020 to estimate chl-*a* concentrations in the lake, using the C2RCC tool within the ESA SNAP package. Overall, 172 images were downloaded and processed (102 Landsat-8 + 100 Sentinel images). Additional measurements required to calculate chl-*a* concentrations with the SNAP package (water temperature, salinity, air

pressure) were taken from the Hydrometeorology and Monitoring Center, SNCO. The calculated algal biomass was compared and validated with 2018 lab measurements received from the Center of Hydroecology and Zoology of the National Academy of Sciences of the Republic of Armenia. Moreover, the results were compared with two relevant studies (publications) to confirm their validity.

Throughout the project, satellite images were complemented with field trips for ground-truthing and to check for issues that would potentially impact the results (*e.g.* appearance of filamentous algae, thick benthic algae in shallow areas, etc.). Concentrations of chemical parameters (including nitrate [NO_3^-], nitrite [NO_2^-], ammonium [NH_4^+], phosphate ion [PO_4^-] and total phosphorus) were retrieved from the Hydrometeorology and Monitoring Center, SNCO and tested for correlations with changes in chl-*a* in Lake Sevan.

Throughout the study period, we recorded spatial and temporal differences in chl-*a* [Fig. 3] and TSM concentrations in Lake Sevan. The South-Eastern section of Major Sevan often exhibited higher algal biomass. Clear monthly variances were recorded in all studied years. Extensive algal blooms were successfully captured in the months between June and August, but the intensity of these blooms were greatest in the years of 2018 and 2019 compared to other years. This coincided with 2018 being the hottest year in Armenia in the past decade, meaning temperature plays an important role in driving algal blooms. We did not find any significant correlations of algal blooms with nitrogen (N) throughout the study years, but phosphate ion (PO_4^-) concentrations showed an interesting dynamic in both basins of the Lake. High concentrations of PO_4^- were generally recorded in spring and autumn but the concentrations diminished in the summer during the excessive algal blooms, hinting at a potential phosphorus limitation for algal growth. The increase of PO_4^- concentrations again during autumn (post-blooms) could be due to internal loading of P either from decomposed biomass or from the hypolimnion when the lake is no longer stratified.

In conclusion, it is apparent that the two most important factors currently driving algal blooms in Lake Sevan are temperature and phosphorus. With climate change progressing, it is expected to have even higher temperatures in the Lake Sevan Basin in the coming years and decades, coupled with diminishing precipitation rates. Thus, in case of inactivity, harmful algal blooms could increase in both intensity and frequency. While temperature increases are unpredictable and beyond our control, sincere efforts to limit the external loading of phosphorus must take place to mitigate these blooms in the near future. These would be in the form of chemical and/or biological sewage treatment before it reaches the Lake, better management of fertilizer usage, and of animal manure and aquaculture activities in the Lake's basin, as well as implementing nature-based solutions around the lake (such as constructed wetlands and macrophyte belts) for filtering and sequestering the nutrient runoff.

Table of Content

Introduction and background

Purpose of the assessment

This report is the final output from the Armenian pilot site of deliverable D.T1.2.5 of the PONTOS project, entitled 'Integrated assessment on chlorophyll concentration and eutrophication dynamics'. It includes the following two objectives:

1. The PONTOS platform will acquire data from land and marine databases (*e.g.* Copernicus, EMODnet, Géoservices Sextant and BLACKSEASCENE) and process space-borne images to assess the dynamics of chlorophyll concentration as an indicator of water eutrophication to operatively monitor nutrient pollution within the pilots for the period 2009-2021.
2. *In-situ* historical and PONTOS field data (*e.g.* TN, DON, NO_3^-, NH_4^+ & TP, PO_4^{3-}) will be used for establishing correlations.

Eutrophication

Eutrophication is a term that describes the biological effects of an increase in concentration of nutrients - usually phosphorus and nitrogen, on aquatic ecosystems. The adjective eutrophe was first used by Weber (1907), a German botanist, to describe the nutrient conditions which determine the plant community in the initial stages of development of raised peat bogs (Harper, 1992). Cultural eutrophication (excessive plant growth resulting from nutrient enrichment by human activity) is a problem currently impacting many surface waters. It is one of the most visible examples of human changes to the biosphere (Fig. 1), affecting aquatic ecosystems from the Arctic to the Antarctic (Smith, 2003). One primary cause has been the rapid intensification of agriculture. In 1950, the entire world's production of agricultural fertilizers resulted in the release of approximately 10 million metric tons of nitrogen, but this number could rise to 135 million metric tons by 2030 (Fig. 2, Gilbert *et al.*, 2005). Substantial N is also applied to croplands in the form of animal manure. Moreover, humans use flowing waters as convenient wastewater disposal systems, and the loading of N and P to the world's surface waters is very strongly influenced by human population density and land use (Smith, 2003).

Unfortunately, increases in nutrient concentrations can have significant effects on water quality. Excess nutrients in aquatic ecosystems are often taken up by phytoplankton (algae), which then accumulate as intense nuisance blooms (Fig. 3). Many phytoplankton species also produce toxins that harm other organisms and human health (Smith and Schindler, 2009).

Fig. 1: Extreme eutrophication event in the Black Sea evident from satellite images. Source: NASA/Science Photo Library.

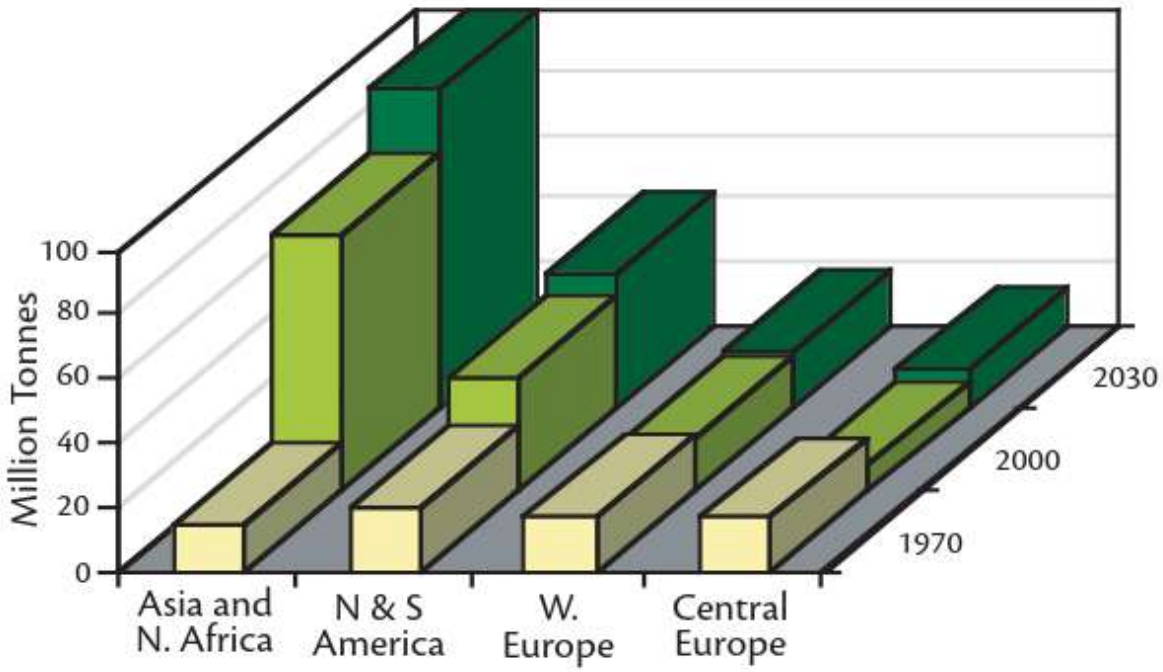

Fig. 2: Estimate of the increase in nitrogen fertilizer consumption through the Year 2030. Source: Gilbert *et al.*, 2005

Impacts of eutrophication

Eutrophication is now recognized to be one of the important factors contributing to habitat change and to spread of harmful algal bloom (HAB) species (Anderson *et al.*, 2002). It is believed that HABs, which frequently accompany an increase in nutrient loading, are increasing in frequency and intensity. Some of the clearest examples of the relationship between HAB frequency and increases in total nutrient loadings to coastal waters come from China. Since the 1970s, when escalation in use of chemical fertilizer began in China, the number of HAB outbreaks has increased over 20-fold, with blooms that now are of greater geographic extent, more toxic, and more prolonged (Anderson et al., 2002). These blooms can result in numerous issues, including accumulations on the surface or shoreline. Although the full economic impact of HABs has not been determined, it is likely that eutrophication will cost billions of dollars per year to fisheries, drinking water treatment, and human and livestock health (Smith and Schindler, 2009). Some common effects of eutrophication are listed in Table 1.

In addition to receiving major inputs of anthropogenic nutrients, surface waters also draw heavy metals, pesticides, pharmaceuticals, hormones and other non-nutrient pollutants. There is mounting evidence that the fates of such contaminants can be significantly influenced by the availability of nutrients, and these interactions require extensive additional research (Smith and Schindler, 2009).

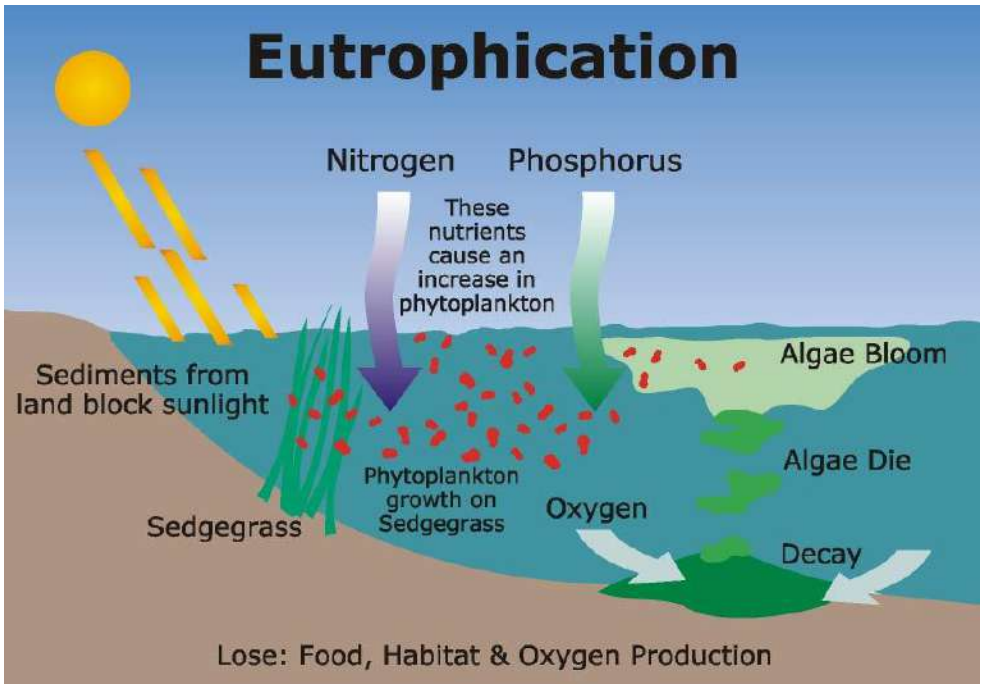

Fig. 3: The drivers and impacts of eutrophication. Source: Online Science Notes.

Table 1 : Adverse effects of freshwater and coastal marine eutrophication. Adapted from Smith, 2003.

Increased productivity and biomass of phytoplankton and suspended algae
Shifts in phytoplankton composi~on to bloom-forming species, many of which may be toxic, or which may not be consumed effectively by aquatic grazers
Increased productivity, biomass, and species composition of attached microalgae (periphyton)
Increased productivity, biomass, and species composition of marine macroalgae
Changes in productivity, biomass, and species composition of aquatic vascular plants
Reduced yields of desirable finfish and shellfish species
Reductions in the health and size of marine coral populations
Threats to endangered aquatic species
Decreases in water column transparency
Taste, odor, and filtration problems in drinking water supplies
Depletion of deep water oxygen
Decreases in the perceived aesthetic value of the water body
Negative economic impacts, including decreased property values and reduced recreational uses

Due to these numerous issues, there have been concerted efforts by researchers and authorities to develop a legal framework to prevent and manage freshwater eutrophication (The EU Water Framework Directive (EU-WFD), The EU Nitrates Directive, OECD 1982, U.S. EPA 2002, etc.). Moreover, ongoing efforts to monitor and to predict the responses of aquatic ecosystems to changes in nutrient loading and their eutrophication dynamics are becoming increasingly common.

Chlorophyll-a as a proxy for eutrophication

Chlorophyll-*a* (Chl-*a*) is a pigment found in green plants and algae, giving them the green color and allowing them to photosynthesize. As such, chl- *a* can be used as a measure of the amount of algae (algal biomass) growing in a waterbody.

The phytoplankton biomass, represented by chl-a, is an important indicator to evaluate the state of eutrophication in water bodies, thus helpful in coastal ecosystem monitoring and management. As such, it is also one of the parameters required to be reported by all European Union (EU) member

states in their implementation of proper water management and estimation of the ecological status of water bodies, according to the EU-WFD (WFD, 2000/60/EC).

Strong (log-linear) relationships between mean and maximum chl-*a* in lakes during the growing season have been found:
$\log_{10}(Chl_{mean}) = 0.91 \log_{10}(Chl_{max}) - 0.20$, $r^2 = 0.91$ (Stadelmann *et al.*, 2001)

Since most lake algal growth is limited by phosphorus (P) availability, Willén (2000) have also reported a strong relationship between annual peak algal biomass and growing-season mean concentrations of total phosphorus:

$\log_{10}(_{\text{Annual Peak Total Volume}}) = 1.512 \log_{10}(TP_{\text{March-October}}) - 1.924$, $r^2 = 0.76$

Monitoring eutrophication via remote sensing

Frequent monitoring and reporting of chl-*a* concentrations (algal biomass) in water bodies is fundamental, but *in-situ* measurements is a time and energy intensive process, which also renders it a costly process. Satellite remote sensing is a feasible way to monitor water bodies when water quality over large regions has to be monitored with regular frequency. There is also the possibility to estimate water quality in non-accessible water bodies. Deriving the chl-*a* concentration associated with algal blooms is an important metric which provides quantitative algal biomass measures useful in documenting the severity of blooms and their long-term trends, especially in relation to nutrient targets and water quality guidelines. Other water quality indicators like total suspended matter (TSM), turbidity, secchi depth and colored dissolved organic matter (CDOM) can also be measured using remote sensing techniques (Toming *et al.*, 2016).

Remote sensing has been used since the 1970s to estimate Chl-*a* concentrations, starting with applications in the oceans (Hu et al., 2012; Mobley, 1995; O'Reilly et al., 1998; Schalles, 2006). Significant progress has also been more recently made in applying remote sensing in inland water bodies with positive outcomes, as described in Palmer *et al.* (2015) and Bukata (2013). The main challenge to use remote sensing is to isolate the Chl-*a* signal from other cell components and other optically active compounds and the effects of the vertical distribution variation of chlorophyll in the water column.

The first satellite sensor developed to evaluate chl-a concentration was the Coastal Zone Color Scanner (CZCS) onboard Nimbus 7 which was launched in late 1978. A two-band ratio of 443–550 nm was calibrated and routinely used for chl-a estimation (O'Reilly *et al.*, 1998). Two more operational sensors were also developed for the monitoring of Chl-a concentration using bands in the blue and the green regions (Sea-viewing Field of view sensor—SeaWIFS- and Moderate resolution Imaging Spectroradiometer — MODIS) (O'Reilly *et al.*, 1998; Schalles, 2006).

The chl-*a* algorithms in ocean waters are based on a simple interaction of phytoplankton density with water, in which usually blue to green band ratios have a robust and sensitive relation to Chl-a during low concentration levels (1–30 mg/m^3). This relationship becomes less sensitive at higher Chl-a concentration (above 30 mg/m^3) and is highly compromised by the effects of colored dissolved organic matter (CDOM) in turbid and optically complex waters (Schalles, 2006). Indeed, chlorophyll retrieval algorithms adopting blue to green band ratios have been shown to be robust for offshore waters, but are known to be sensitive to interference from non-algal constituents (particularly CDOM), as well as uncertainties brought about by atmospheric correction failure over highly turbid waters.

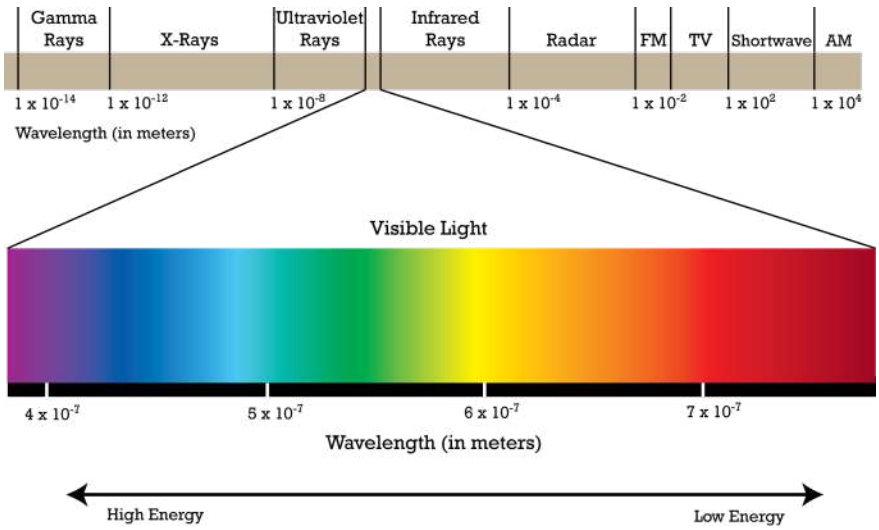

Fig. 4: The wavelengths of the light spectrum. Source: ubc.ca

The distinct scattering/absorption features of chl-*a* are the strong absorption between 400–500 nm (blue) and 680 nm (red), and the reflectance maximums at 550 nm (green) and 700 nm (near-infrared-NIR) (Han, 1997). Wavelength range for characterizing chl- *a* is between 400 nm and 900 nm (Han and Jordan, 2005). Therefore, the four bands mostly associated with chl- *a* are the blue, green, red and NIR bands (Han, 1997; Yew-Hoong Gin *et al.*, 2002).

According to Schalles (2006), low chl-*a* concentration (<2 mg/m^3) shows higher reflectance in the blue part of the spectrum (400–500 nm) and reflectance decreases as wavelength increases, with extremely low reflectance values, near 0, in the near infrared spectrum (NIR, 700–800 nm); Chl- *a* concentrations between 2 and 30 mg/m^3 show higher reflectance in the green (500–600 nm) and red bands (600–700 nm), with peak reflectance in the green part of the spectrum; and chl-*a* concentrations over 300 mg/m^3, show peak reflectance in the NIR and minimum high in the green part of the spectrum, the blue and red bands show low reflectance.

These principles are used to select bands and develop algorithms to retrieve chl-*a* from satellite images since it is evident that spectral signature changes depending on the content of chl-*a* in water. Usually, local-based algorithms are needed for inland water bodies, and they vary

significantly from one site to another since their development is based on the specific optical constituents of a water body.

These operational algorithms are based on comparing blue to green ratios and have been generated for oceanic waters in which color is dominated by phytoplankton. The largest value of the ratios is used in a fourth-order polynomial regression equation, as the exponential term in a power function equation. These exponential equations best represent the sigmoidal relationship between chl-*a* and the band ratio calculations (O'Reilly *et al.*, 1998). The good performance of blue and green ratios in oceanic waters is due to the general tendency that as the phytoplankton concentration increases, reflectance decreases in the blue (400–515 nm) and increases in the green (515–600 nm) (Kirk, 1994). Ocean color and meteorological instruments have a coarse spatial resolution which precludes their applications to small inland lakes (Cao *et al.*, 2020).

Some efforts have been made to find suitable sensors, but none were specifically designed for inland waters. Many lake chl-*a* estimations were performed using ocean satellites color sensors including the Coastal Zone Color Scanner (Antoine *et al.*, 1996), SeaWiFS (Dall'Olmo *et al.*, 2005) and Earth Observation Systems, *e.g.*, Moderate Resolution Imaging Spectroradiometer (Gitelson *et al.*, 2008), Medium Resolution Imaging Spectrometer (MERIS) (Gitelson *et al.*, 2008; Gurlin *et al.*, 2011), meteorological satellite, like Advanced Very High Resolution Radiometer (Ibelings *et al.*, 2003), and medium to high resolution land resources satellite, such as Landsat Operational Land Imager (OLI) (Liu *et al.*, 2020) and Sentinel Multispectral Imager (MSI) (Toming *et al.*, 2016).

The launch of Multispectral Imager's (MSI) onboard Copernicus Sentinel-2 mission in 2015 opened a great new potential in small water bodies remote sensing. The derived imagery comes with a spatial resolution of 10 m, 20 m and 60 m, depending on the band, exposing the monitoring of small waterbodies with more sophisticated algorithms based on neural networks, like the Case-2 Regional CoastColour (C2RCC) developed by ESA CoastColour project.

The Sentinel 3A satellite sensor OLCI (Ocean and Land Colour Instrument) launched in February 2016 by the European Space Agency (ESA) is particularly useful for chlorophyll retrievals due to their waveband selection in the red and near-infra-red (R-NIR) portion of the spectrum.

Algorithm approaches exploiting the R-NIR perform well in turbid eutrophic waters and line-height algorithms, such as the Maximum Chlorophyll Index (MCI), the Cyanobacteria Index (CI) and the Maximum Peak Height (MPH), are particularly favorable due to their relative insensitivity to uncertainties in atmospheric correction. Indeed, the application of line-height algorithms to uncorrected or partially atmospherically-corrected (using the bottom of Rayleigh reflectance) aquatic colored satellite data has become increasingly popular. The MCI, CI and MPH indices are well validated for the detection of dense surface algal blooms and have been calibrated for quantitative mapping of chlorophyll concentrations in a range of coastal and inland waters.

Similarly, phycocyanin (PC) is a frequently used cyanobacteria marker pigment and forms the basis of many proposed remote sensing algorithms for detecting cyanobacteria.

Satellites used for chlorophyll-*a* analysis

Landsat 8 (formerly the Landsat Data Continuity Mission, or LDCM) was launched on an Atlas-V rocket from Vandenberg Air Force Base, California on February 11, 2013. The Instruments Operational Land Imager (OLI) and Thermal Infrared Sensor (TIRS) are housed on the satellite. The OLI measures in the spectral regions of the visible, near infrared, and shortwave infrared (VNIR, NIR, and SWIR). Utilizing a brand-new method that makes use of quantum physics to detect heat, the TIRS measures the temperature of the land surface in two thermal bands. Along a 185 km wide swath, Landsat 8 images have a panchromatic resolution of 15 meters and a multispectral resolution of 30 meters (Ihlen, 2019).

Landsat 8 orbits the Earth in a sun-synchronous, near-polar orbit (98.2 degrees inclination) at an altitude of 705 km and completes one Earth orbit every 99 minutes. It has a 16-day repeat cycle with an equatorial crossing time of 10:00 a.m. +/- 15 minutes. The satellite acquires about 740 scenes a day on the Worldwide Reference System-2 (WRS-2) path/row system, with a swath overlap (or sidelap) varying from 7% at the equator to a maximum of approximately 85% at extreme latitudes (Ihlen, 2019).

Landsat 8 carries two sensors:

1. The Operational Land Imager sensor is built by Ball Aerospace & Technologies Corporation.
2. The Thermal Infrared Sensor is built by NASA Goddard Space Flight Center.

Landsat 8's Operational Land Imager (OLI) has 9 spectral bands, including a pan band (Bands 1-9 in Table 1). The OLI captures data with improved radiometric precision over a 12-bit dynamic range, which improves overall signal to noise ratio. This amounts to 4096 potential grey levels, whereas Landsat 1-7 8-bit instruments only have 256 grey levels. The state and condition of land cover can be better characterized with improved signal to noise performance. In the Level-1 data products, the 12-bit data are scaled up to 16-bit integers. The product metadata file (MTL file) contains radiometric rescaling coefficients that can be used to rescale the product to the Top of Atmosphere (TOA) reflectance and/or radiance. The products are scaled to 55,000 grey levels The Thermal Infrared Sensor (TIRS) has 2 additional spectral bands (Bands 10 and 11 in Table 2, Ihlen, 2019).

Table 2: Landsat 8's bands, wavelengths and respective resolutions

Bands	Wavelengths	Resolution
Band 1 Coastal Aerosol	0.43 - 0.45 µm	30 m
Band 2 Blue	0.450 - 0.51 µm	30 m
Band 3 Green	0.53 - 0.59 µm	30 m
Band 4 Red	0.64 - 0.67 µm	30 m
Band 5 Near-Infrared	0.85 - 0.88 µm	30 m
Band 6 SWIR 1	1.57 - 1.65 µm	30 m
Band 7 SWIR 2	2.11 - 2.29 µm	30 m
Band 8 Panchromatic (PAN)	0.50 - 0.68 µm	15 m
Band 9 Cirrus	1.36 - 1.38 µm	30 m
Band 10 TIRS 1	10.6 - 11.19 µm	100 m
Band 11 TIRS 2	11.5 - 12.51 µm	100 m

Sentinel-2 launched as part of the European Commission's Copernicus program on June 23, 2015. The satellite has a 13-spectral opto-electronic multispectral sensor for surveying with a resolution of 10 to 60 m in the visible, near infrared (VNIR), and short-wave infrared (SWIR) spectral zones (Table 3). This ensures that differences in the state of the vegetation, including changes over time, are captured, and it also minimizes the impact on atmospheric photography quality. The two satellites in the mission make it possible to conduct repeated surveys every five days at the equator and every two to three days at middle latitudes. The orbit has an average height of 785 kilometers (sentinel.esa.int).

Sentinel-2 has a systematic global coverage of land surfaces from 56° S to 84° N, coastal waters, and all of the Mediterranean Sea. It revisits every 10 days under the same viewing angles. However, some regions at high latitudes will be observed twice or more every 10 days, but with different viewing angles. The satellite's field of view is 290 km. To achieve frequent revisits and high mission availability, two identical Sentinel-2 satellites (Sentinel-2A and Sentinel-2B) operate together. The satellites are phased 180 degrees from each other on the same orbit. This allows for what would be a 10-day revisit cycle to be completed in 5 days (sentinel.esa.int).

The orbit is Sun synchronous at 786 km (488 mi) altitude, 14.3 revolutions per day, with a 10:30 a.m. descending node. This local time was selected as a compromise between minimizing cloud

cover and ensuring suitable Sun illumination. It is close to the Landsat local time and matches SPOT's, allowing the combination of Sentinel-2 data with historical images to build long-term time series. The Sentinel-2 satellites each carry a single multi-spectral instrument (MSI) with 13 spectral channels in the visible/near infrared (VNIR) and short wave infrared spectral range (SWIR). Within the 13 bands, the 10 meter spatial resolution allows for continued collaboration with the SPOT-5 and Landsat-8 missions (Table 3).

Sentinel-2 operates under a free and open data policy. Its data provide services for the GMES (Global Monitoring for Environment and Security) program, which is run by the EC and ESA (European Space Agency). These services include monitoring of natural disasters and humanitarian operations, as well as land management, agricultural production, and forestry (sentinel.esa.int).

Table 3: Sentinel 2 bands and their characteristics (Source: https://sentinel.esa.int)

Band name	**Sensor**	**Band number**	**Sentinel-2A**		**Sentinel-2B**		**Resolution (meters)**
			Central wavelength (nm)	**Bandwidth (nm)**	**Central wavelength (nm) – 2**	**Bandwidth (nm) – 2**	
Coastal aerosol	MSI	1	443.9	20	442.3	20	60
Blue	MSI	2	496.6	65	492.1	65	10
Green	MSI	3	560.0	35	559	35	10
Red	MSI	4	664.5	30	665	30	10
Vegetation Red Edge	MSI	5	703.9	15	703.8	15	20
Vegetation Red Edge	MSI	6	740.2	15	739.1	15	20
Vegetation Red Edge	MSI	7	782.5	20	779.7	20	20
NIR	MSI	8	835.1	115	833	115	10
Narrow NIR	MSI	9	864.8	20	864	20	20
Water vapour	MSI	10	945.0	20	943.2	20	60
SWIR – Cirrus	MSI	11	1373.5	30	1376.9	30	60
SWIR	MSI	12	1613.7	90	1610.4	90	20
SWIR	MSI	13	2202.4	180	2185.7	180	20

Algorithms used for chl-*a* measurement

The Case 2 Regional processor, originally developed by Doerffer and Schiller (2007) uses a large database of radiative transfer simulations of water leaving radiances ("water signal") as well as top-of-atmosphere radiances ("satellite signal"). Neural networks are the fundamental technology that perform the inversion of the satellite signal as well as the water signal. The idea was first introduced in the MERIS ground segment at the end of the 1990s. Later, it was further developed, and the BEAM EO data processing Toolbox (Case 2 Regional Processor) made it available to the public as an open source processor.

Special versions for lakes were also made available, using bio-optical models specifically designed for inland waters (MERIS Lakes processors). MERIS 3 reprocessing utilized the Case 2 Regional algorithm (Bourg *et al.*, 2012). Incorporating a coastal aerosol model and a 5-component bio-optical model into the ESA DUE CoastColour project resulted in a significant improvement to the algorithm (Fig. 5).

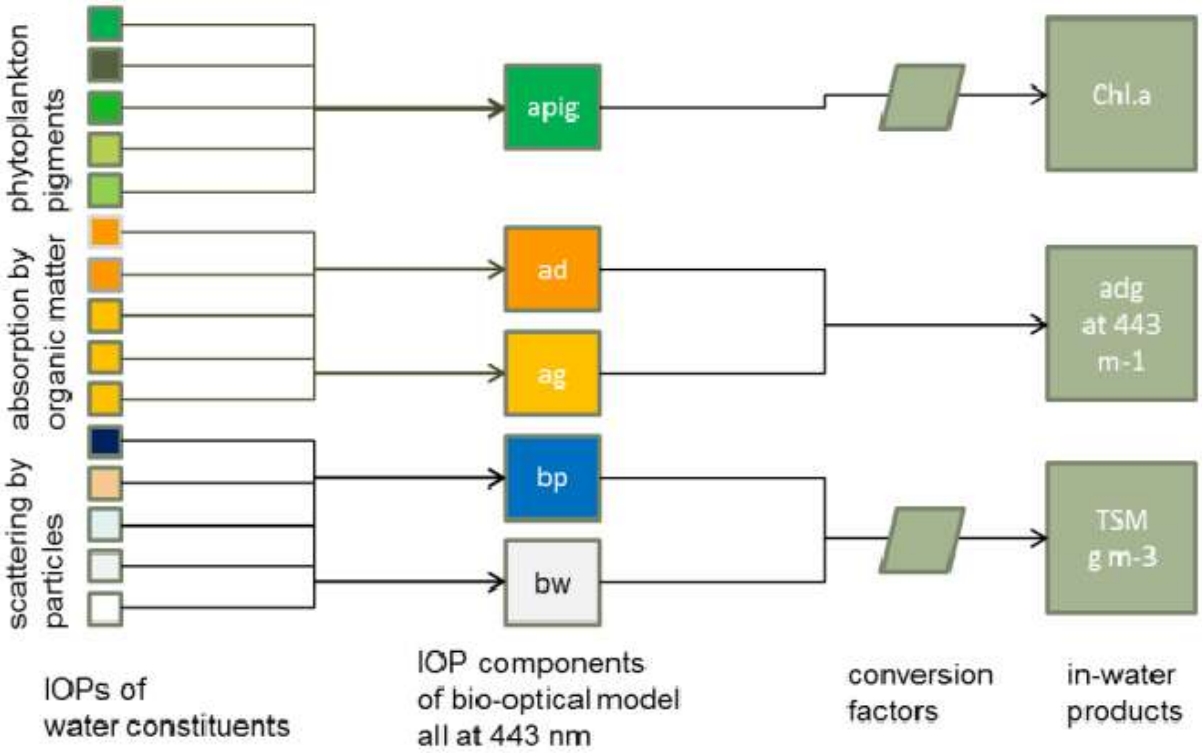

Fig. 5: C2RCC bio-optical model. Source: Brockmann *et al.*, 2016.

The current version, called C2RCC (Case 2 Regional CoastColour) version is further developed and made available through ESA's Sentinel Toolbox SNAP (Fig. 6), available to download freely at https://earth.esa.int/eogateway/tools/snap. For more information about the C2RCC processor and its evolution, refer to Brockmann *et al.* (2016) and https://c2rcc.org/.

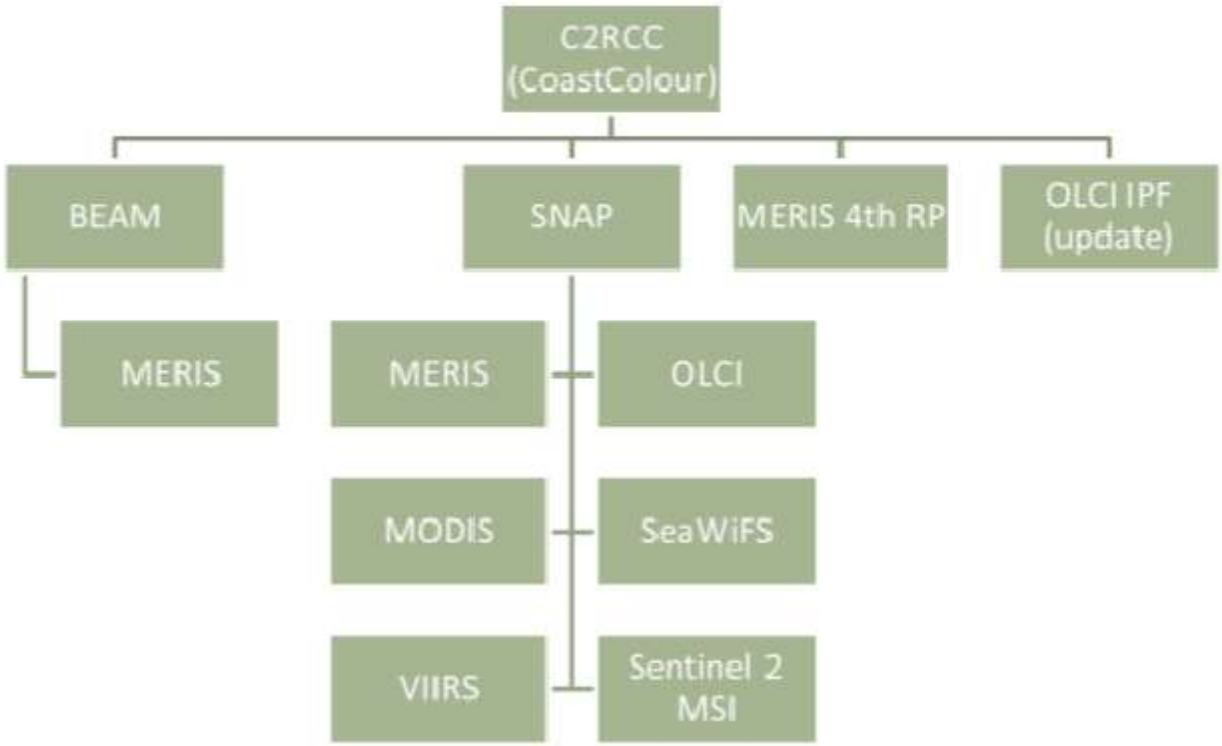

Fig. 6: C2RCC family tree. Source: Brockmann *et al.*, 2016.

Methods

Pilot site

Lake Sevan (Coordinates: 40°19′N 45°21′E) is the largest freshwater body in Armenia and the Southern Caucasus with a surface area of 1279 km^2 and a volume of about 34.0 ×109 m^3, constituting 96.5% of the national water reserve of the country (Arakelyan *et al.*, 2021). It is one of the largest alpine lakes worldwide, situated at an altitude of about 1900 m. Two capes and an underwater shaft-threshold divide the Lake Sevan into two basins: Major Sevan (910 km^2) and Minor Sevan (345 km^2) (Arakelyan *et al.* 2019, Fig. 7). There are 28 rivers flowing into Lake Sevan (Table 4), but it has one major outflow, the Hrazdan River, which eventually enters the Araks River along the border with Turkey. Along the river, numerous cities and villages are situated, accounting for about 1,130,000 people, including the population of Yerevan city (Kachvoryan *et al.* 2008). As such, it is vitally important to Armenia as a source of irrigation, ecotourism, and the generation of hydroelectric power (HP). It is also a food source, producing the majority of Armenia's fish and crayfish catches (Babayan et al. 2006). Furthermore, Lake Sevan and its peripheral marshlands are considered a biodiversity hotspot, hosting many endemic species, including no less than 167 endemic and migratory birds (Hovhanissian & Gabrielyan, 2000). Since 1993, the lake has been a protected site according to the Ramsar convention.

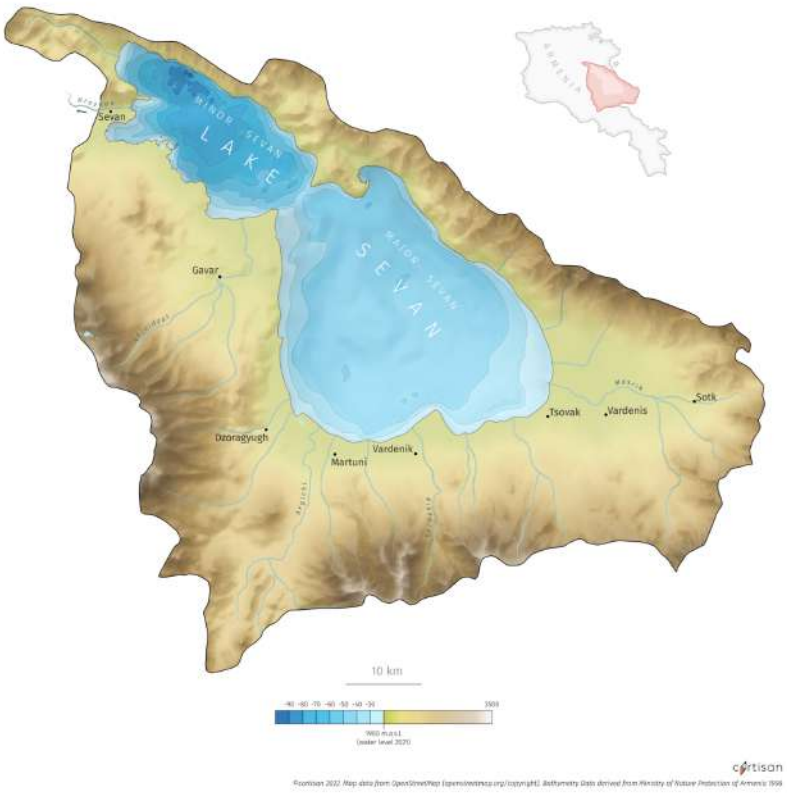

Fig. 7: Morphometry of Lake Sevan with its two basins and its location in Armenia. Source: Cartisan

Table 4: The main rivers of the Sevan Lake Basin and their characteristics. Source: Arakelyan *et al.*, 2019.

River Name	Length, km	Watershed Area, km^2	Altitude at Source, m	Altitude at Mouth, m	Average incline, ‰
Argichi	56	367,2	2520	1900,6	11,1
Artanish	8	16,7	2612	1900,6	88,9
Bakhtak	31	152,1	3220	1900,6	42,6
Daranak	8	23,3	2850	1900,6	118,7
Areguni	9	11,7	2820	1900,6	102,2
Jil	10	17,5	2780	1900,6	87,9
Artsvanist	20	82,7	3260	1900,6	68,0
Astghadzor	21	48	3220	1900,6	62,8
Vardenis	30	110	3160	1900,6	42,0
Gavaraget	50	480	3130	1900,6	24,6
Dzknaget	22	86,3	2310	1900,6	18,6
Zolakar	14	31,5	2840	1900,6	67,1
Karchaghbyur	24	109,6	2905	1900,6	41,9
Lichk	8	36,9	2006	1900,6	13,2
Martuni	28	96,5	3070	1900,6	41,8
Masrik	51	675	2880	1900,6	19,2
Pambak	10	23,2	2762	1900,6	86,1
Drakhtik	11	39,5	2670	1900,6	69,9
Tsakkar	23	67,2	3180	1900,6	55,6
Geghamasar	12	21,6	3030	1900,6	94,1
Yeranos	4	7,9	1960	1900,6	14,9
Selavagetak	15	19	2650	1900,6	50,0
Pokr Masrik	15	69	2800	1900,6	60,0
Sarinar	11	14,2	3094	1900,6	108,5
Shishkert	9	18,6	2600	1900,6	77,7
Tsapatagh	8	17,3	2670	1900,6	96,2
Dali	5	7,4	2422	1900,6	104,3
Spitakajur	12	23,9	2405	1900,6	42,0

The Sevan National Park was established in 1978, the area of which is 147,343 ha with Lake Sevan (without the lake = 22,585 ha). The reserve zone of the Sevan National Park occupies 342,920 ha. It was established to conserve fresh-water resources of Lake Sevan: its vegetation, endemic fish (Sevan trout, Sevan barble, Khrami carp- *Varicorhinus capoeta sevangi*), and animal species including Armenian seagulls and birds.

The lake basin is home to approximately 1,600 species of vascular plants, or 50% of Armenia's flora. Armenia's Red Data Book contains 48 species, six of which are endemic: *Isotis arnoldiana*, *Isotis sevangensis, Ribes achurjani, Acantholimon gabrieljanae, Astragalus shushaensis* , and *Alyssum hajastanum.* The mountain steppe, sub-alpine, and alpine vegetation communities of Lake Sevan's basin feature a variety of Astragalus and Acantholimon species. Junipers (*Juniperus policarpos, J.*

oblonga) are the region's most distinctive arboreal plants. The ' *Sevan Mountains*' still harbor natural oak forests. Sweetbrier (*Rosa canina*) and other species of Rosa sp. are prevalent in the Vardenis and Geghama Mountains. On Lake Sevan, emergent vegetation, including reedbelts (*Potamogeton spp*.) are abundant to depths of 2-5 m. Stoneworts (*Chara spp*.) cover the littoral zone to depths of 4-8 m (Babayan *et al*., 2006).

In the Lake Sevan basin there are six species of fishes (two species are in the Red Data Book of Armenia, another two are endemic). All native fish species of ishkhan (*Salmo ischchan*), Sevan barbel (*Barbus goktschaikus*), Sevan koghak (*Varicorhinus capoeta sevangi*) are in decline or have already disappeared from parts of the Lake. Additionally, there are four species of amphibians and 18 species of reptiles, two of which are in the Red Data Book of Armenia. Two-hundred ten species of birds have been recorded in the Lake's Basin. Of those, 36 are in the Red Data Book of Armenia, one is endemic, and 83 are included in the Agreement on the Conservation of African-Eurasian Migratory Waterbirds of the Convention on the Conservation of Migratory Species of Wild Animals. The Eurasian coot (*Fulica atra*), mallard (*Anas platyrhynchos*) and endemic Armenian gull (*Larus armenicus*) are presently abundant (Babayan *et al*., 2006).

Throughout the past century (Between 1933–2002), excessive demands on the water resources of Lake Sevan, brought about by hydropower generation and abstraction for irrigation and aquaculture, coupled with incorrect policies for the management of Lake Sevan water resources, had resulted in a water-level reduction of about 20 m (Fig. 8). This led to significant morphological, physical, chemical, and biological changes that ultimately induced eutrophication of the system (Kachvoryan *et al.* 2008; Hovsepyan & Gevorgyan, 2017).

After the decrease of the water level, the exposed regions of the former lake bottom were forested by alien species of plants. Artificial forests composed of pine (*Pinus caucasica*), poplar (*Populus canadensis, Populus simoni*), acacia (*Caragana brevespina, Caragana trutex*), and willow (*Salix viminalis*) were planted. In some areas, the sallow thorn (*Hippopae ramnoides*) forms thick, impassable bushes (Babayan *et al*., 2006). The artificial water-level decrease also negatively impacted the population of breeding waterfowl. From about 60 breeders, only 25 species are now reported as breeding in the basin (Babayan *et al*., 2006).

In 2001, active measures to restore the lake ecosystem by raising the water level by at least 6 m within 30 years were implemented (Hovsepyan & Gevorgyan, 2017). Since then, the water-level has risen by a few meters (Table 6, Krylov *et al*., 2019). Nonetheless, the recent water-rise hasn't come without its problematic developments. Upon the flooding of ephemeral ponds in the coastal region and the formation of shallower and warmer sites, new species typical for temporary water bodies have been recorded in the flora (Gabrielyan *et al*., 2019) and fauna of the lake (Krylov *et al*.. 2013). The flooding of the newly forested areas also led to the leaching of humic substances and nutrients into the water, further deteriorating its quality.

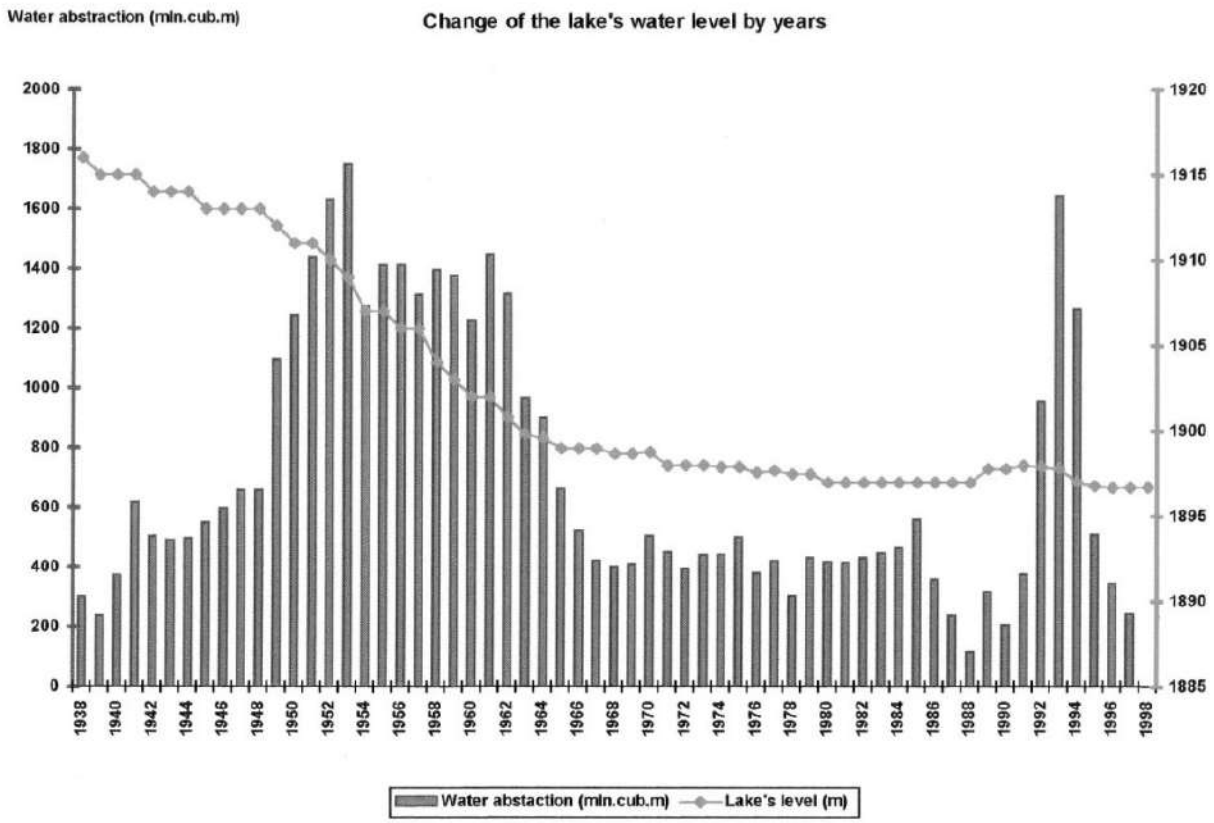

Fig. 8: Water level changes in Lake Sevan in the 20th century due to excessive water abstraction. Source: Hovhanissian and Gabrielyan, 2000.

Table 5: Lake Sevan water balance in the 20th century (in million m^3/year). Source: Babayan *et al.*, 2006.

Components of balance	1927-1933	1949-1962	1970-1979	1984-1990	1992-1997	1998-2003
Surface inflow	811	669	774	990	1,144	986
Precipitation	509	475	479	486	466	498
Underground inflow	31	48	56	81	65	76
Summary income	**1,351**	**1,192**	**1,309**	**1,557**	**1,675**	**1,560**
Surface outflow	42	1,383	430	329	831	167
Evaporation	1,136	1,041	1,039	1,102	1,081	1,262
Underground outflow	84	26	9	9	15	20
Summary expenditure	**1,262**	**2,450**	**1,478**	**1,440**	**1,927**	**1,431**
Discrepancy	**+89**	**-1,258**	**-169**	**+117**	**-252**	**+129**

Table 6: Water level and surface area fluctuations of Lake Sevan in the previous two decades. Source: Arakelyan *et al.*, 2019.

Year	Annual Average		
	Level, m	Surface Area, km^2	Volume, km^3
2002	1896.72	1240.50	33.49
2003	1897.18	1245.24	33.98
2004	1897.64	1249.94	34.55
2005	1898.03	1253.79	35.05
2006	1898.34	1256.91	35.44
2007	1898.68	1260.39	35.87
2008	1899.01	1263.50	36.28
2009	1899.17	1265.48	36.49
2010	1899.69	1270.74	37.15
2011	1900.19	1275.58	37.79
2012	1900.26	1276.26	37.87
2013	1900.30	1276.57	37.92
2014	1900.28	1276.40	37.89
2015	1900.29	1276.51	37.91
2016	1900.52	1278.74	38.21
2017	1900.60	1279.46	38.30

In July and August, the lake's surface reaches a maximum temperature of about 24-25°C, with slightly higher temperatures along the eastern coast. Major Sevan typically experiences higher temperatures than the Minor Sevan. The reason for this is that the wind moves the warm waters from north to south. During the day, there are little changes in the lake's surface water temperature, ranging from 1.5°C to 2°C and rarely reaching 3-4°C. During the summer, Major Sevan forms a "dome" of cold water with a 5-6°C drop in temperature at its center.

At its depth, water has a temperature of 4-5°C throughout the year, and there are no noticeable seasonal changes (Arakelyan *et al.*, 2019). The lake stratifies twice a year

The eutrophication of Lake Sevan is exacerbated by increased pollution of its tributaries from industrial, agricultural, and domestic sources. Untreated sewage continues to flow into the lake from all cities and towns in the catchment, leading to a high nutrient loading into the lake, thus driving its eutrophication. Intensive land reclamation, as well as uncontrolled building of reservoirs for fish breeding, have changed the course of rivers and streams in the catchment and altered their physicochemical characteristics (Kachvoryan et al. 2008). These transformations are usually associated with a decline in water quality that may have an impact on fish populations (Hovhanissian & Gabrielyan, 2000).

Constant fluctuations in the lake's water-level and biochemical parameters have also resulted in significant changes in the lake's algal composition and production rates (Parparov, 1990; Minasyan A. & Karrasch B., 2015; Sakharova *et al.*, 2020). Within the last few decades, numerous different algal groups have dominated the pelagic production of the lake's water column and many new species have been reported (Hovsepyan & Gevorgyan, 2017). To this day, it does not appear that the lake has reached a stable condition and it is still undergoing significant changes (Fig. 9; Asatryan et al., 2022). Furthermore, during the last few years, new harmful cyanobacteria blooms have appeared on the lake's shores (Ovsepyan & Khachikyan, 2016; Sakharova *et al.*, 2020; Asatryan *et al.*, 2022), initiating widespread local and regional concern (Gevorgyan et *al.*, 2020).

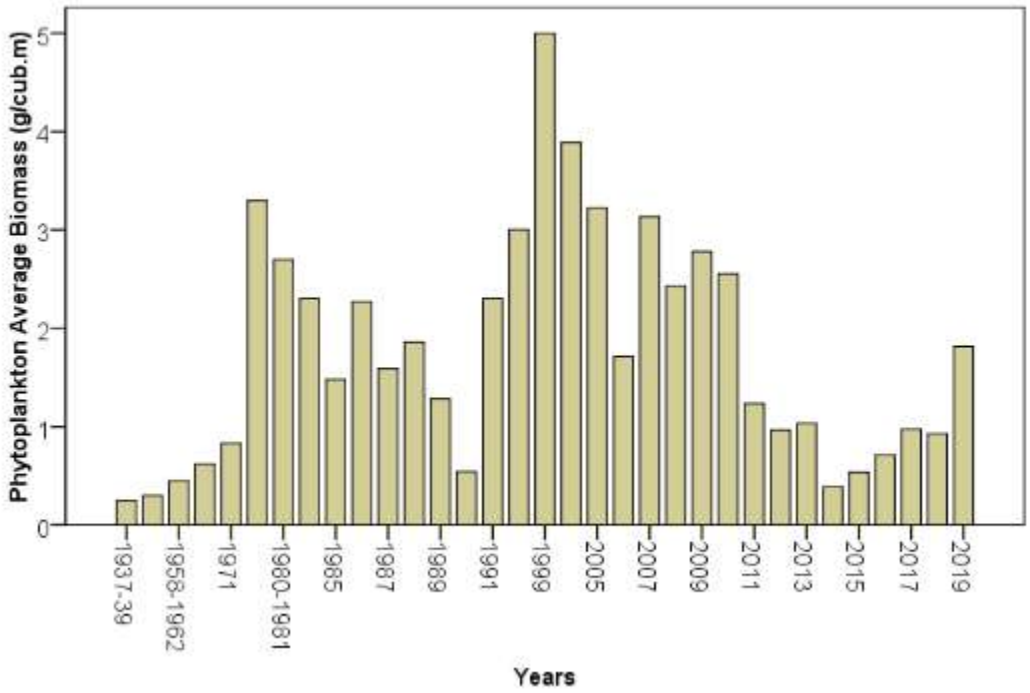

Fig. 9: Phytoplankton average biomass (g/m^3) fluctuations over time in Lake Sevan.

Contemporary global issues, such as climate change, are expected to make matters worse by reduced precipitation rates, altering the bacterial composition of the water (Kachvoryan et al. 2008) and promoting the spread of harmful algal blooms, as cyanobacteria generally grow better at higher temperatures (Paerl & Huisman, 2008). This will have drastic consequences on the lake's ecosystem services and will likely lead to significant economic losses to the nation. Thus, the need to develop tools to predict the effects of future changes on the sustainable development of the lake basin are paramount (Hovhanissian & Gabrielyan, 2000), as well as making the correct recommendations to improve the lake's water quality, ensure its biodiversity, and the ecosystem services it provides the nation.

However, for knowledge-based policymaking the availability of long term monitoring data is paramount. In the case of Lake Sevan, due to financial and capacity restrictions, hydrobiological monitoring measurements have been conducted intermittently and there are large gaps in chl-a data, making long term ecosystem analyses extremely challenging (Kazanjian and Asatryan, *in press*).

Methods and process

One of the objectives of the PONTOS project was to develop a standardized methodology of remote sensing that could be easily learnt and adopted to improve the national long-term monitoring of eutrophication dynamics in Lake Sevan. To that aim, we developed the following strategy (Fig. 10):

- Initially, two satellites were chosen that could provide free to use images with enough spatial resolution and bands for chl-a identification in inland waters. From the year 2017 onwards, Sentinel-2's MSI was chosen to be the best alternative with a spatial resolution of up to 10m. For the years preceding the availability of regular images from Sentinel-2, Landsat-8's offerings could cover the gap dating back to 2013. The downloaded satellite images were stored locally for processing (see section below for details).
- Concurrently, literature reviews and interviews with local stakeholders were conducted to obtain relevant historical data and *in-situ* measurements. Additional field surveys were conducted to clarify uncertainties in the analyzed data (outliers, suspicious readings, etc.).
- The calculated chl-*a* data from satellite images were then compared to and validated by in-situ chl-*a* measurements from 2018.
- Two sets of trainings were conducted to familiarize the relevant stakeholders with the used methodology for adoption, as well as a training module developed for further use. The results of this assessment were presented to the public during the PONTOS final conference, held in October 2022 in Yerevan, Armenia.

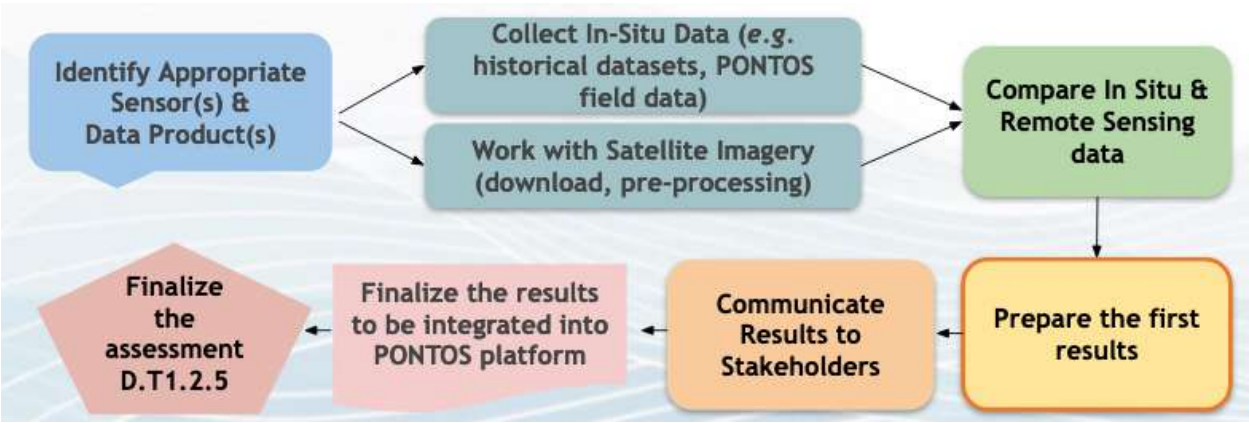

Fig. 10: Description of steps for the PONTOS deliverable D.T1.2.5.

Image retrieval and pre-processing

To achieve the study aims within the stated time period, freely available images from 2 satellites were downloaded. For the period dating from 2013 to 2017, Landsat-8 satellite images were used, downloaded from the USGS Earth Explorer (Fig. 11). In total, 102 Landsat-8 images were downloaded and processed. The breakdown of downloaded images per year can be seen in Table 7. The Landsat 8 images were pre-processed in the ESA SNAP software, resampled to a resolution of 15 m, and subsetted to the desirable coordinates.

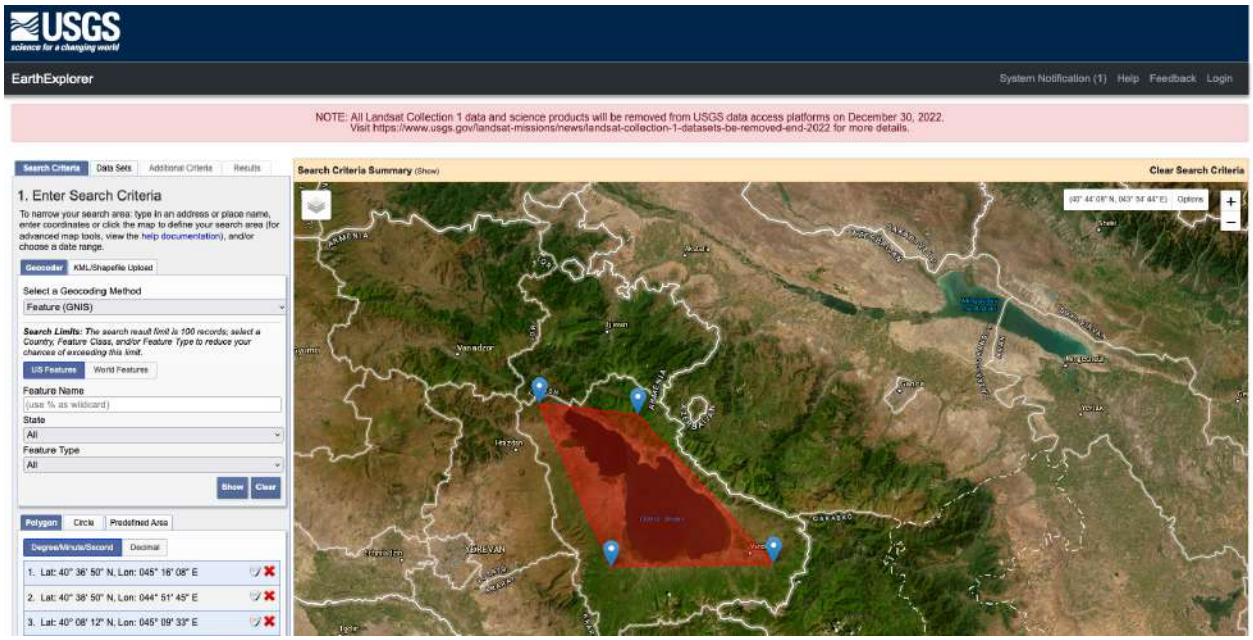

Fig. 11: Landsat-8 satellite images were downloaded from USGS Earth Explorer [https://earthexplorer.usgs.gov/]

Table 7: Number of Landsat 8 images downloaded per year.

Years	Number of images downloaded and processed
2013	18
2014	19
2015	22
2016	22
2017	21

Sentinel-2A images from 2017 to 2021 were downloaded from Copernicus Sentinel Hub (Fig. 12) provided that cloud cover did not surpass 30%. Overall, 100 images were downloaded (Table 8). Thereafter, the downloaded images were processed in ESA's SNAP package. The bands of each image were resampled to match the resolution of Sentinel-2A's 2nd band (10 m, Fig. 13).

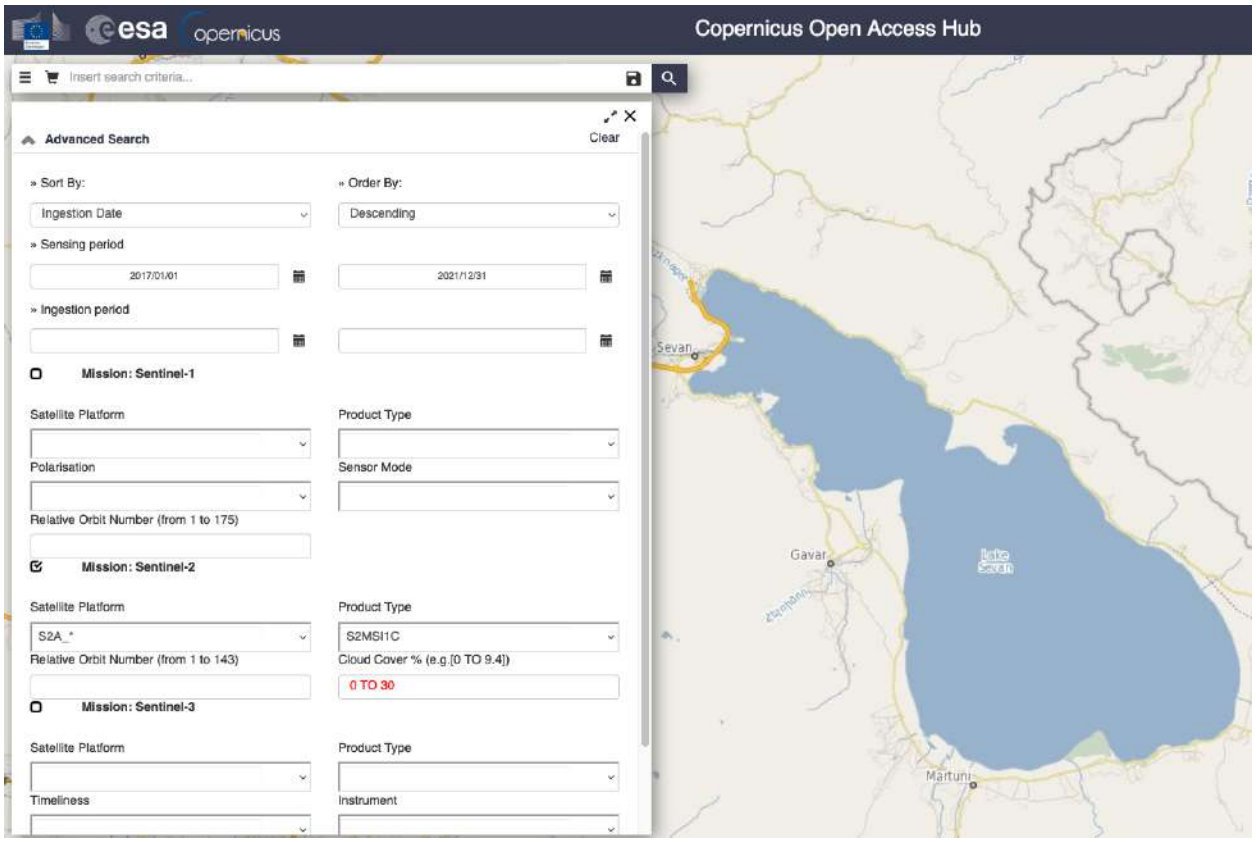

Fig. 12: Sentinel 2A images were downloaded from Copernicus Open Access Hub [https://scihub.copernicus.eu/]

Table 8: Number of Sentinel-2 images downloaded per year.

Years	Number of images downloaded and processed
2017	19
2018	23
2019	16
2020	19
2021	23

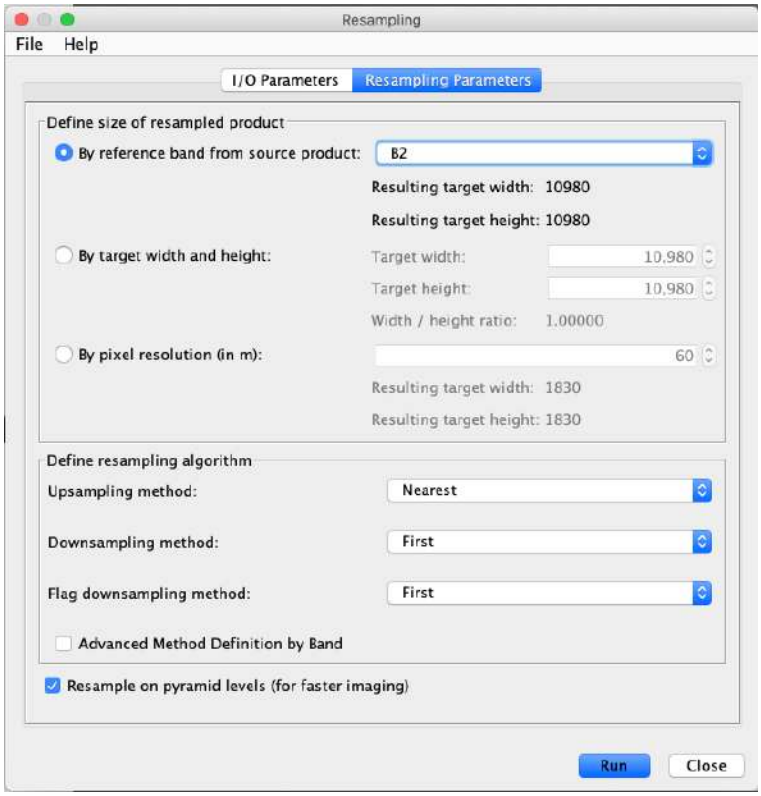

Fig. 13: Resampling Sentinel-2 satellite image bands to 10m resolution in SNAP.

Thereafter, the desired area on the map corresponding to the Lake was selected using the subset function (Fig. 14). All the image pre-processing steps are highlighted in Fig. 15.

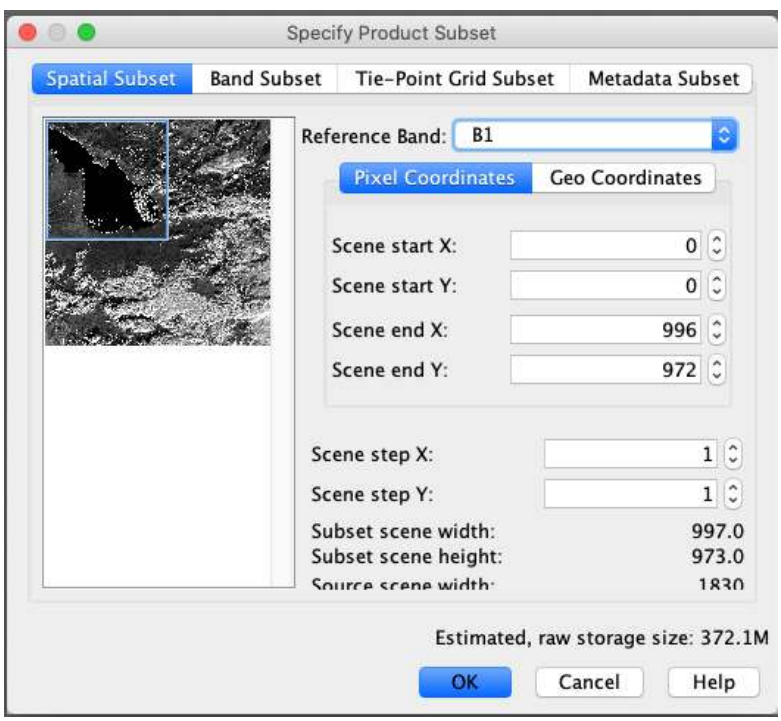

Fig. 14: Subsetting satellite image to select the required area.

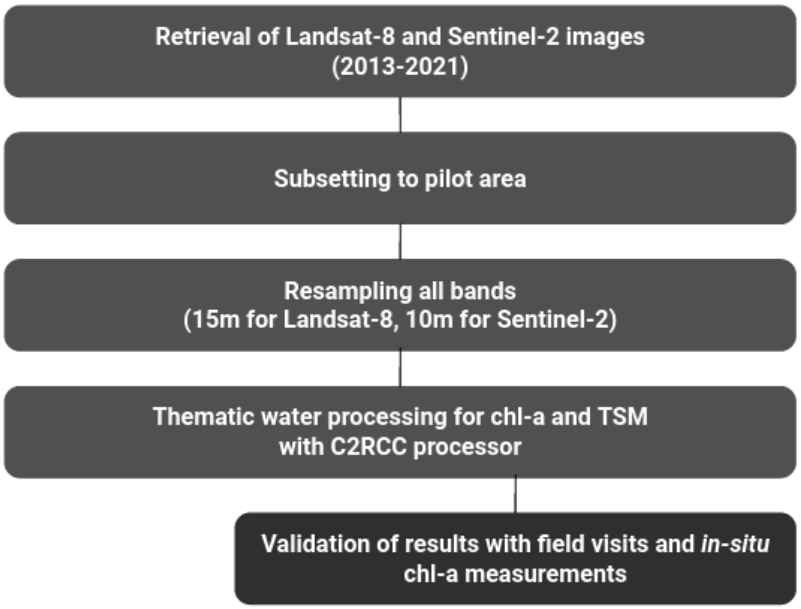

Fig. 15: Description of steps for image preparation, processing and validation.

Image processing

Resampled and subsetted images were then processed using the C2RCC processor available within ESA's SNAP software, using the Landsat 8 and S2-MSI for Landsat and Sentinel images, respectively (Fig. 16). Before image processing initiation, several parameters, namely temperature, salinity, and elevation were changed to match the site and time specificities of when the images were captured (Fig. 17).

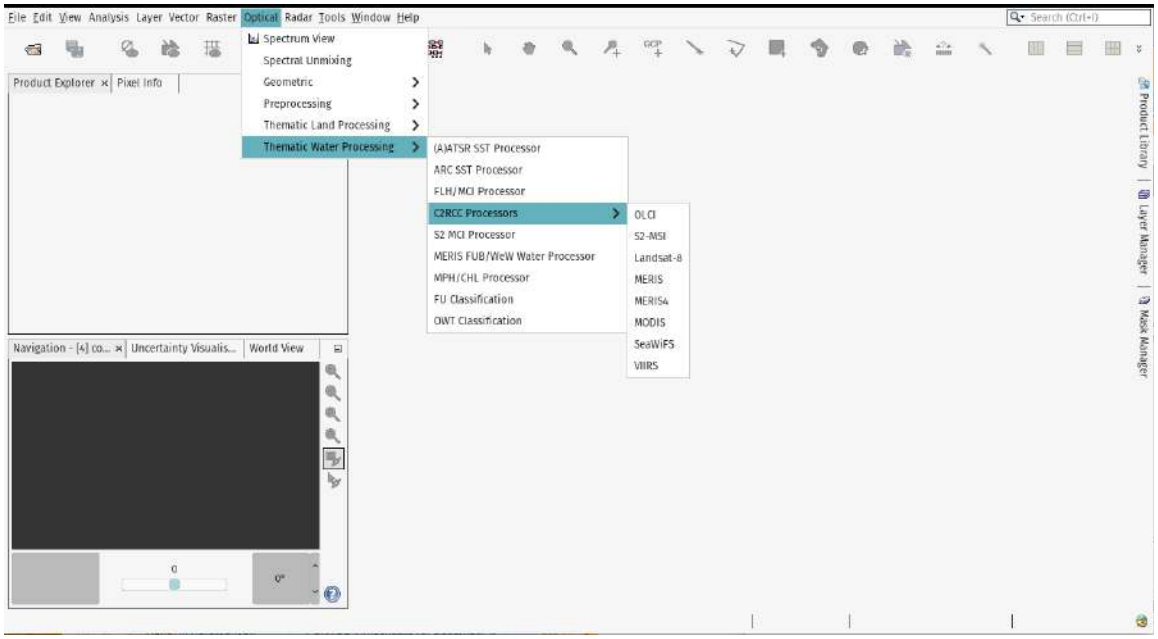

Fig. 16: C2RCC processor within SNAP's Thematic Water Processing options.

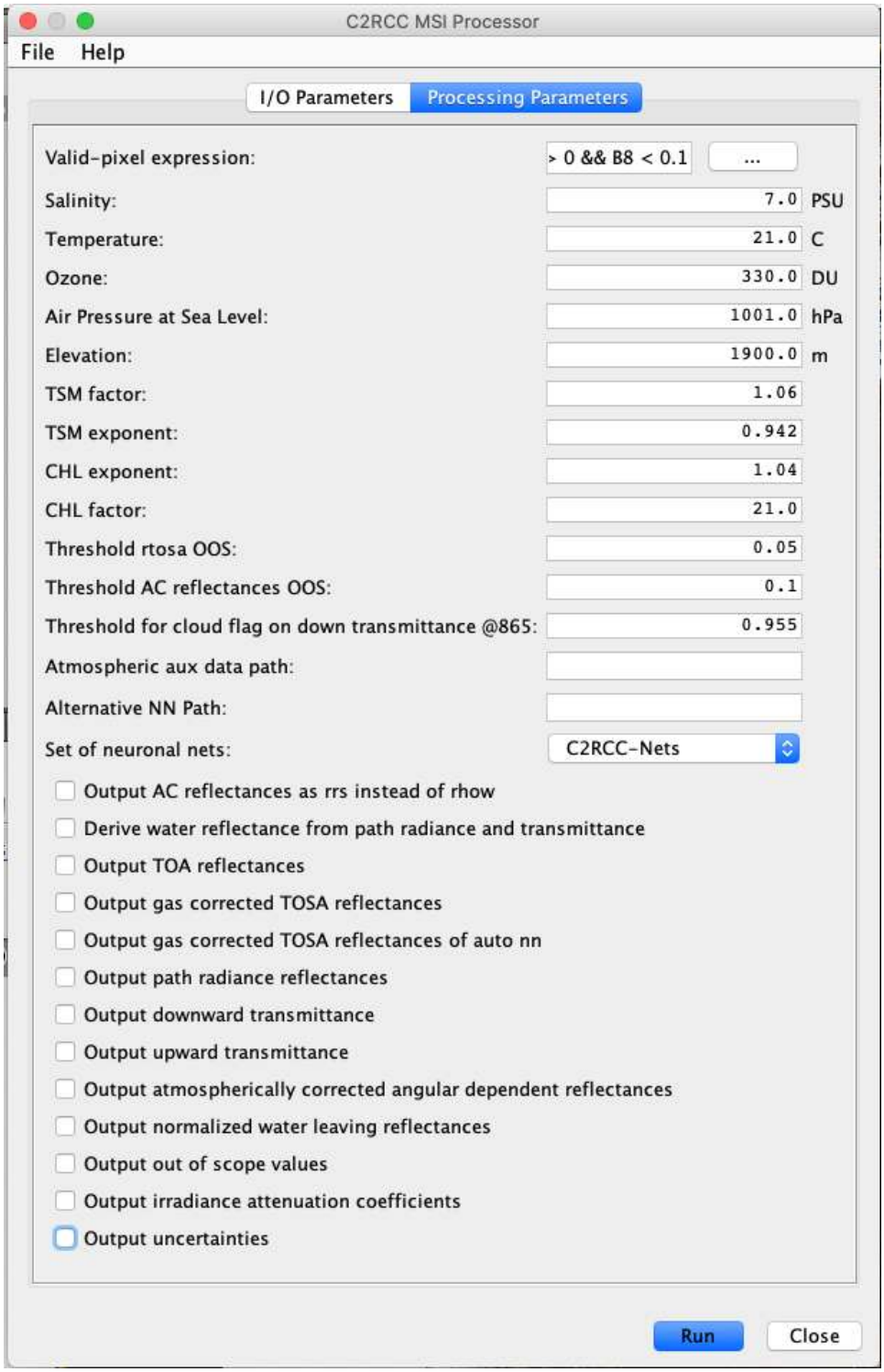

Fig. 17: Updating the processing parameters within C2RCC MSI processor.

Upon running the image analysis, we obtain two new images, corresponding to the distribution of chl-*a* and TSM concentrations in the lake, respectively. The color palette of the images can be then changed as desired, as well as their scale (legend). The produced images could be exported and saved in a wide variety of file formats.

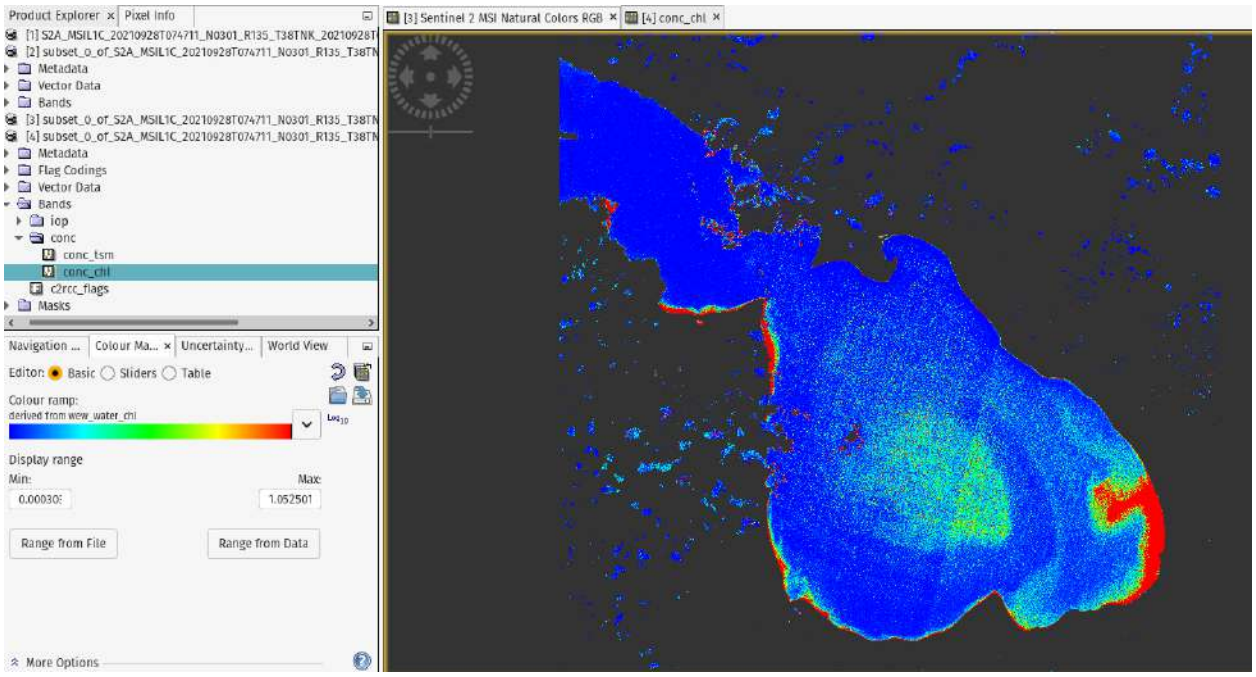

Fig. 18: The distribution of chl-a concentrations in the lake as a function of the C2RCC S2-MSI processor.

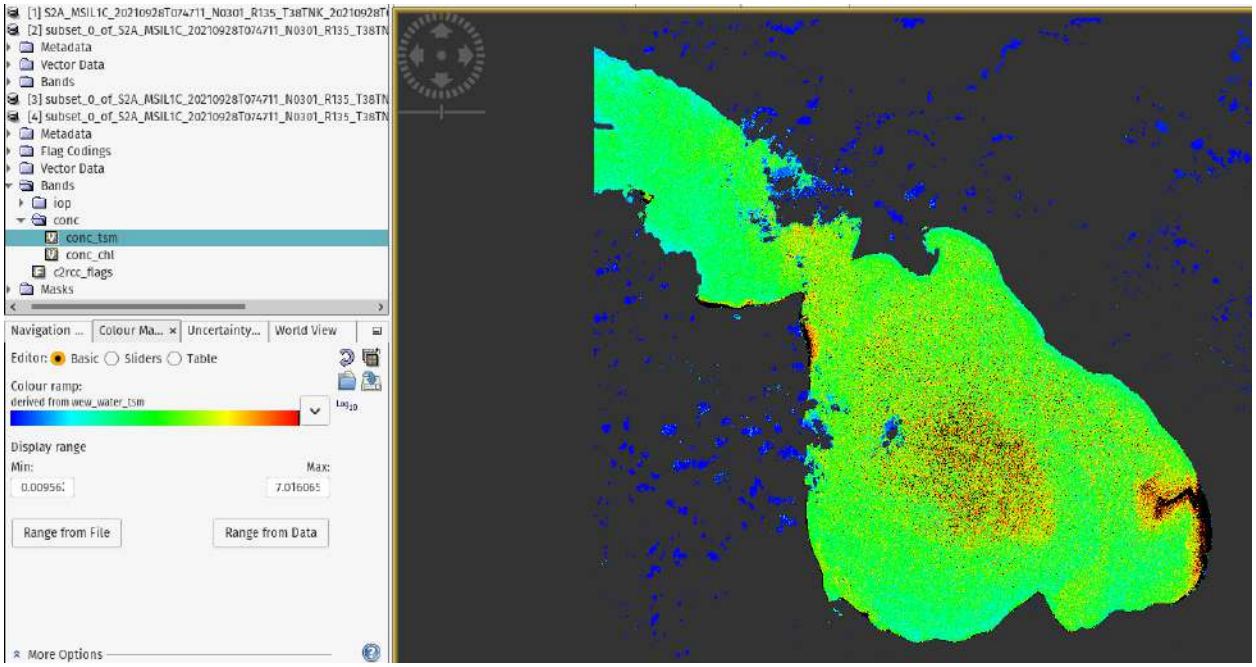

Fig. 19: The distribution of TSM concentrations in the lake as a function of the C2RCC S2-MSI processor.

Field visits for validation

Several field surveys were conducted during the project, particularly in the summer, for ground-truthing results obtained by satellite image analysis, and to validate (or refute) outliers, extreme events, and unexpected results.

Fig. 20: Images taken in August 2021 at Karchaghbyur river estuary, showing intensive growth of filamentous algae along the coast.

Fig. 21: Images from the Norashen reserve - an important bird habitat (shallow lagoon-like environment with significant submerged and emergent vegetation).

Fig. 22: Images taken in July 2022 from the southern coast (close to the Martuni river estuary) depicting extreme cyanobacterial blooms.

Validation with in-situ measurements

Algal biomass (chl-*a* concentrations) retrieved from satellite images via the C2RCC processor for the year 2018 were compared with laboratory chl-*a* measurements obtained from the Institute of Hydroecology and Zoology of the National Academy of Sciences of the Republic of Armenia (NASRA). The laboratory measurements were sampled from two locations, one from Major Sevan (40°22.350'N 45°22.705'E) and the other from Minor Sevan (40°36.136'N 45°03.544'E). The samples were taken by a Friedinger sampler, approximately once a month from May to December 2018, at depths of 0.5, 5, 10, 20, and 30m in Major Sevan and additionally at depths of 55, 70, and 80m in Minor Sevan. Thereafter, the samples were transported to the laboratory at the Institute of Hydroecology and Zoology of NASRA, where they were filtered through glass fiber filters (Whatman GF/F) and stored in a freezer at −20°C until extraction by 90% ethanol and analyzed by spectrophotometry (DV-8200; Drawell Scientific) according to Nusch (1980).

The results derived from satellite images closest in time to the actual sampling date (at a maximum of ∓ 3 days difference) were collected for validation. The samples taken from the different depths corresponding to those of the photic zone in Lake Sevan were averaged. The satellite image-derived chl-*a* values of the pixel at the coordinates of sampling, as well as those in its immediate vicinity were also averaged to smooth out pixel inconsistencies. A linear regression with the equation Measured chl-*a* = 0.628 x calculated chl-*a* + 0.646 yielded an R^2 = 0.79.

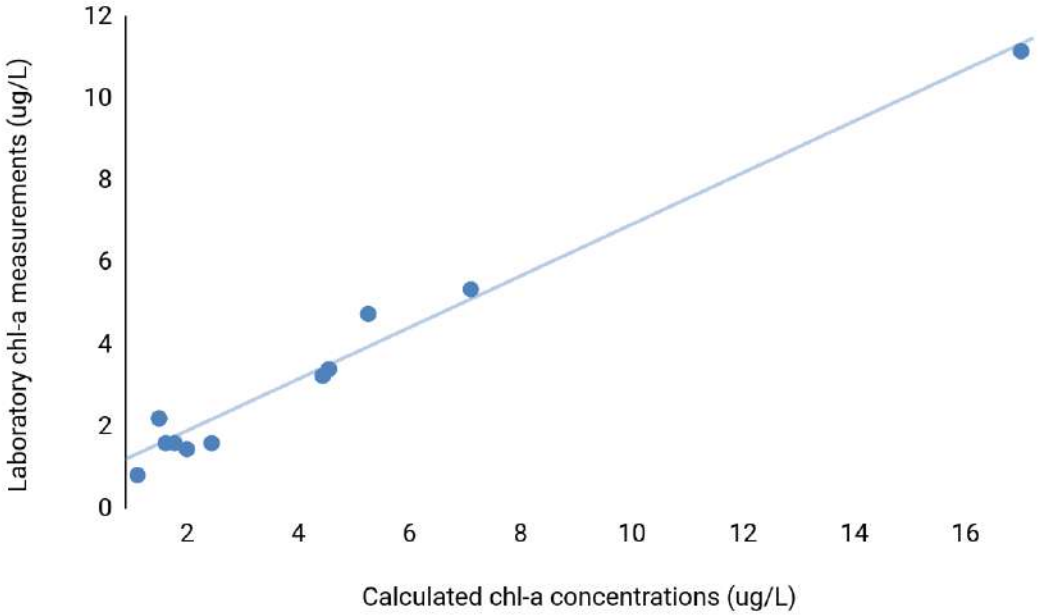

Monthly *In-situ* water chemistry and water quality data (including nitrate, nitrite, ammonium, phosphate ion, suspended matter, dissolved oxygen, BOD, and others) from 2016 to 2021 were received from the Hydrometeorology and Monitoring Center SNCO.

Results

Chl-*a* concentration dynamics

Landsat 8 images

Overall, 102 Landsat images were downloaded corresponding to the period between 2013 and 2017. The number of images downloaded and processed for every year is described in Table 7. All the images were resampled to a resolution of 15 m and analyzed in ESA's SNAP Tool using C2RCC's Landsat 8 algorithm. The number of images analyzed per In general, the images showed higher concentrations of chl-*a* in the SE basin of Major Sevan compared to the rest of the lake (Fig. 23).

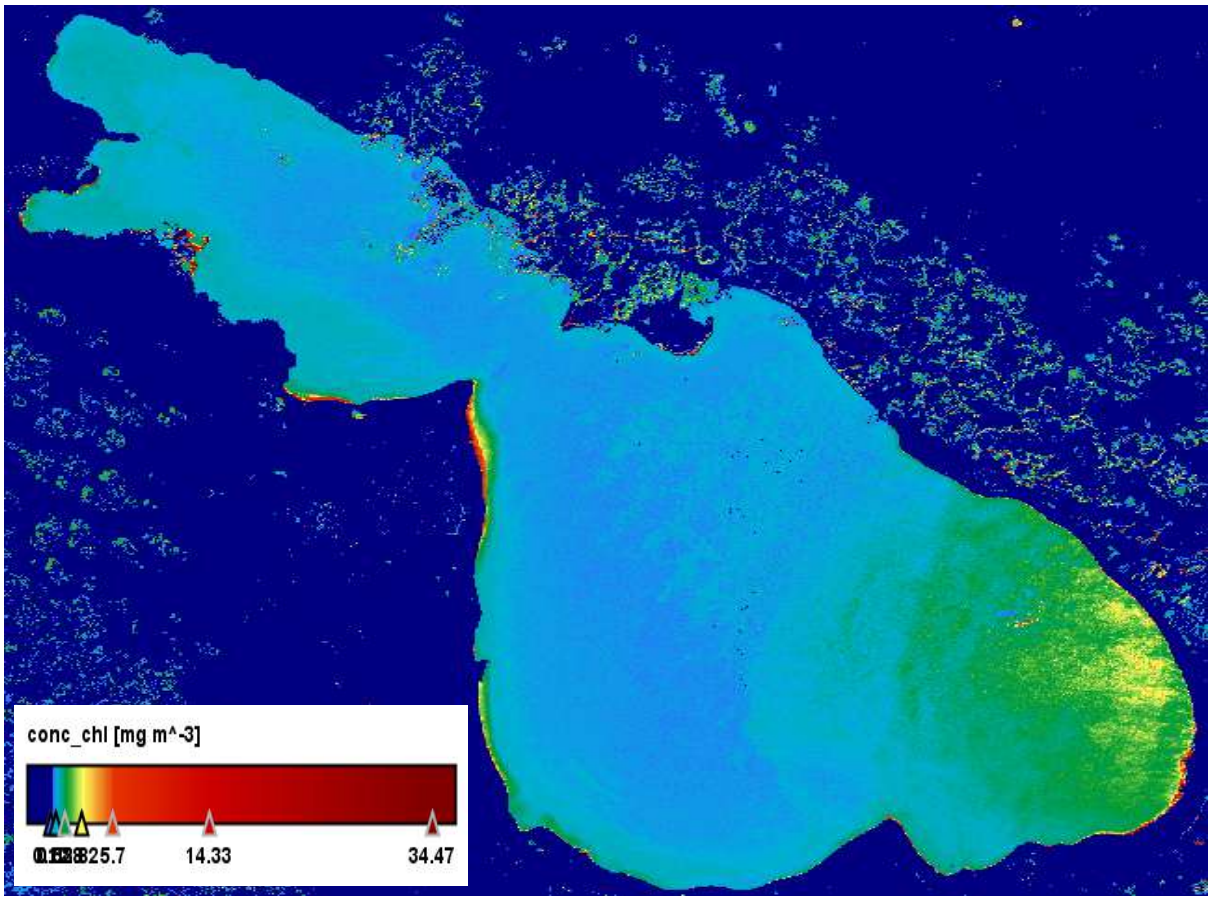

Fig. 23: Landsat 8 image of Lake Sevan in July 2014, analyzed for chl- *a* concentrations using the C2RCC processor.

Algal biomass was also recorded to be highest in the month of July across years, although there were significant inter-annual variations in bloom intensity (Fig. 24). The highest concentrations within the Landsat-8 analyzed data spectrum (2013 - 2017) occurred during 2014, with the second most intensive blooms occurring the following year, in 2015. Despite the differences in bloom

intensities, the temporal bloom dynamics were comparable across years, with most blooms occurring in the summer months and dying off before October (Fig. 25).

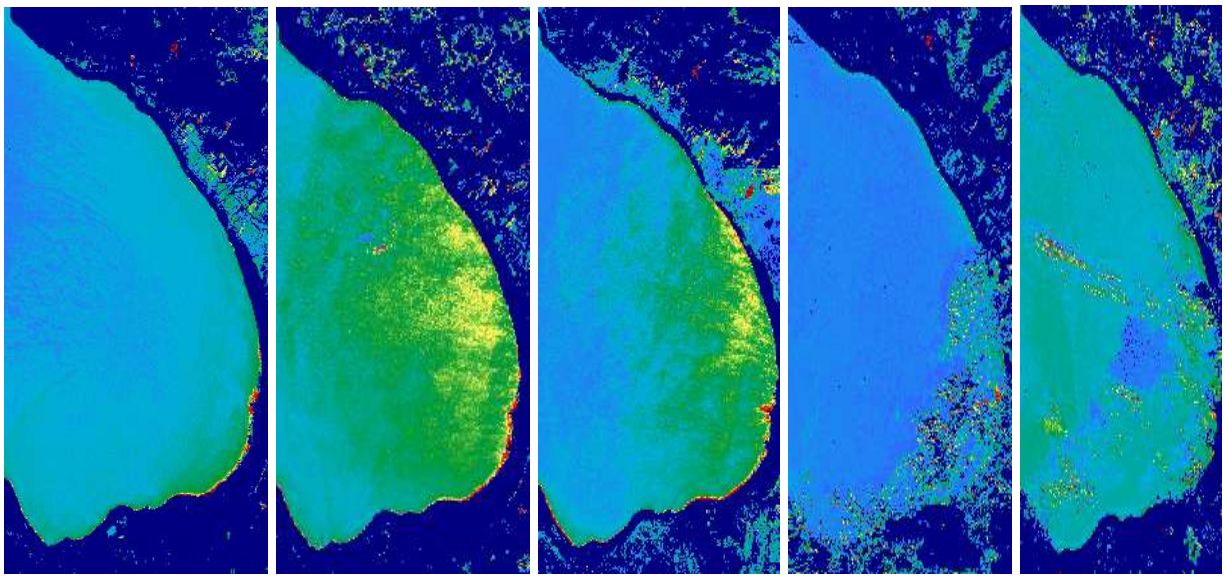

Fig. 24: Landsat 8 images of the SE basin of Lake Sevan in the month of July from 2013 to 2017(left to right). Images analyzed with C2RCC processor's Landsat 8 algorithm.

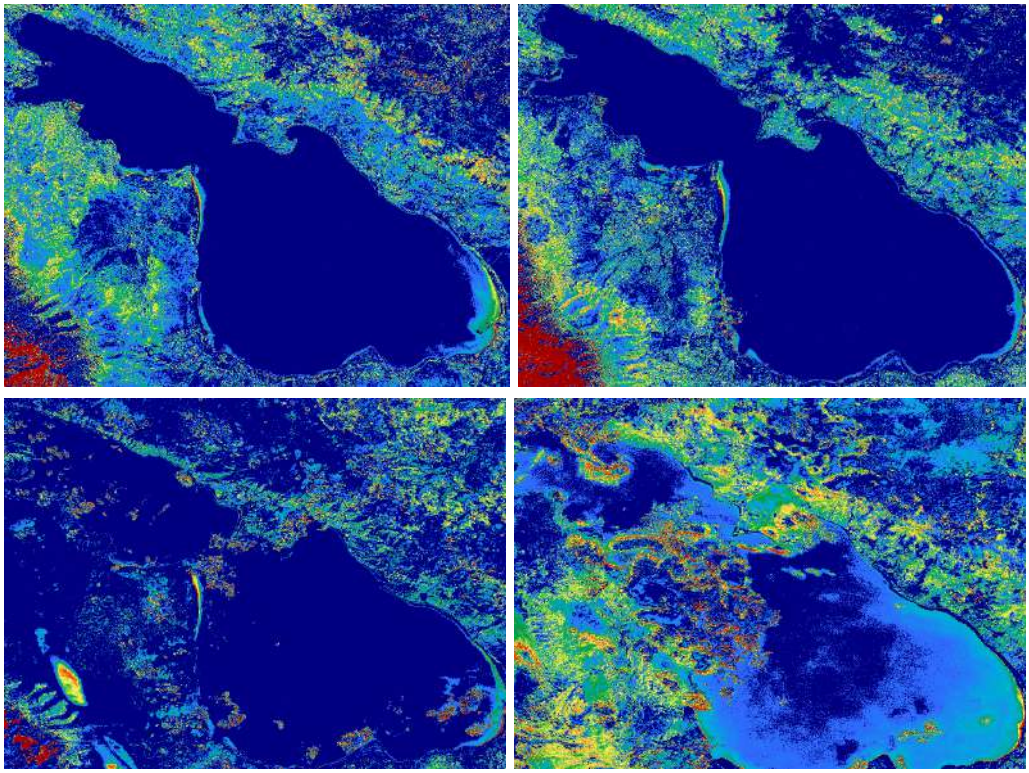

Fig. 25: Landsat 8 images of Lake Sevan in the month of October from the years 2013 (upper left), 2014 (upper right), 2015 (lower left), and 2016 (lower right). Images analyzed with C2RCC processor's Landsat 8 algorithm.

Sentinel-2 Images

In total, 100 Sentinel-2 images were downloaded and analyzed corresponding to the period between 2017 and 2021. The number of images downloaded and processed for every year is shown in Table 8. Below is the description of the eutrophication dynamics for every year in this period.

2017

During the year 2017, strong algal blooms were observed in Spring, with median chl- *a* concentrations in April reaching 4.68 µg.L^{-1} (Table 9). Localized elevated algal biomass was recorded in June and July, particularly in SE of Major Sevan, however, HABs in the summer of 2017 were not captured via our images. Throughout most of the year, higher chl-a concentrations were recorded in Major Sevan compared to Minor Sevan (Fig. 26; Table 9).

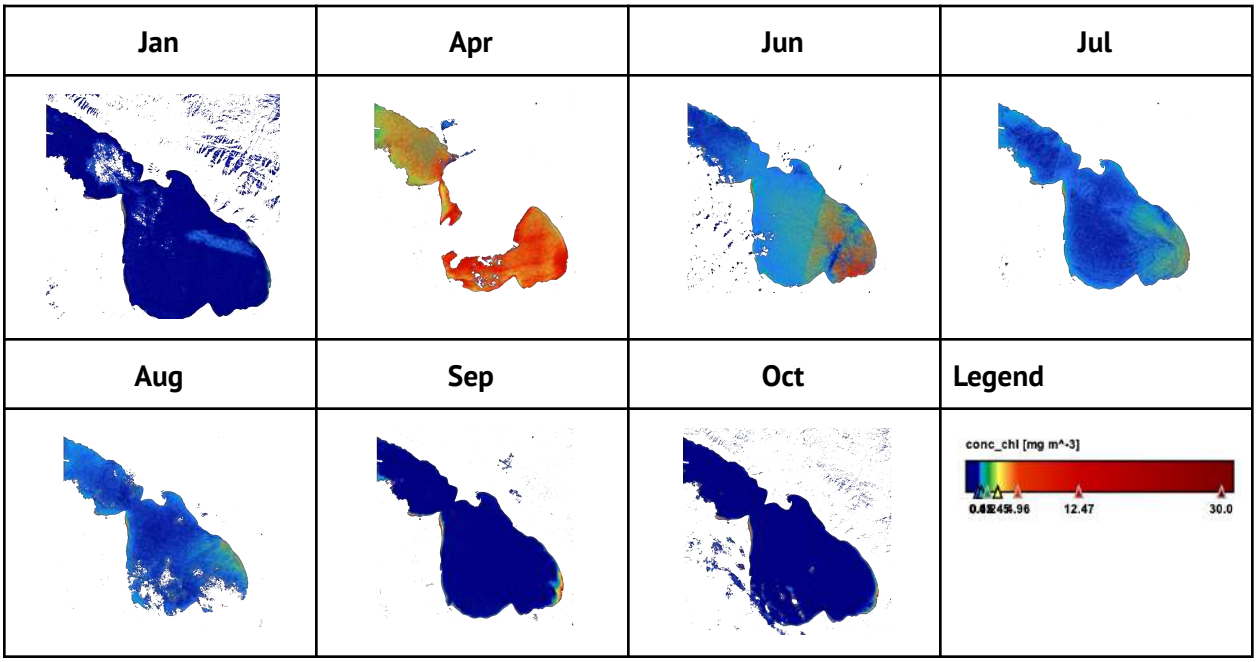

Fig. 26: Monthly algal biomass (chl-a concentrations) in Lake Sevan in 2017. Images from Sentinel-2. Processed by C2RCC processor in ESA SNAP software.

Table 9: Phytoplankton biomass (chl-*a*, in µg.L^{-1}) dynamics in Lake Sevan and its 2 basins during the year 2017.

Lake Sevan - 2017							
Months	**1**	**4**	**6**	**7**	**8**	**9**	**10**
Average	0.0570	5.1948	1.2157	0.3809	0.4513	0.1327	0.1625
Maximum	34.9571	33.6357	44.1757	46.8137	48.7961	47.1113	45.9301
Median	0.0001	4.6755	0.3536	0.1406	0.1465	0.0002	0.0002
Minimum	0.0001	0.0002	0.0002	0.0002	0.0002	0.0002	0.0002
p90_threshold	0.1050	9.9900	3.5342	0.6556	0.5857	0.0473	0.0920
p95_threshold	0.2099	11.6045	6.2731	1.3110	1.2689	0.2358	0.2298
sigma	0.4218	3.3542	2.2881	0.9387	1.5782	0.9407	1.2267
Major Sevan							
Average	0.0494	6.1416	1.4854	0.4155	0.4857	0.1268	0.1367
Maximum	22.9939	27.7583	31.8604	27.9589	36.9950	34.9249	37.1178
Median	0.0001	5.5796	0.4462	0.1680	0.1481	0.0003	0.0002
Minimum	0.0001	0.0002	0.0002	0.0002	0.0002	0.0003	0.0002
p90_threshold	0.0921	10.4928	4.4606	0.7551	0.7031	0.0701	0.0744
p95_threshold	0.1841	11.9362	7.2324	1.6218	1.6649	0.2447	0.1857
sigma	0.3450	3.0959	2.4675	0.9210	1.6194	0.8050	1.0447
Minor Sevan							
Average	0.0829	3.8083	0.3711	0.2792	0.3452	0.1189	0.0945
Maximum	34.9571	33.6357	44.1757	46.8137	48.7961	47.1113	45.9301
Median	0.0001	2.8929	0.1769	0.1406	0.1466	0.0002	0.0002
Minimum	0.0001	0.0002	0.0002	0.0002	0.0002	0.0002	0.0002
p90_threshold	0.1400	8.0727	0.6628	0.5152	0.4393	0.0473	0.0462
p95_threshold	0.2099	10.5281	0.9720	0.6088	0.5857	0.1887	0.0921
sigma	0.5738	3.2314	1.1175	0.9041	1.3671	1.1041	1.0005

2018

The year 2018 produced the strongest algal blooms recorded throughout the studied months during the month of July, with the median chl-a concentrations in the Minor Sevan surpassing 11 $\mu g.L^{-1}$ (Table 10). These were mostly driven by HABs, the majority of the phytoplankton consisting of cyanobacteria, some which were reported to contain harmful cyanotoxins. The harmful algal blooms started in Major Sevan and moved a few days later into Minor Sevan. The HABs started subsiding in August and had altogether disappeared by the end of it (Fig. 27).

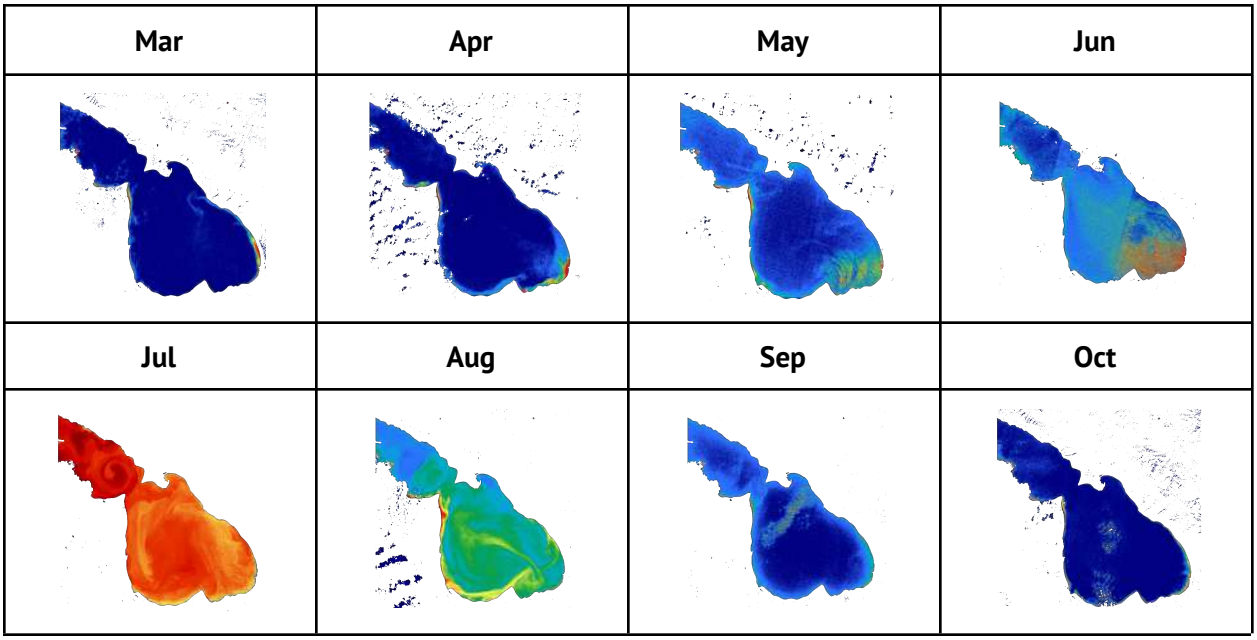

Fig. 27: Monthly algal biomass (chl-a concentrations) in Lake Sevan in 2018. Images from Sentinel-2. Processed by C2RCC processor in ESA SNAP software.

Table 10: Phytoplankton biomass (chl-*a*, in µg.L^{-1}) dynamics in Lake Sevan and its 2 basins during the year 2018.

Lake Sevan - 2018								
Months	**3**	**4**	**5**	**6**	**7**	**8**	**9**	**10**
Average	0.1213	0.1693	0.3236	0.9451	6.9114	1.0187	0.2254	0.1918
Maximum	36.6682	37.1669	36.9623	44.4041	45.8537	45.5143	46.6947	47.5961
Median	0.0002	0.0002	0.1111	0.3110	5.0155	0.8649	0.0936	0.0002
Minimum	0.0002	0.0002	0.0002	0.0002	0.0003	0.0002	0.0002	0.0002
p90_threshold	0.1102	0.1860	0.5177	2.4868	13.2548	1.7752	0.2804	0.1906
p95_threshold	0.2568	0.3718	1.1091	4.8402	18.0909	2.2303	0.4671	0.4285
sigma	0.8216	0.9309	0.9067	1.8948	4.6657	0.9891	0.8895	1.1559
Major Sevan								
Average	0.0964	0.1646	0.3398	1.1282	5.1902	1.1808	0.2352	0.1902
Maximum	30.5796	31.7275	36.2770	33.1751	39.2031	44.3787	30.5334	39.2777
Median	0.0002	0.0002	0.1091	0.3319	4.7438	1.0210	0.0918	0.0002
Minimum	0.0002	0.0002	0.0002	0.0002	0.0003	0.0003	0.0002	0.0002
p90_threshold	0.0919	0.2223	0.6169	3.2513	6.6256	1.9085	0.3361	0.1573
p95_threshold	0.2142	0.4126	1.3787	5.6067	8.2721	2.3523	0.5498	0.5501
sigma	0.6454	0.8416	0.8618	2.0439	2.1319	0.8147	0.8673	1.1118
Minor Sevan								
Average	0.1354	0.1603	0.2756	0.3185	12.4304	0.6625	0.2159	0.1725
Maximum	36.6682	37.1669	36.9623	44.4041	45.8537	45.5143	46.6947	47.5961
Median	0.0003	0.0374	0.1481	0.1778	11.1427	0.4098	0.1404	0.0002
Minimum	0.0003	0.0002	0.0003	0.0002	0.0004	0.0002	0.0003	0.0002
p90_threshold	0.1470	0.1489	0.3329	0.6219	21.4139	1.0925	0.2805	0.1906
p95_threshold	0.2570	0.2975	0.4808	0.7995	24.1651	1.4111	0.3272	0.2857
sigma	0.9619	1.0352	0.9907	0.9497	5.8676	1.2553	0.8658	1.1242

2019

In 2019, strong harmful blooms continued to occur in Lake Sevan albeit they did not reach the same magnitude as the year before (Fig. 28, Table 11). Early localized blooms occurred in Spring, mostly in Major Sevan and particularly along its south-eastern regions. Stronger blooms occurred in the months of June and July when the median chl-*a* concentration in the former month reached 5.2 $\mu g.L^{-1}$ in the whole lake and 5.7 $\mu g.L^{-1}$ in Major Sevan. The blooms gradually subsided in the months of August and September and clearer waters returned in October (Fig. 28).

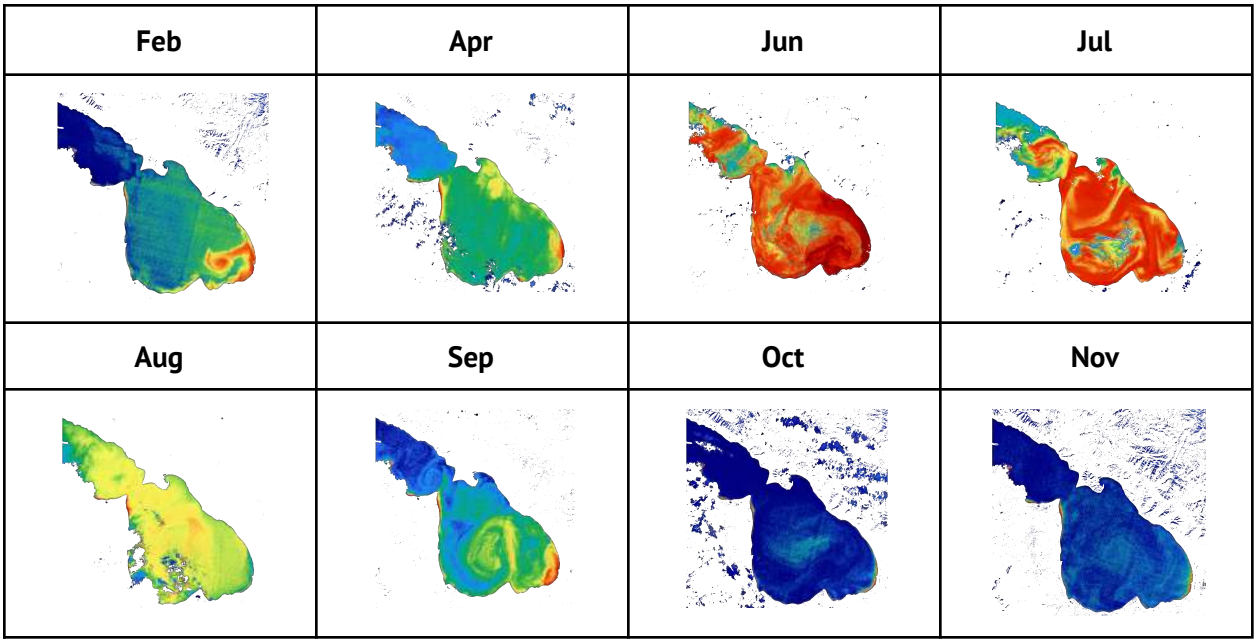

Fig. 28: Monthly algal biomass (chl-a concentrations) in Lake Sevan in 2019. Images from Sentinel-2. Processed by C2RCC processor in ESA SNAP software.

Table 11: Phytoplankton biomass (chl-*a*, in µg.L^{-1}) dynamics in Lake Sevan and its 2 basins during the year 2019.

Lake Sevan - 2019								
Months	**2**	**4**	**6**	**7**	**8**	**9**	**10**	**11**
Average	0.9563	1.1788	6.7405	4.2694	2.3033	1.0136	0.2100	0.2831
Maximum	37.4539	36.2770	43.8037	46.5927	44.8106	47.0347	45.0055	43.2295
Median	0.6369	0.9796	5.2128	4.3799	2.3751	0.7058	0.0002	0.0434
Minimum	0.0002	0.0002	0.0002	0.0002	0.0002	0.0002	0.0002	0.0002
p90_threshold	2.1350	2.1405	17.3463	7.3152	2.9128	2.1638	0.3602	0.7350
p95_threshold	3.2961	2.7209	22.2961	8.0607	3.1817	2.7282	0.7653	1.1241
sigma	1.1912	1.3143	6.1513	2.4288	1.1563	1.1857	1.1237	0.9964
Major Sevan								
Average	1.2128	1.4085	7.5948	4.9127	2.3756	1.2366	0.2131	0.3106
Maximum	28.7218	35.5303	37.5770	46.5927	44.8106	34.9893	31.2914	33.2464
Median	1.0341	1.1726	5.7119	4.9856	2.4199	1.0149	0.0002	0.0666
Minimum	0.0002	0.0002	0.0002	0.0002	0.0002	0.0003	0.0002	0.0002
p90_threshold	2.5564	2.3096	19.4650	7.5481	3.0025	2.3445	0.4695	0.8646
p95_threshold	3.6191	2.8781	23.1475	8.2936	3.2713	2.9743	0.8763	1.1970
sigma	1.1419	1.2257	6.4112	2.1452	1.1832	1.1219	0.9219	0.7932
Minor Sevan								
Average	1.7626	0.5561	3.7045	2.5665	2.1769	0.3110	0.1271	0.1604
Maximum	43.0591	36.2770	43.8037	40.5429	44.3787	47.0347	45.0055	43.2295
Median	1.5116	0.3266	3.1978	1.8651	2.2636	0.1413	0.0002	0.0002
Minimum	0.0047	0.0002	0.0002	0.0002	0.0003	0.0002	0.0002	0.0002
p90_threshold	2.9755	0.9796	7.4906	6.2437	2.7518	0.5176	0.0902	0.1731
p95_threshold	3.3199	1.4149	8.1038	7.3789	2.8405	0.8469	0.1802	0.4757
sigma	1.2215	1.2131	2.6892	2.2807	1.0007	1.0297	1.0703	1.0814

2020

The year 2020 was characterized by milder blooms compared to the previous 2 years, with chl-*a* concentrations reaching their maximum in the month of July (median = 1.96 µg.L^{-1} in the whole lake and 2.96 µg.L^{-1} in Major Sevan). Unfortunately, the images downloaded for the month of August all yielded errors during processing in SNAP, thus data from that month is missing. Nonetheless, by the month of September, algal biomass had decreased to very low levels (Table 12, Fig. 29). A slight increase in algal biomass in the month of November was likely due to the lake mixing after months of stratification.

Feb	May	Jun	Jul
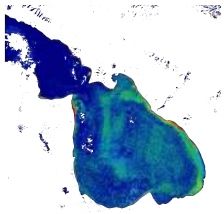	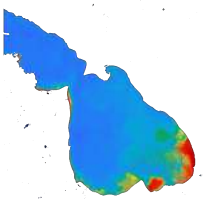	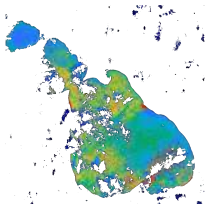	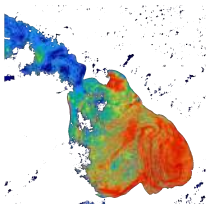
Sep	**Oct**	**Nov**	
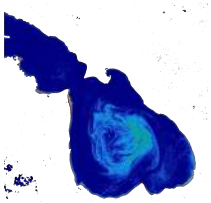	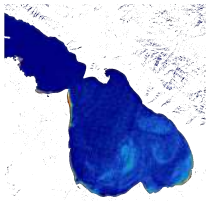	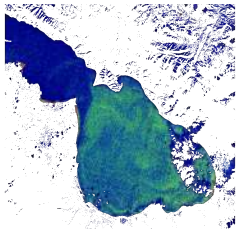	

Fig. 29: Monthly algal biomass (chl-a concentrations) in Lake Sevan in 2020. Images from Sentinel-2. Processed by C2RCC processor in ESA SNAP software.

Table 12: Phytoplankton biomass (chl-*a*, in µg.L^{-1}) dynamics in Lake Sevan and its 2 basins during the year 2020.

Lake Sevan - 2020							
Months	**2**	**5**	**6**	**7**	**9**	**10**	**11**
Average	0.4613	0.7769	1.4715	3.0493	0.1426	0.1805	0.1813
Maximum	32.5667	39.4769	39.5766	40.0425	45.5482	44.1418	48.2088
Median	0.0653	0.3161	0.8313	1.9622	0.0002	0.0443	0.0002
Minimum	0.0002	0.0002	0.0002	0.0002	0.0002	0.0002	0.0002
p90_threshold	1.2702	1.2635	3.4037	7.0476	0.3190	0.3091	0.2894
p95_threshold	1.5633	3.3952	4.7889	8.4091	0.5467	0.5299	1.0125
sigma	1.0916	1.7017	1.9805	3.2235	0.6837	0.9051	1.0472
Major Sevan							
Average	0.5394	0.8993	1.6220	3.6579	0.1616	0.2003	0.7311
Maximum	32.5667	37.5688	38.9130	40.0425	33.6278	35.9112	29.4778
Median	0.1956	0.3384	0.9730	2.9633	0.0339	0.0721	0.2949
Minimum	0.0002	0.0003	0.0002	0.0002	0.0002	0.0003	0.0002
p90_threshold	1.3679	1.6909	3.6191	7.4080	0.3701	0.3594	1.8278
p95_threshold	1.6285	4.3207	5.0588	8.8896	0.6055	0.6107	2.0636
sigma	1.0452	1.8153	2.0532	3.2309	0.5814	0.8340	1.2630
Minor Sevan							
Average	0.1166	0.3439	1.1350	0.4519	0.0897	0.1103	0.1813
Maximum	24.4240	39.4769	39.5766	39.1119	45.5482	44.1418	48.2088
Median	0.0002	0.2371	0.4751	0.1957	0.0002	0.0002	0.0002
Minimum	0.0002	0.0002	0.0002	0.0002	0.0002	0.0002	0.0002
p90_threshold	0.0978	0.3161	3.0080	0.8215	0.0457	0.0443	0.2894
p95_threshold	0.3665	0.4740	4.1161	1.3300	0.1368	0.1326	1.0125
sigma	0.7064	1.0314	1.6800	1.2255	0.8831	0.9772	1.0472

2021

The last year in our study, 2021, showed somewhat similar dynamics. Algal biomass increased in May and reached its peak in June (median chl-*a* 2.55 µg.L^{-1} in the whole lake and a higher 5.24 µg.L^{-1} in Major Sevan). Unlike other years, July was characterized by lower biomass and by August the median chl-*a* concentration was already <0.1 µg.L^{-1} (Fig. 30, Table 13).

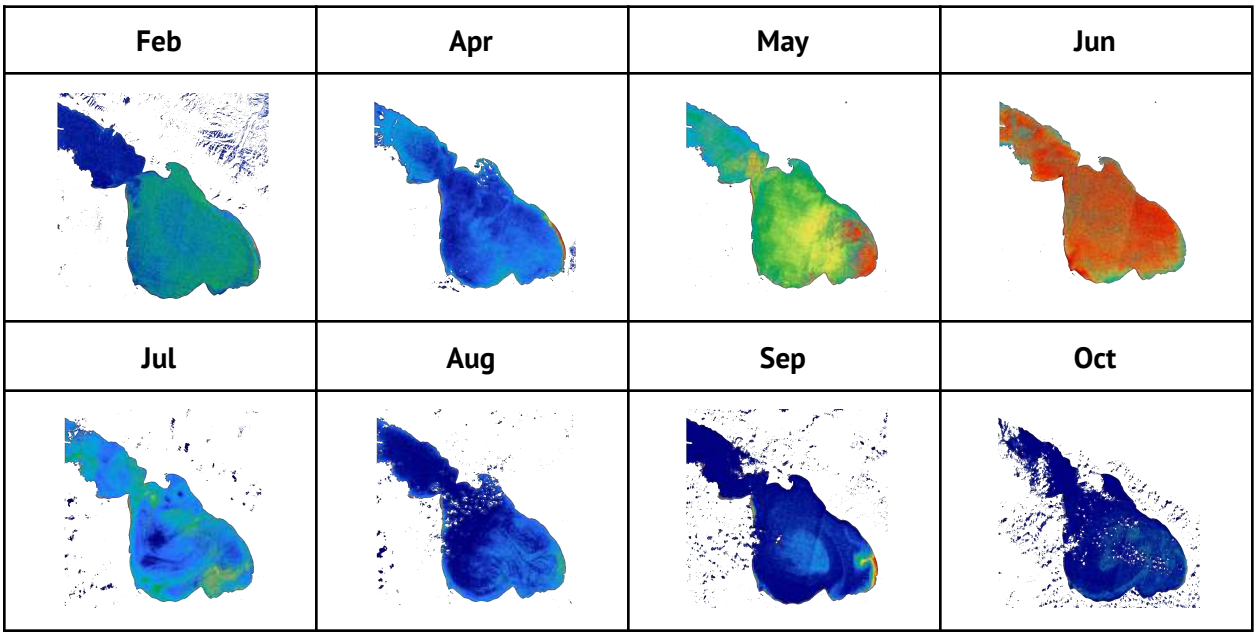

Fig. 30: Monthly algal biomass (chl-a concentrations) in Lake Sevan in 2021. Images from Sentinel-2. Processed by C2RCC processor in ESA SNAP software.

Table 13: Phytoplankton biomass (chl-*a*, in µg.L^{-1}) dynamics in Lake Sevan and its 2 basins during the year 2021.

Lake Sevan - 2021								
Months	**2**	**4**	**5**	**6**	**7**	**8**	**9**	**10**
Average	0.5604	0.3236	1.8399	2.9984	0.5141	0.2335	0.2485	0.2651
Maximum	32.6533	28.4216	42.4123	43.8877	45.8877	48.2343	47.0943	31.5637
Median	0.3593	0.1707	1.5694	2.5513	0.3214	0.0966	0.0002	0.0002
Minimum	0.0002	0.0002	0.0002	0.0061	0.0002	0.0002	0.0002	0.0002
P90_threshold	1.2736	0.5117	3.1811	5.0086	0.9638	0.3378	0.3298	0.4420
P95_threshold	1.4369	0.6538	4.7079	6.3690	1.5145	0.5307	0.7537	0.9786
sigma	0.7671	0.8570	1.4435	1.8205	0.8671	1.1024	1.2122	1.3431
Major Sevan								
Average	0.6972	0.3100	2.0662	5.5873	1.8523	0.2427	0.2361	0.2638
Maximum	28.4816	28.4216	34.6273	41.2537	42.0146	45.7943	34.4828	31.5637
Median	0.6837	0.1423	1.7662	5.2394	1.7711	0.0917	0.0346	0.0002
Minimum	0.0002	0.0002	0.0002	0.0003	0.0068	0.0002	0.0002	0.0002
P90_threshold	1.3388	0.4549	3.4283	10.5199	2.3592	0.3665	0.4140	0.5052
P95_threshold	1.4812	0.7107	5.1250	13.8614	2.6533	0.5955	0.7933	1.0418
sigma	0.6346	0.8856	1.3789	3.8554	0.5294	1.0288	0.9117	1.2812
Minor Sevan								
Average	0.1378	0.3389	1.1990	5.4669	0.5526	0.2002	0.2342	0.2475
Maximum	32.6533	26.2121	42.4123	41.3962	45.8877	48.2343	47.0943	27.6546
Median	0.0328	0.2361	0.8061	5.0505	0.3673	0.0484	0.0002	0.0002
Minimum	0.0002	0.0002	0.0003	0.0002	0.0002	0.0002	0.0002	0.0002
P90_threshold	0.3267	0.5768	2.5026	11.0943	0.9179	0.1931	0.0473	0.1384
P95_threshold	0.4573	0.6292	3.3932	14.1990	1.2391	0.2896	0.2356	0.4979
sigma	0.5067	0.6915	1.2752	4.1987	1.1143	1.2709	1.6345	1.4708

Total Suspended Matter (TSM)

Total suspended matter in general followed the same trends as chl-*a*, with minor deviations.

2017

In 2017, the highest amount of TSM recorded was in April (Fig. 31), corresponding to the algal blooms that were recorded in the same month of that year (see Fig. 26). In contrast, TSM concentrations were lowest in August. In general, TSM concentrations were found to be higher in littoral areas compared to the pelagic zone. The eastern coast of Minor Sevan (North of Shorzha) recorded lower TSM concentrations than the rest of the shoreline.

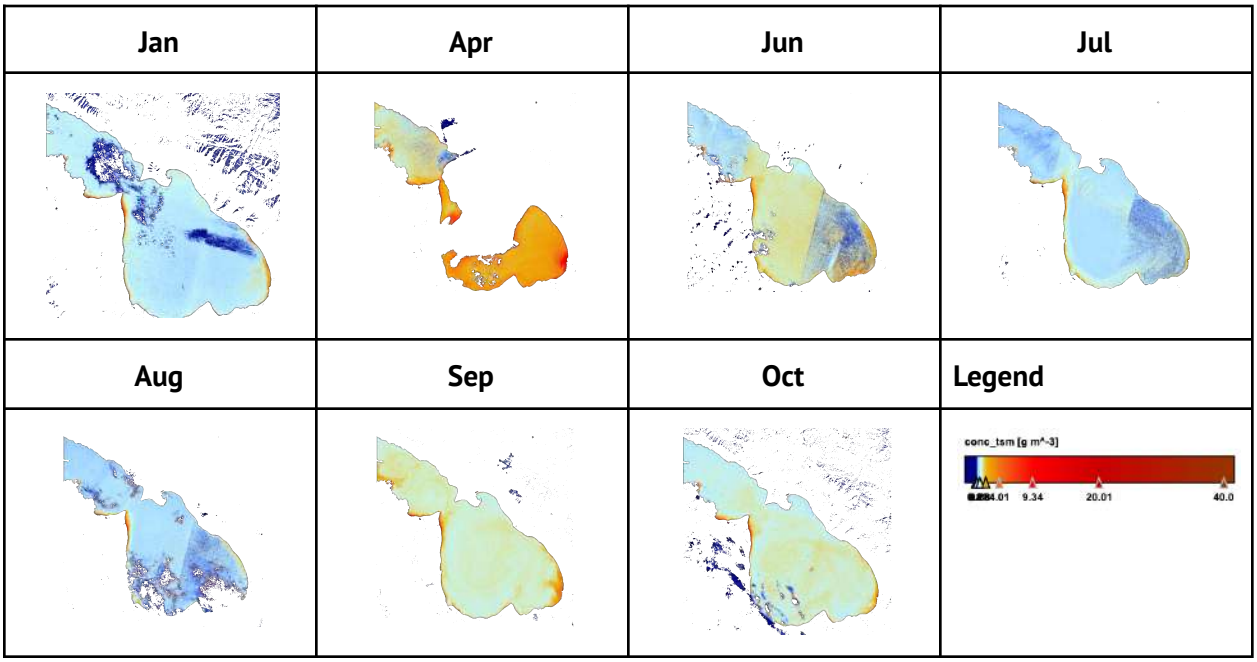

Fig. 31: Monthly Total Suspended Solids (TSM) in Lake Sevan in 2017. Images from Sentinel-2. Processed by C2RCC processor in ESA SNAP software.

2018

In 2018 TSM concentrations were highest in the month of July coinciding with the strong algal bloom that occurred in Lake Sevan during that year. In contrast, the lake water was relatively clearer in March and September (Fig. 32).

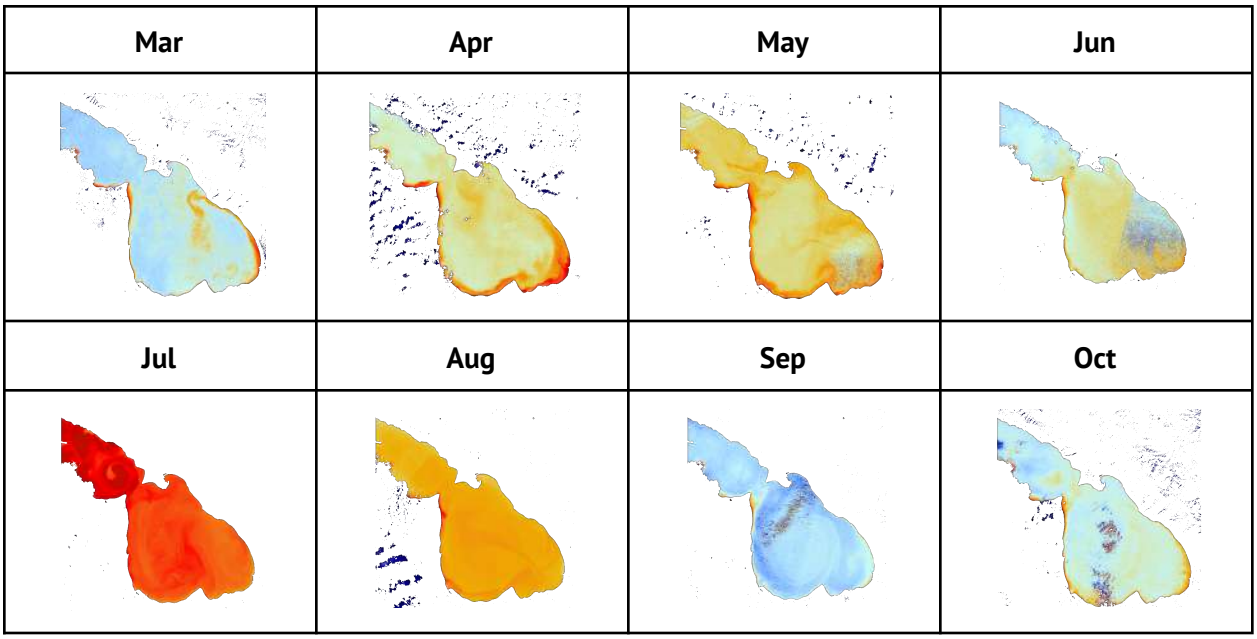

Fig. 32: Monthly Total Suspended Solids (TSM) in Lake Sevan in 2018. Images from Sentinel-2. Processed by C2RCC processor in ESA SNAP software.

2019

The year 2019 was characterized by high TSM concentrations almost year round, with the peak reaching in July, coinciding with the strong algal blooms. TSM concentrations only declined in autumn (October and November; Fig. 33).

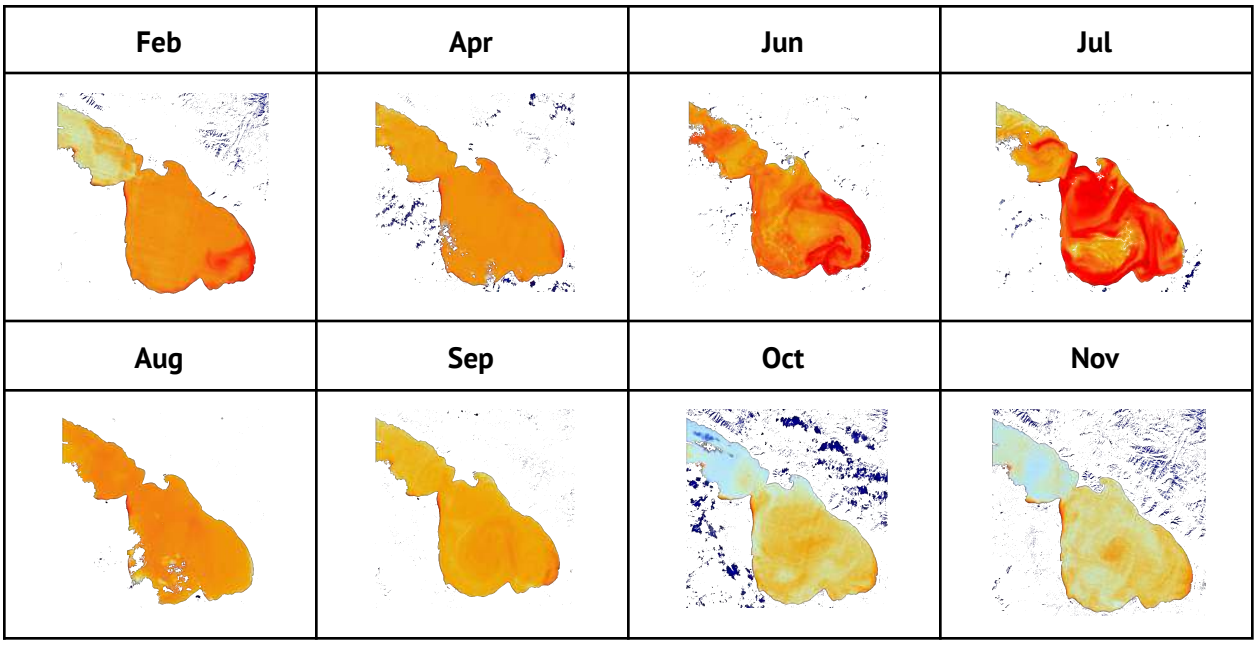

Fig. 33: Monthly Total Suspended Solids (TSM) in Lake Sevan in 2019. Images from Sentinel-2. Processed by C2RCC processor in ESA SNAP software.

2020

The year 2020 was characterized by slightly lower TSM concentrations compared to the previous year, with peak concentrations reaching yet again in the month of July.

Feb	May	Jun	Jul
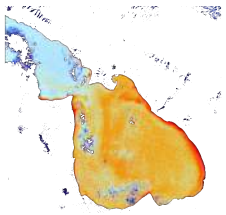	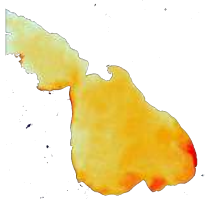	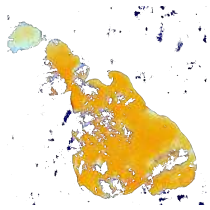	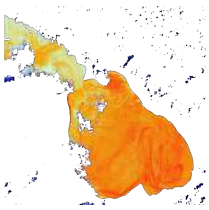
Sep	**Oct**	**Nov**	
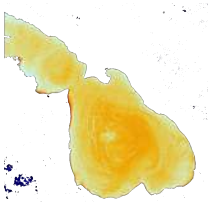	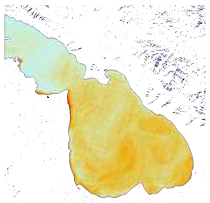	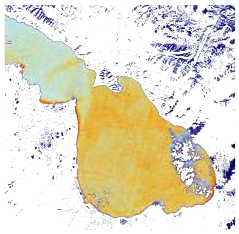	

Fig. 34: Monthly Total Suspended Solids (TSM) in Lake Sevan in 2020. Images from Sentinel-2. Processed by C2RCC processor in ESA SNAP software.

2021

In 2021, low TSM concentrations were recorded in February, however suspended matter in the lake increased in April, reaching its highest values in June (same time as the highest algal biomass that year). TSM concentrations in the lake decreased in August but registered a slight increase again in September (Fig. 35).

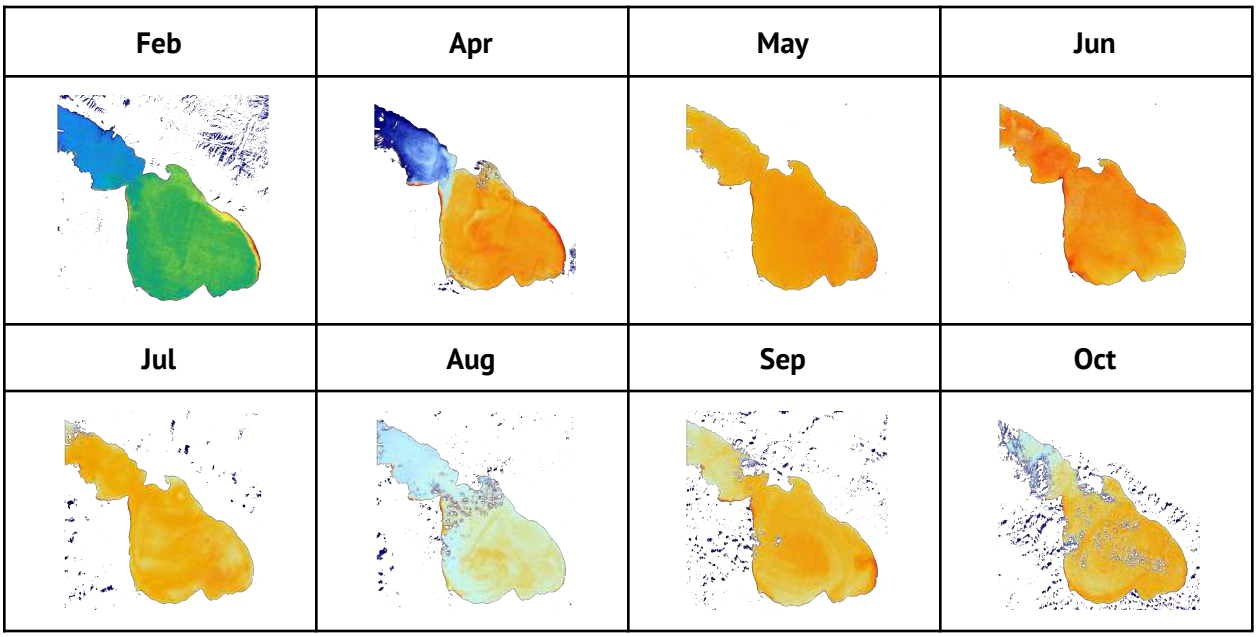

Fig. 35: Monthly Total Suspended Solids (TSM) in Lake Sevan in 2021. Images from Sentinel-2. Processed by C2RCC processor in ESA SNAP software.

Eutrophication drivers

To better understand the factors driving eutrophication in Lake Sevan we compared algal biomass (chl-*a* concentrations) derived from satellite images to a few abiotic parameters.

Firstly, we looked into annual temperature fluctuations in the Lake Sevan Basin to explain potential inter-annual differences. Despite some differences between years in mean surface water temperatures (Fig. 36), we could not find any significant statistical differences that could explain the variations.

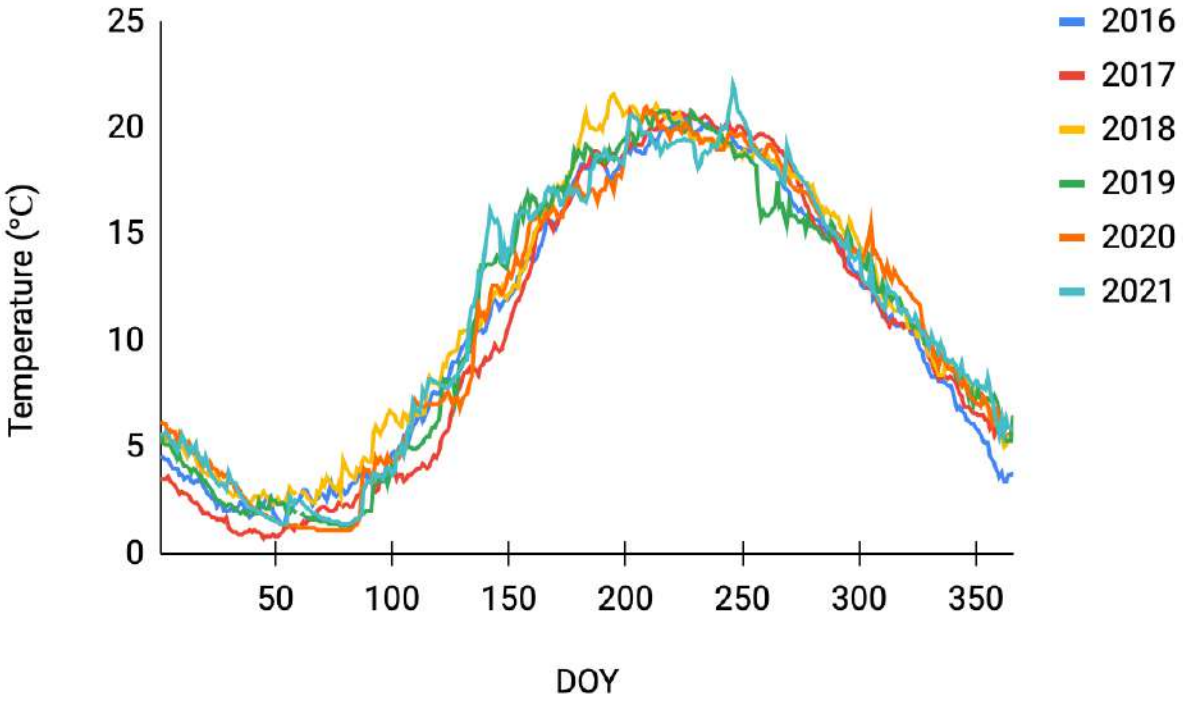

Fig. 36: Daily fluctuations of surface water temperature (in ℃) in Lake Sevan between 2016 and 2021.

However, upon closer inspection into the temperature of summer months, we noted a few interesting observations about July temperatures, the month during which algal blooms were most prevalent. In 2018, the year with the highest chl- *a* concentrations recorded throughout our study period, the surface water temperatures in Lake Sevan were also the highest in the previous years (20.7 ℃, Fig. 37). In 2019, the year with the second highest algal blooms, the July water surface temperatures dropped slightly (19.4 ℃) but still constituted the second highest mean temperature in the studied years. In 2020, lower temperatures throughout the spring (Fig. 36) and in the month of July (18.7 ℃, Fig. 37) potentially partially inhibited the algal blooms and led to lower chl-a concentrations compared to previous years (Figs. 29, 38, Table 12).

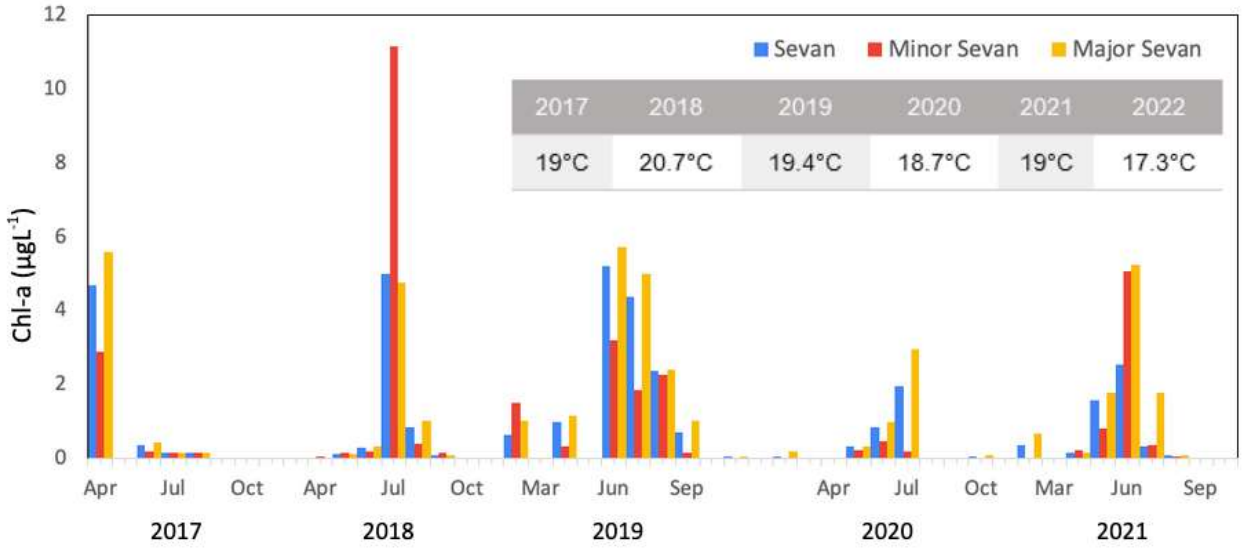

Fig. 37: Fluctuations in median chl-*a* concentrations in Lake Sevan and its two basins. The embedded table shows mean surface water temperatures in the month of July between 2017 and 2022.

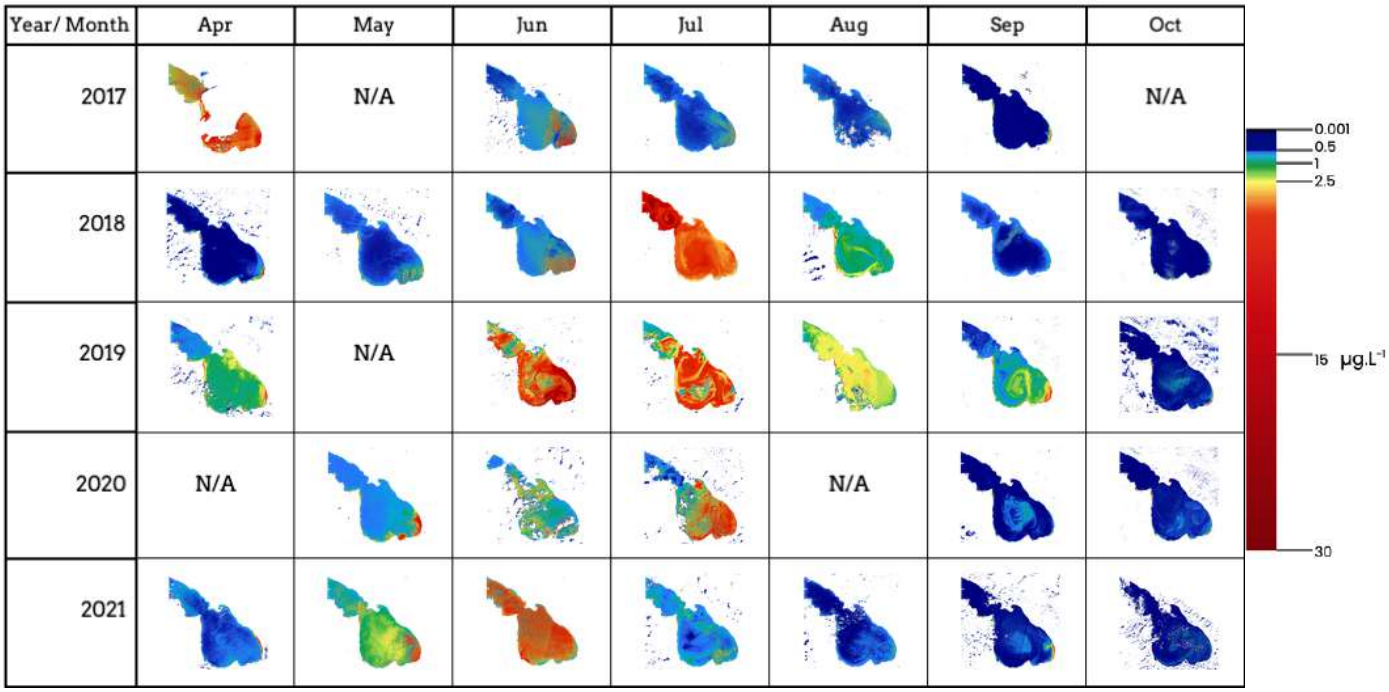

Fig. 38: Interannual fluctuations in chl-*a* concentrations in Lake Sevan, derived from Sentinel-2 images.

To further investigate anthropogenic impacts and nutrient loading on the eutrophication dynamics of Lake Sevan, we also looked into correlations between nutrient concentrations and algal biomass.

We looked into water N concentrations (Nitrates (NO_3^-), Nitrites (NO_2^-), Ammonium (NH_4^+) and Total Nitrogen (TN)) but found no significant correlations (Fig. 40). There are two factors that might contribute to this. Firstly, it is likely that N is no longer a limiting factor in algal stoichiometry. Secondly, some of the reported cyanobacterial strains in Lake Sevan (Gevorgyan *et al.*, 2020, Asatryan *et al.*, 2022) have the ability to fix atmospheric nitrogen, thus rendering the link between water N concentrations and algal biomass weaker.

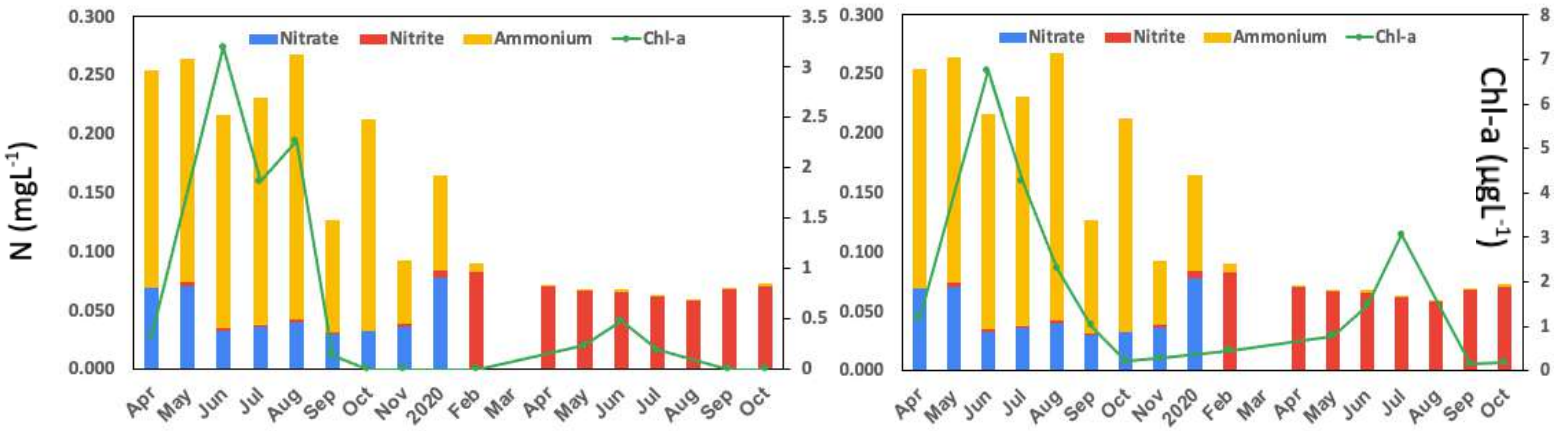

Fig. 40: Fluctuations in concentration of Nitrogen compounds and chl-a concentrations across months.

Next, we looked into correlations between phosphate ion (PO_4^{3-})and Total Phosphorus (TP) concentrations and algal biomass (Fig. 41). While there were no correlations between TP and algal biomass, it was noteworthy that strong algal blooms were always accompanied by a near full depletion of phosphate ion concentrations (Fig. 41). This potentially indicates a strong phosphate limitation in the lake and a possible cause for algal bloom termination.

Fig. 41: Fluctuations in concentration of TP, phosphate ion and chl- *a* concentrations across months.

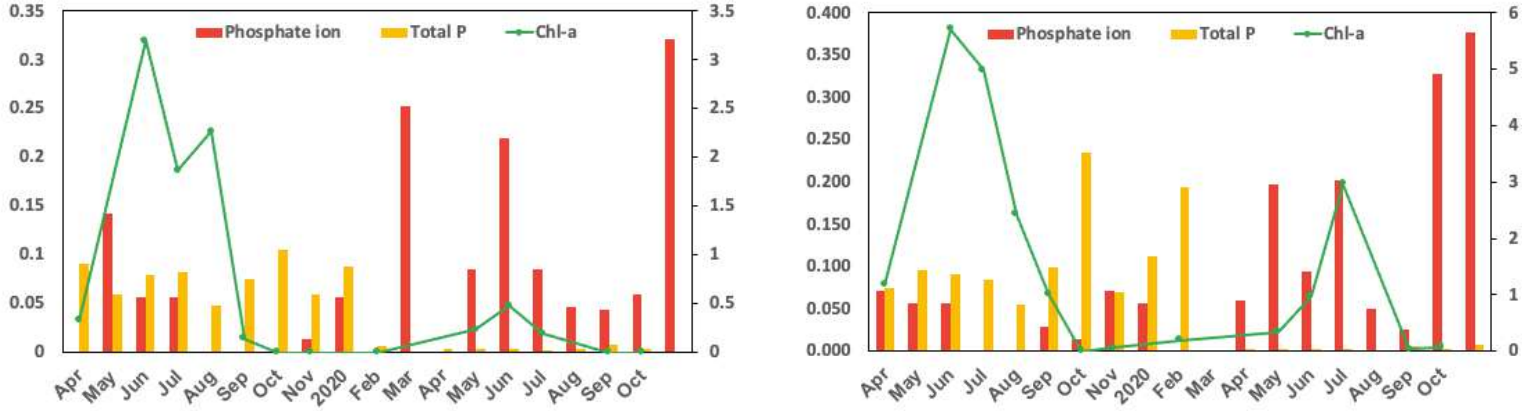

Discussion

Using freely available satellite images, we were able to reconstruct the changes in algal biomass and eutrophication dynamics that occurred in Lake Sevan over the past decade. This allowed us to investigate spatial and temporal variations (within and between years) to better understand the drivers leading to eutrophication.

There were significant differences between years, as we recorded a number of years where Lake Sevan underwent Spring blooms (*e.g.* 2017, 2019; Fig. 38), while in other years algal (e.g. 2018, 2021) biomass in Spring was relatively lower. Most years, with the exception of 2017, experienced strong algal blooms in the summer, though maximum chl-*a* concentrations were reached in June in some years and in July in others.

Temperature seems to be an important determinant of the time and intensity of algal occurrence (Fig. 37) with lower surface water temperatures potentially limiting algal blooms in 2020, after 2 years of intensive HABs in 2018 and 2019. Similarly, earlier temperature peaks in 2021 led to increase in algal biomass production in early June but subsided in July and August due a drop of temperature lower than annual averages in July.

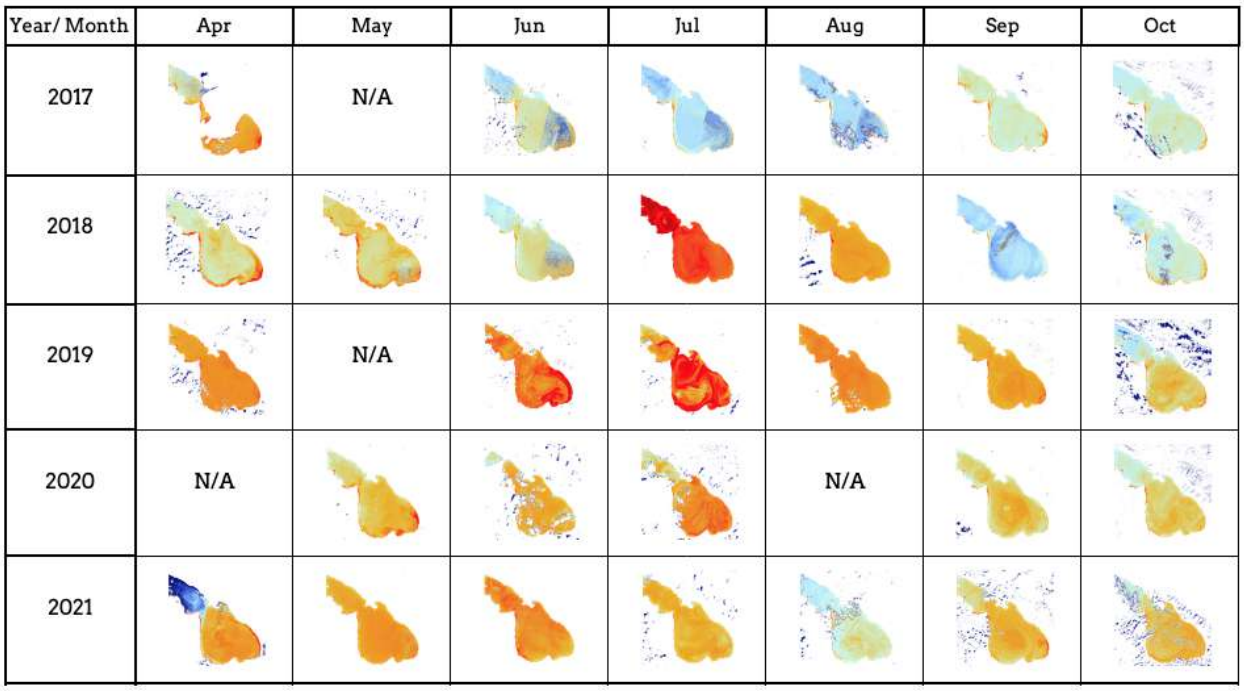

Fig. 42: Interannual differences in TSM concentrations in Lake Sevan.

There were also evident spatial variations in Lake Sevan throughout the years, with some areas exhibiting higher eutrophication profiles than others. The eastern coast of Minor Sevan (North of Shorzha) recorded lower TSM concentrations than the rest of the shoreline (Fig. 42). This is not surprising given the low number of rivers flowing into the Lake along that coast and fewer urban developments in the region, leading that section of the Lake to potentially experience less anthropogenic pressures than the rest of it.

In contrast, the higher TSM and algal biomass was recorded in the western coasts of Minor and Major Sevan and along the south-east shoreline of Major Sevan. Given the presence of the majority of the cities (Sevan, Gavar, Martuni, Vardenis) and larger urban settlements in the lake basin along these parts, in addition to the majority of river inflow reaching the lake in its southern basin, organic matter and nutrients loading is expected to be higher in this region, as reflected in the eutrophication dynamics (Fig. 43, Appendix I).

The Lake Sevan basin is heavily impacted by untreated sewage flowing from urban settlements into its rivers and, eventually, the lake. During our field surveys, we often came across heavily polluted rivers (*e.g.* Gavaraget, Masrik (Fig. 42), Karchaghbyur (Fig. 43)) flowing uninterrupted into Lake Sevan. There are only three sewage treatment facilities in the basin, however they only conduct primary (physical) treatment and lack the capacity for any chemical and biological treatment (Mesropyan, 2022). Many of the smaller urban settlements and businesses (resorts, restaurants, etc.) along the lake's shoreline lack proper sewage collection, increasing the potential of non-point source pollution, in addition to agricultural runoff (fertilizers, pesticides, herbicides) after heavy rainfall events and snowmelt. This acts as one of the core drivers of the increase in N and P loading into the lake and, ultimately, to the occurrence of HABs.

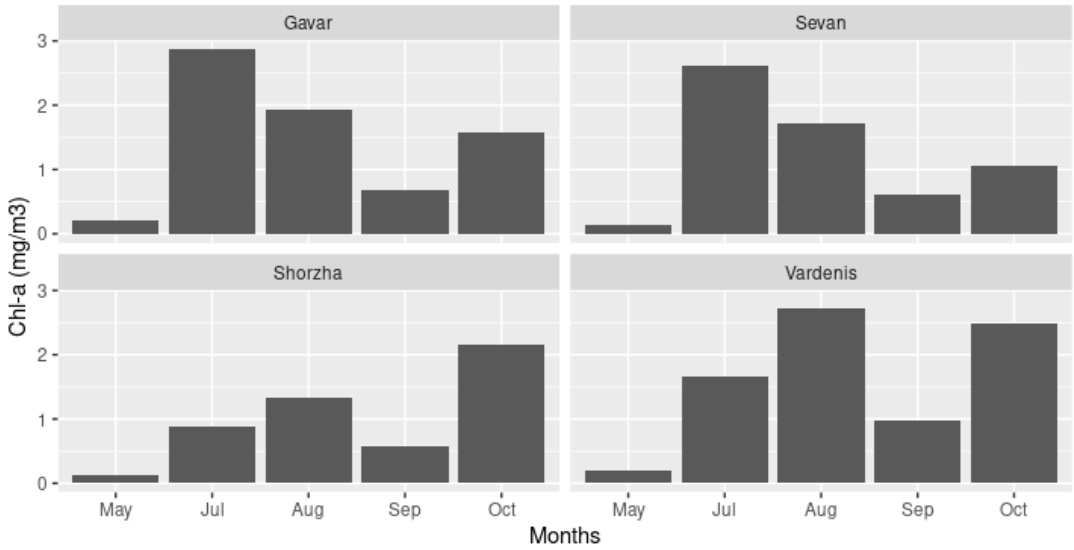

Fig. 43: Elevated chl-*a* concentrations along the coasts of cities in Lake Sevan. See Appendix I.

The Lake Sevan basin is heavily impacted by untreated sewage flowing from urban settlements into its rivers and, eventually, the lake. During our field surveys, we often came across heavily polluted rivers (*e.g.* Gavaraget, Masrik (Fig. 44), Karchaghbyur (Fig. 45)) flowing uninterrupted into Lake Sevan. There are only three sewage treatment facilities in the basin, however they only conduct primary (physical) treatment and lack the capacity for any chemical and biological treatment (Mesropyan, 2022). Many of the smaller urban settlements and businesses (resorts, restaurants, etc.) along the lake's shoreline lack proper sewage collection, increasing the potential of non-point source pollution, in addition to agricultural runoff (fertilizers, pesticides, herbicides) after heavy rainfall events and snowmelt. This acts as one of the core drivers of the increase in N and P loading into the lake and, ultimately, to the occurrence of HABs.

Fig. 44: River Masrik in August 2021. A significant source of organic pollution and nutrient input into Lake Sevan.

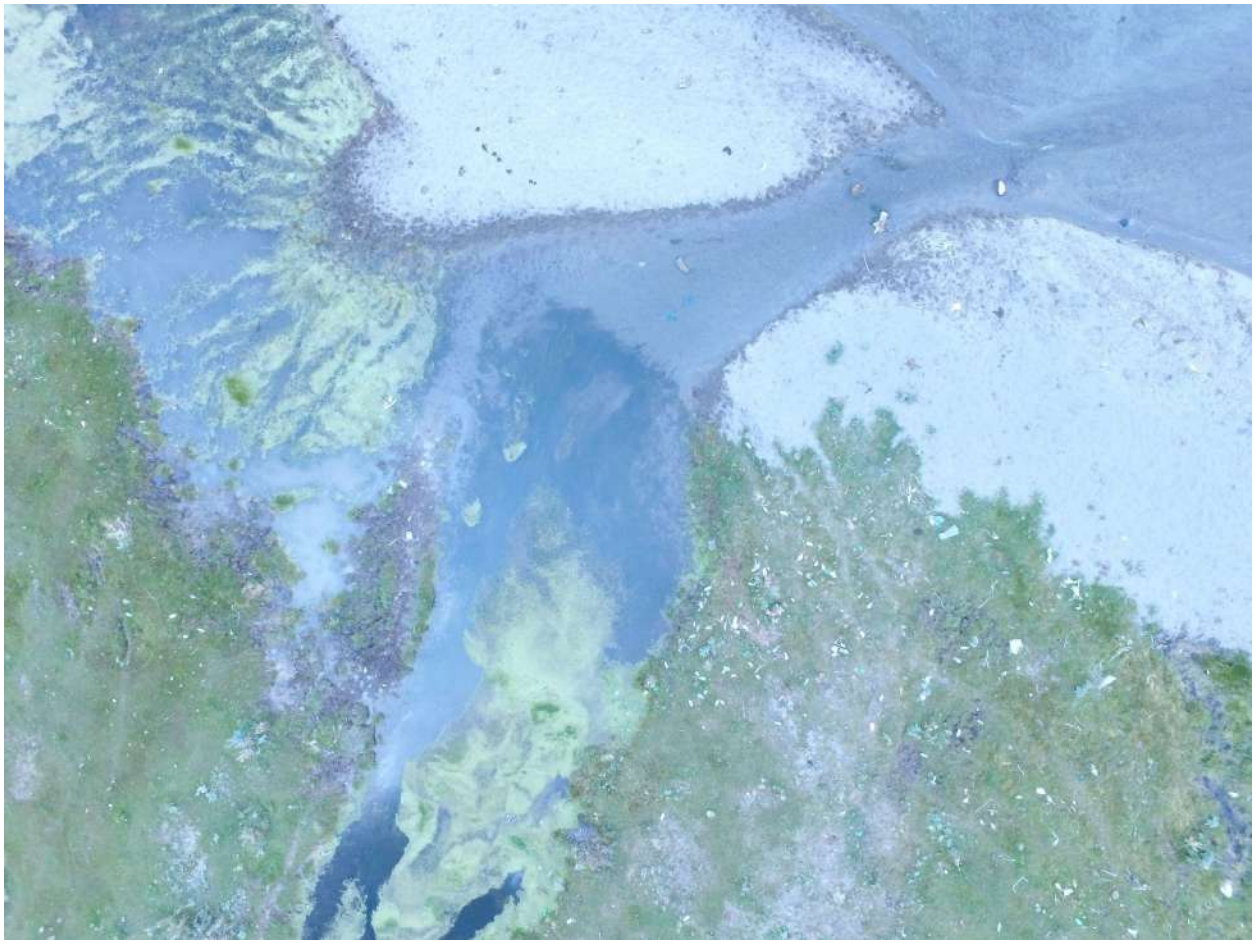

Fig. 45: Drone image of Karchaghbyur river flowing into Lake Sevan (2021). Signs of eutrophication at the estuary are evident.

A minor limitation of this method (and remote sensing in general) is the inaccuracies generated particularly looking into coastal and shallow waters, due to a high reflectance from the bottom (sediments and submerged vegetation) skewing the results. This was also an issue that we noticed in this study with some very shallow regions producing very high chl-*a* year round. This limitation was partially alleviated by using median chl-a concentrations in our analyses (as opposed to means) to decrease the impact of outliers in the calculations. Additionally, complimenting our satellite image analysis with frequent field trips, we could confirm whether high chl-*a* concentrations were indeed due to algal blooms or because of interferences from other factors.

For instance, we noticed the growth and spread of filamentous algae in September 2021 (and again the current year, 2022) along the southern and south-eastern coast resulting in extremely high chl-*a* concentrations in our satellite image analyses. Based on field observations, we could easily disregard this information as a potential algal bloom.

In general, the results shown in this study are in agreement with other recent publications (*e.g.* Gevorgyan et al., 2020, Asatryan et al., 2022, See Appendix II) and further corroborate the

increased eutrophication in Lake Sevan in recent years. It also provides an easy-to-use methodology to improve the ecosystem's long term monitoring capacity for all relevant stakeholders (relevant ministries, local public authorities, national park management, academic institutions, etc.).

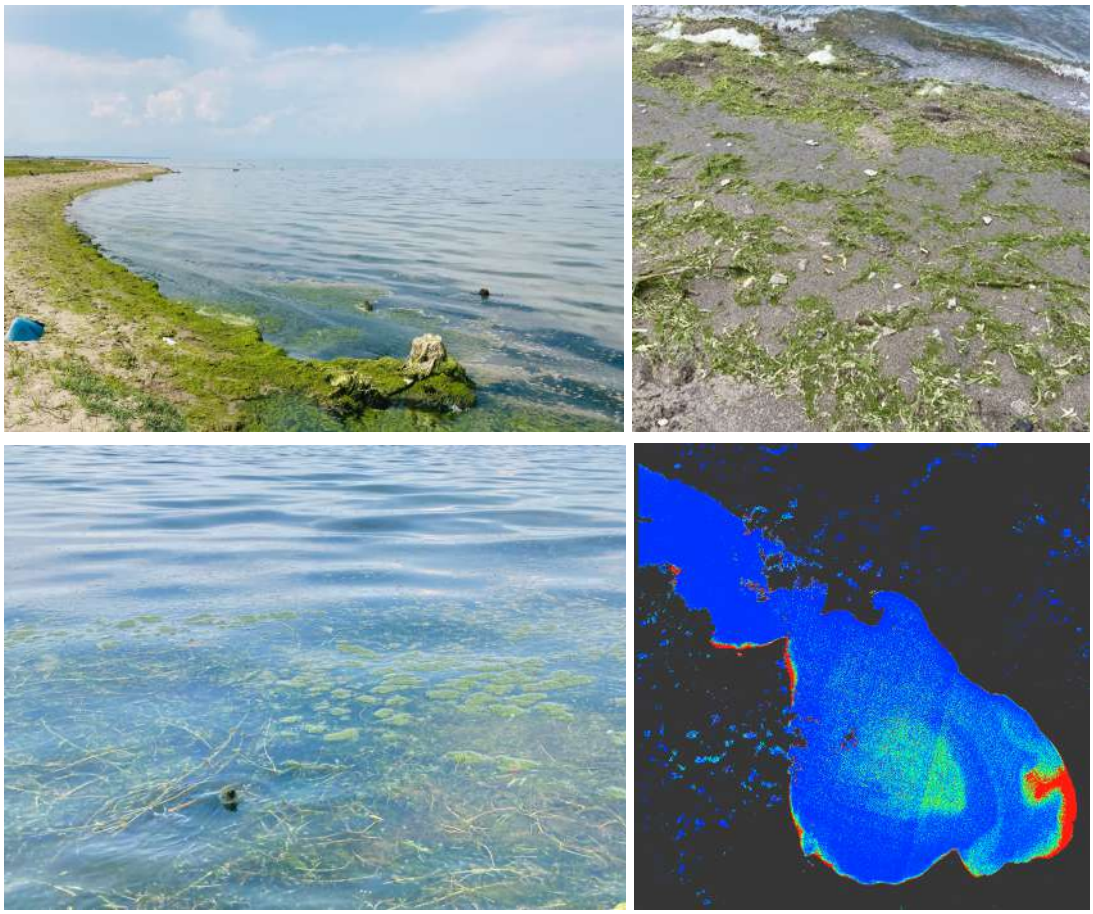

Fig. 46: Growth and spread of filamentous algae along the southern coast in Sep 2021 resulted in extremely high chl-*a* concentrations.

It is expected that the water temperature will rise by 2°C in 2070 and by 4°C in 2100 (Arakelyan *et al.*, 2021). This will further increase the occurrences of intensive algal blooms and, in particular, cyanobacterial HABs, as it is well reported that cyanobacteria thrive in warmer temperatures (Paerl & Huisman, 2008). This will have very dire consequences for the Lake Sevan ecosystem, its food webs, its biodiversity, and the ecosystem services it provides. Thus, it might create huge economic losses, higher unemployment, while putting the country's water and energy security at risk.

There are also model projections that, with climate change, Lake Sevan will shift from a dimictic to a monomictic lake (Shikhani *et al.*, 2021). This will definitely alter the lake's ecosystem metabolism and nutrient fluxes, with numerous unpredictable consequences related to its eutrophication dynamics. With less mixing, the potential for anoxia might increase, promoting higher anoxia-driven P release from the sediments.

Global phenomena like climate change are difficult to control for a small nation-like Armenia. However, developing climate adaptation plans are paramount to its security. For Lake Sevan, this can be done by limiting the nutrient loading into the lake, to mitigate its eutrophication and HABs.

This study showed that nitrogen is no longer a limiting factor. Moreover, the ability of specific cyanobacterial species to fix atmospheric nitrogen further diminishes the impact of further reducing the nutrient concentrations in the lake. However, unlike a century ago in Lake Sevan, phosphorus is currently a limiting factor. Reducing phosphorus loading into the lake via proper sewage treatment, reducing non-point P loading through better management of nearby agriculture, regulating the tourism sector, improving the infrastructure, and better implementation of environmental regulations can have significant impacts in mitigating algal blooms and safeguarding the sustainability of Lake Sevan's ecosystem.

Appendix I

Spatiotemporal analysis of chl-*a* concentrations along the major urban settlements in Lake Sevan in 2018

Aleksandr Hakobyan

Introduction:

To study Sentinel 2-A Satellite's Multi Spectral Instrument (MSI) data during the months of May to October 2018 to extract average Chlorophyll-*a* (Chl-*a*) concentration in the waters of the lake, especially around 4 major cities of the lake area – Sevan, Vardenis, Gavar, and Shorja.

Methods:

Visualization:

Polygon Creation – Firstly, a complete polygon of the lake was created keeping a margin of ~100 m from the shoreline to avoid considering distorted data from the satellite. After acquiring the polygon, for decreasing the computational requirements and the ease of observing and analyzing the data, the polygon was further divided into 400 individual zones. The following is the procedure:

- 4000 points were placed in the original polygon randomly
- The points were then clustered using the K-Means Clustering algorithm into 400 different subsets
- Each cluster was then aggregated further to provide a larger number of points within each region
- Centroids were calculated for each of the aggregated clusters
- Thiessian Polygons tool from SAGA GIS Toolbox was used to create individual polygons around each of the 400 centroids
- An intersection between the Thiessian Polygons and the original polygon was made, yielding the final polygon covering the Sevan River-Basin with 400 individual computation zones.

After the zones were created, raster files containing the Chl-*a* band (Band 5) were imported and the Zonal Statistics tool was used to calculate the mean concentration for each zone. The attributes table of the Polygons with extracted average Chl-*a* data was exported for further calculation in Excel. The vector was then rasterized to obtain the final rasters used for visualization. All analyses and computations performed using QGIS software and SAGA GIS Toolbox

City Coast Analysis:

The exported attribute tables were used in this method to come up with average concentrations of Chl-*a* around 4 of the major cities in the Sevan Lake area. For each city the closest 4-5 polygons to the shoreline were selected. The Chl-*a* concentration data was identified by their polygon Id and for each polygon and the average was calculated. This procedure was repeated for each of the months for each major city.

Results:

The data from each month was visualized using pseudocolor single band setting for the raster file. Concentrations of each month were taken into consideration when adjusting the weight of the legends for the maps. Figures 1 through 5 represent the visualized data for each month from May to October respectively, excluding June due to data corruption.

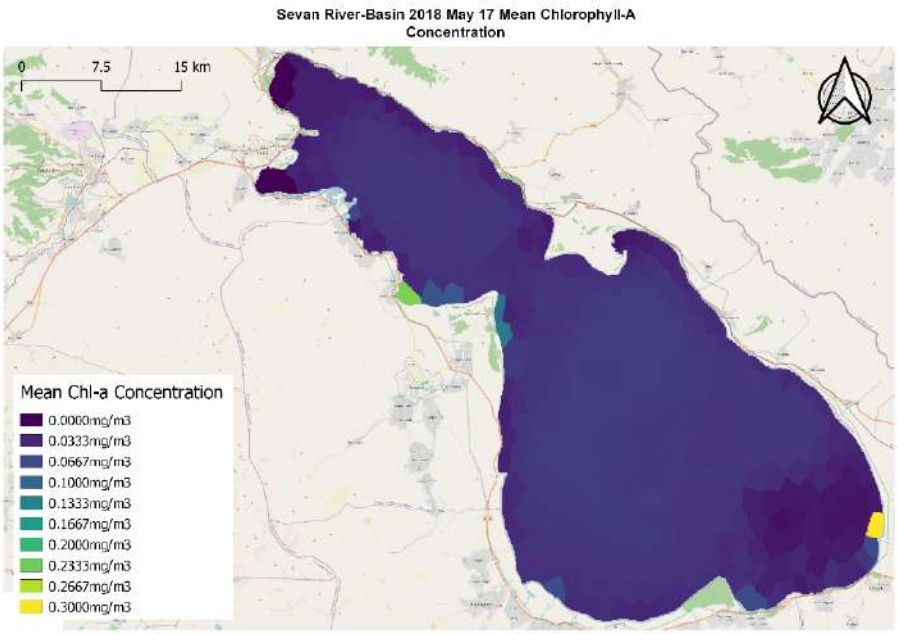

Figure 1

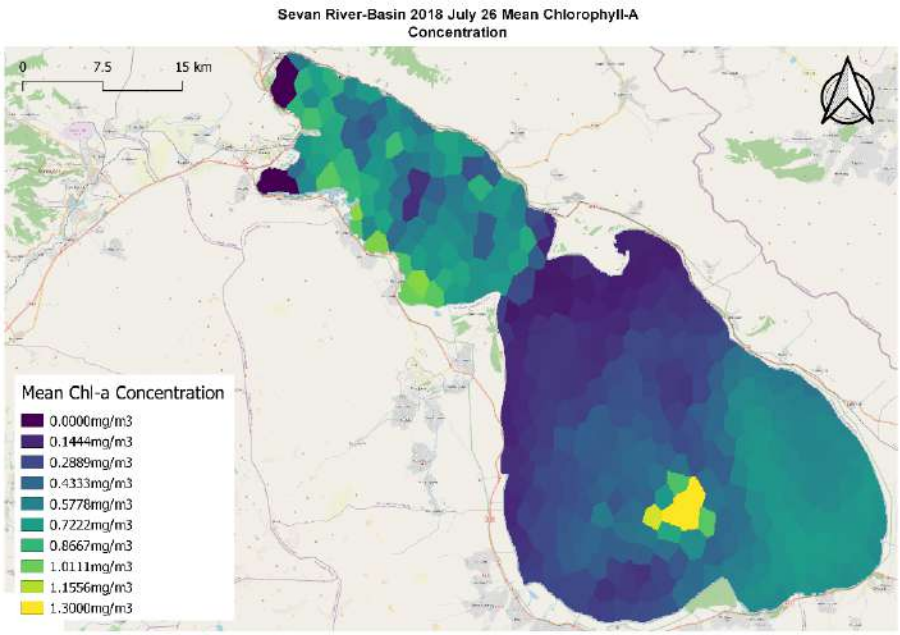

Figure 2

In Figure 2 the raster file included some cloud disturbance around Big Sevan yielding in a concentration of 3.2 mg/m^3. This was discarded and can be seen as a bright yellow spot.

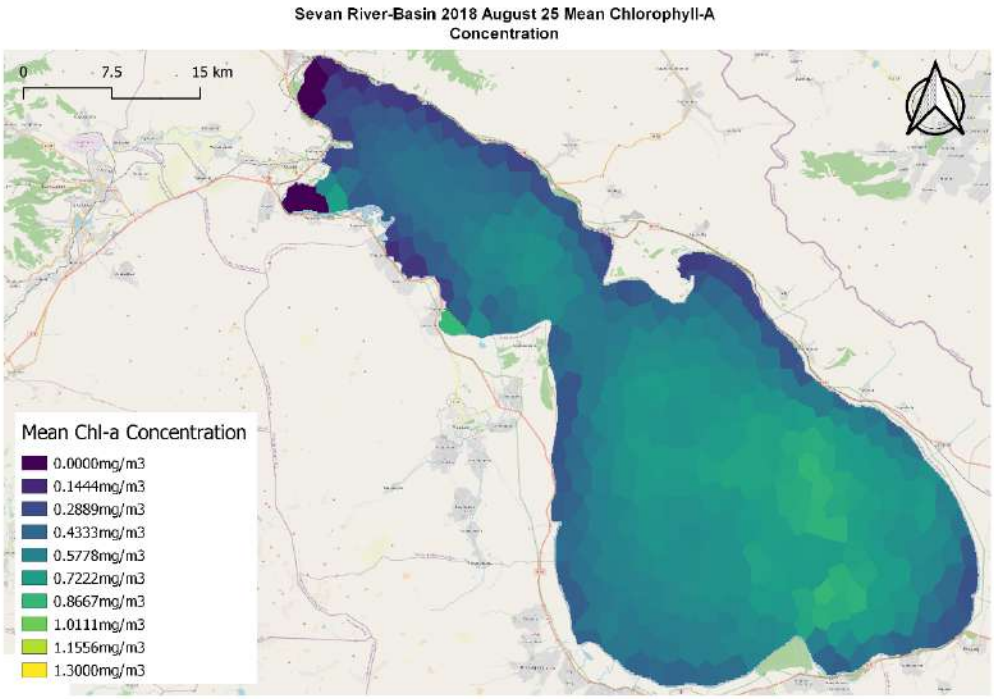

Figure 3

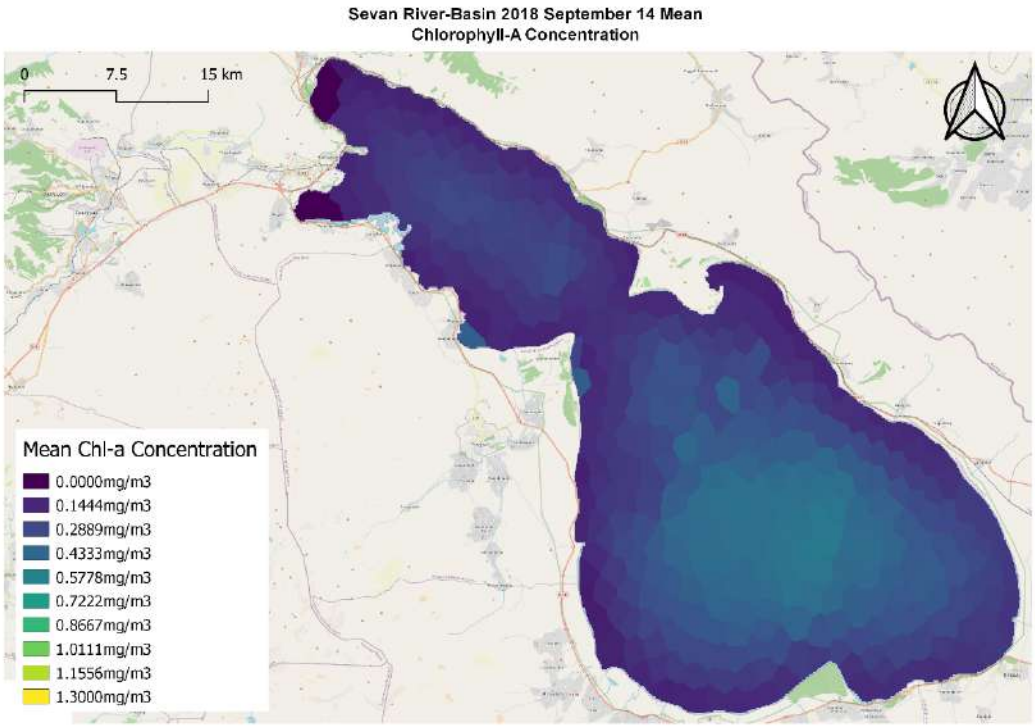
Sevan River-Basin 2018 September 14 Mean
Chlorophyll-A Concentration
0
7.5
15 km
Mean Chl-a Concentration
0.0000mg/m3
0.1444mg/m3
0.2889mg/m3
0.4333mg/m3
0.5778mg/m3
0.7222mg/m3
0.8667mg/m3
1.0111mg/m3
1.1556mg/m3
1.3000mg/m3

Figure 4

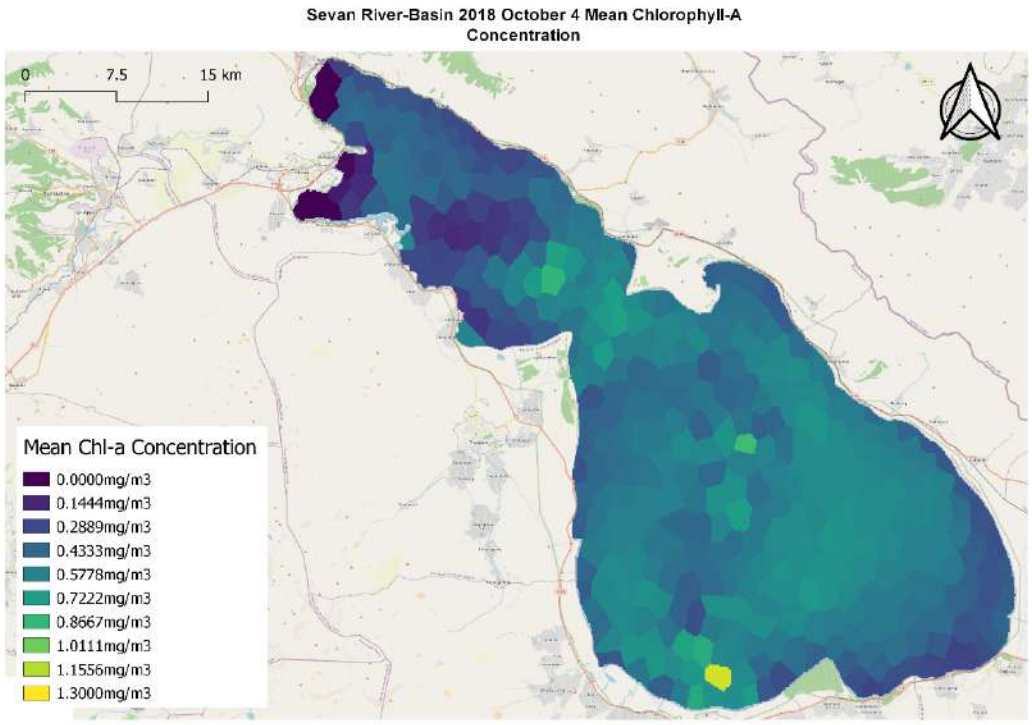

Figure 5

For the individual city calculation please refer to Figure 6 below which shows the selected areas near the shores of each of the major cities as well as the Polygon of the Sevan River-Basin divided into 400 sections.

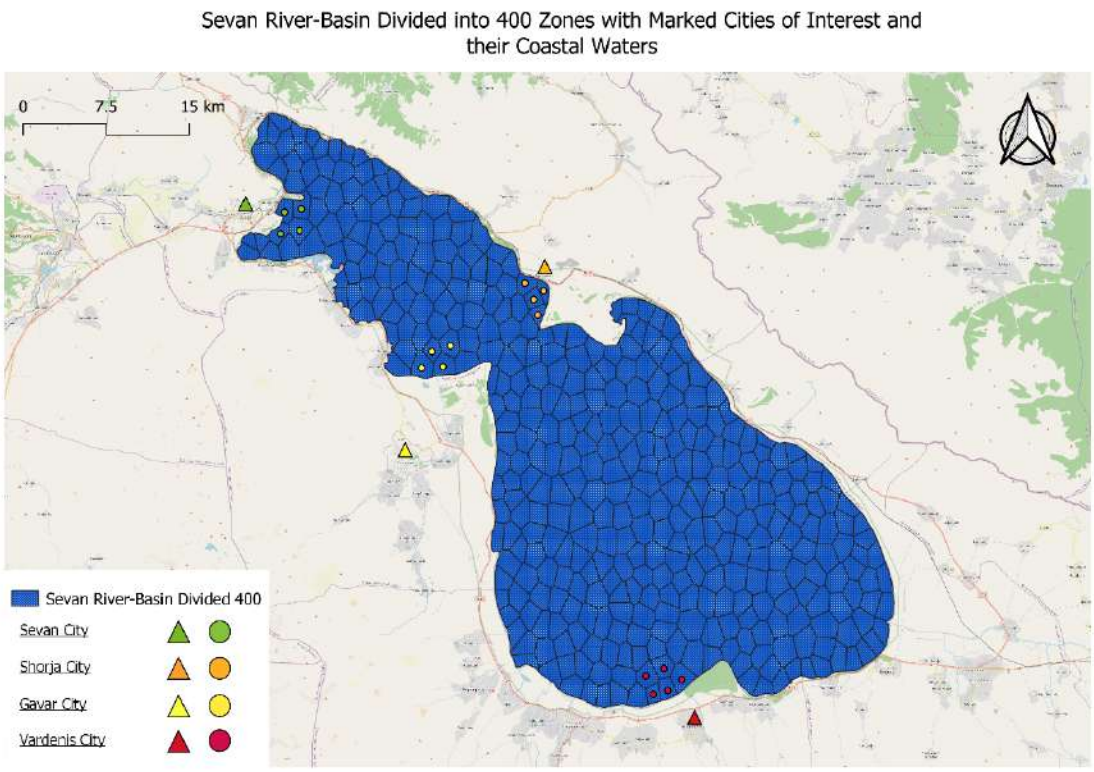

Figure 6

From Figure 6 and the Calculations mentioned in the Methodologies section, Chl-A was calculated for each of the cities and can be seen in Graphs 1 through 4 for Sevan, Shorja, Vardenis and Gavar respectively.

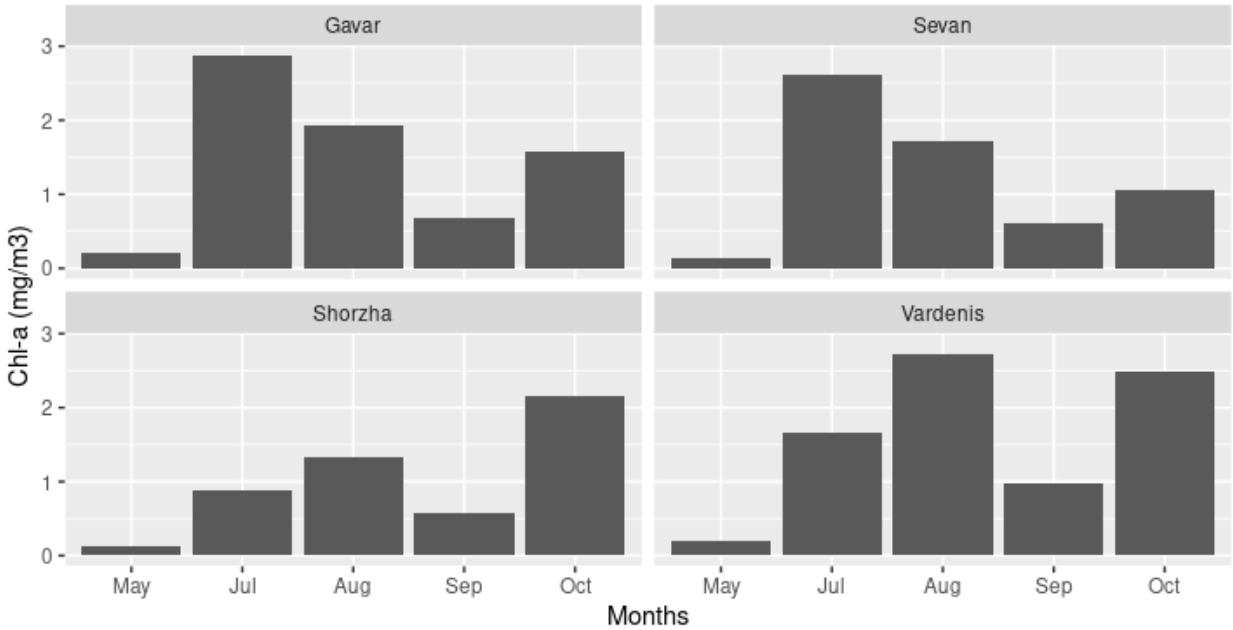

Results Analysis:

Temporal Analysis:

We can see in Figure 1 that the lake was experiencing the lowest concentration of Chl-A from all the months which correlates with the factual clarity of the lake during those months. The temperature is cold enough in May that blooming of Algae does not occur. Following Figures 2 and 3 we see a dramatic increase in concentration. This occurs during the months of June, July, and August when the lake is in the phase of active blooming. In September sedimentation occurs after the active blooming phase due to a decrease in ambient temperature. This slows down the eutrophication processes going on in the lake as can be seen in Figure 4. Following the sedimentation process, the lake clears up allowing sunlight to penetrate further. This increases the photosynthesis yielding a secondary bloom in the month of October as can be seen in Figure 5.

Looking at the concentrations of Chl-A around the shores of major cities around the lake we see this temporal trend continue. All the points of interest follow the same trend with slight changes in values which can be attributed to a greater or smaller amount of anthropogenic pollution (sources of nutrients for algae). All the cities have a decrease in Chl-A concentrations during the month of September followed by a spike in the month of October. This can be seen in Graph 1.

Spatial Analysis:

Chl-A concentrations regardless of the month are highest around the shore, specifically near major cities. This can be attributed to shallow waters, where the temperature of the water is higher in combination with the wastewater flowing into the lake from said cities carrying needed nutrients for algal blooming. When looking at the temporal trends of spiked concentrations in the month of October at different locations near the shore, we see a different increase in concentrations. In other words, not all locations have the same amount of increase in Chl-A concentrations. This could likely be the result of the internal hydraulics and waterflow patterns of the lake. The variance of anthropogenic pressure could also be the result of the inconsistent increase in concentration. The spatial trend is that the northern shores (Sevan city to the northwest and Shorja city to the North) tend to be less concentrated than the southern shores (Vardenis city to the South and Gavar city to the southwest).

Appendix II

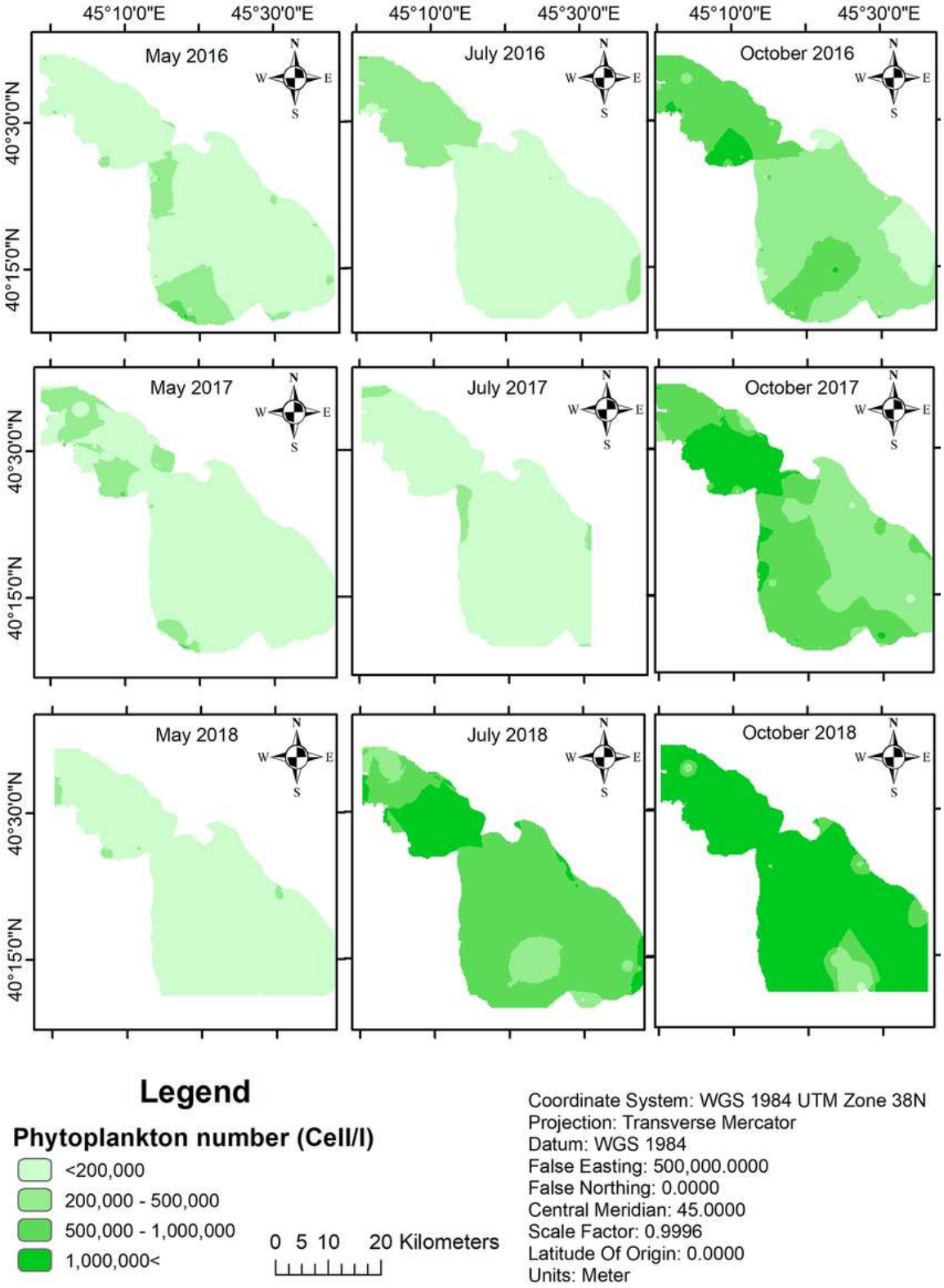

Fig: Spatiotemporal dynamics of phytoplankton count from 2016 to 2018. Source: Asatryan *et al.*, 2022

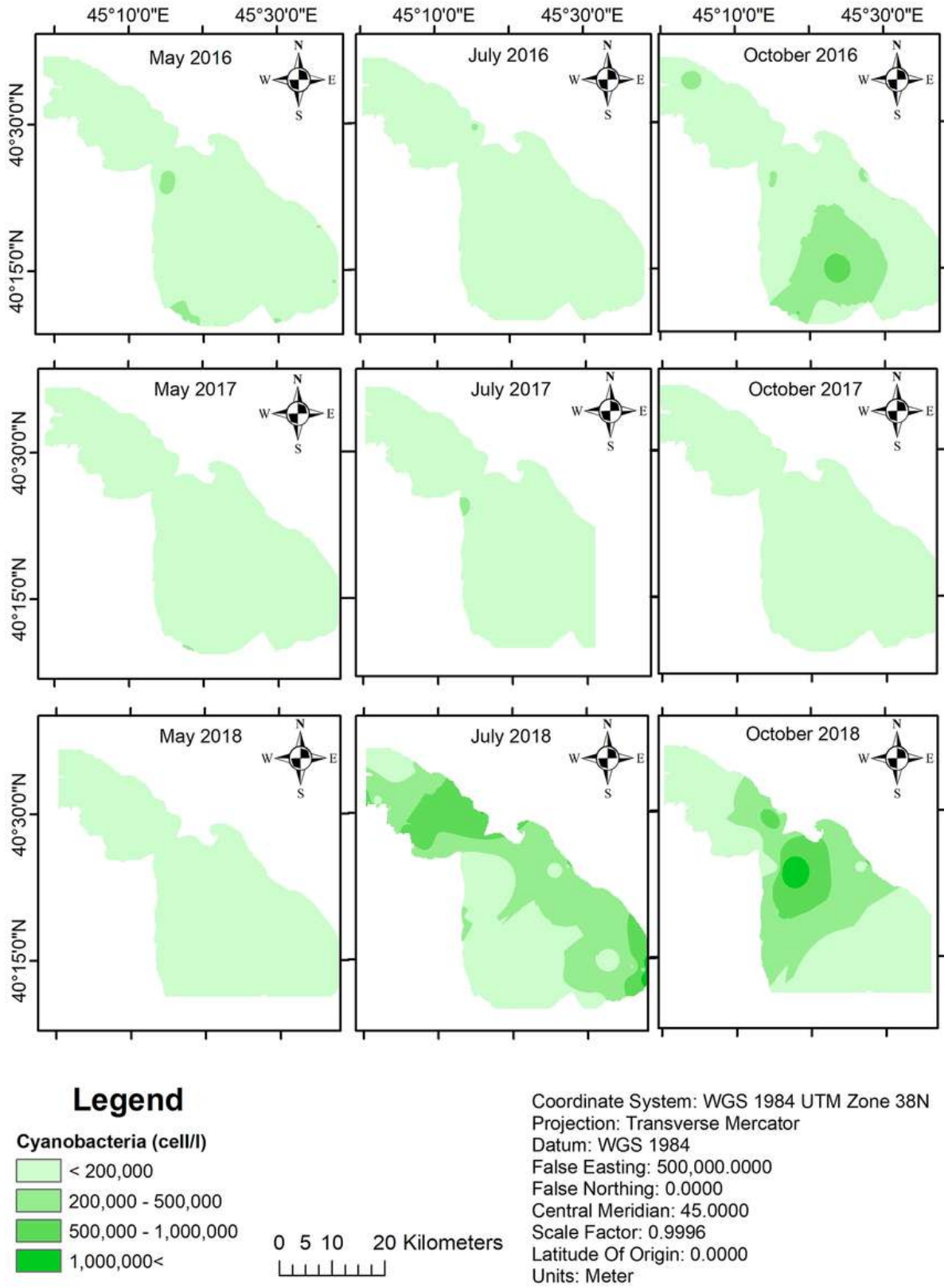

Fig: Spatiotemporal dynamics of cyanobacterial count from 2016 to 2018. Source: Asatryan *et al.*, 2022.

Acknowledgments

We would like to thank the ENI CBC "Black Sea Basin Joint Operational Programme 2014-2020" for funding the PONTOS project, without which this work would not have been possible.

We would also like to express our gratitude to all our partners within this project for a smooth and productive collaboration, despite many of the challenges we and the whole world faced during the past years. In alphabetical order, they are The Centre for Research and Technology Hellas (CERTH), The Democritus University of Thrace (DUTH), The Environmental Protection and Mining Inspection Body of the Republic of Armenia (EPMIB), Green Alternative, Georgia (GRAL), and The Odessa National University, Ukraine (ONU).

Our thanks also extend to the Hydrometeorology and Monitoring Center SNCO for sharing with us water chemistry data from Lake Sevan and to the Institute of Hydroecology and Zoology of the National Academy of Sciences of the Republic of Armenia for the results of laboratory chl-*a* analyses.

We would like to thank Haykanush Martirosyan, Valeria Komysh, Siniorita Chatziapostolidoua, Aleksandr Hakobyan and a number of volunteers and interns at the AUA Acopian Center for the Environment who contributed with their valuable to completing this work.

Lastly, we are grateful for the participation of a number of local stakeholders in our trainings, workshops, and hackathon. You made the project more vibrant and successful.

References

Anderson D., P.M. Glibert, and J.M. Burkholder. 2002. Harmful algal blooms and eutrophication: Nutrient sources, composition, and consequences. Estuaries **25**: 704-726.

Antoine, D., André, J.-M., Morel, A. 1996. Oceanic primary production: 2. Estimation at global scale from satellite (Coastal Zone Color Scanner) chlorophyll. Global Biogeochemical Cycles **10**: 57-69.

Aleksandr Arakelyan, Arshavir Avagyan, Gayane Shahnazaryan, Narek Tarasyan, Lilit Sargsyan, Harutyun Uloyan, A. N. 2019. Development of draft river basin management plan for Sevan river basin district in Armenia.

Arakelyan, A., Burmanyan, A., Geghamyan, O., Manoukyan D., Markaryan L., Pintus F., 2021. Development of Water Sector Adaptation plan in Armenia. UNDP/GCF National Adaptation Plan to Advance Medium and Long-Term Adaptation Planning in Armenia Project. OiEau International Office for Water. pp. 107.

Asatryan, V., Stepanyan, L., Hovsepyan, A. et al. 2022. The dynamics of phytoplankton seasonal development and its horizontal distribution in Lake Sevan (Armenia). Environ Monit Assess **194**: 757. https://doi.org/10.1007/s10661-022-10446-5

Babayan, A., Hakobyan, S., Jenderedjian, K., Muradyan, S., & Voskanov, M. 2006. Lake Sevan: Experience and Lessons Learned Brief. In: Towards a Lake Basin Management Initiative and a Contribution to the Third World Water Forum: Sharing Experiences and Early Lessons in GEF and non-GEF Lake Basin Management Projects: Experience notes and Lessons Learned (Vol. 1).

Bourg et al. 2012. MERIS 3rd validation report. Available from: https://earth.esa.int/documents/700255/707222/A879-NT-017-ACR_v1.0.pdf/6fa86bec-9945-4e39-808e-3801f2e3962b

Bukata, R.P. 2013. Retrospection and introspection on remote sensing of inland water quality:"Like Déjà Vu All Over Again". Journal of Great Lakes Research, 2-5.

Cao, Z., Ma, R., Duan, H., Pahlevan, N., Melack, J., Shen, M., Xue, K. 2020. A machine learning approach to estimate chlorophyll-a from Landsat-8 measurements in inland lakes. Remote Sensing of Environment **248**: 111974.

Dall'Olmo, G., Gitelson, A., Rundquist, D., Leavitt, B., Barrow, T., Holz, J. 2005. Assessing the potential of SeaWiFS and MODIS for estimating chlorophyll concentration in turbid productive waters using red and near-infrared bands. Remote Sensing of Environment **96**: 176-187.

Doerffer, R., & Schiller, H. 2007. The MERIS case 2 water algorithm. International Journal of Remote Sensing, **28**(3): 517–535.

Gabrielyan, I., Yepremyan, H. v., Hakobyan, E., Elmasakyan, A., Hayrapetyan, N., Sahakyan, T., & Bruch, A. A. 2019. Ruppiaceae (Magnoliophyta , Liliopsida, Alismatidae) the new family for the flora of Armenia. Takhtajania, **5**: 9–13.

Gevorgyan, G., Rinke, K., Schultze, M., Mamyan, A., Kuzmin, A., Belykh, O., Sorokovikova, E., Hayrapetyan, A., Hovsepyan, A., Khachikyan, T., Aghayan, S., Fedorova, G., Krasnopeev, A., Potapov, S., & Tikhonova, I. 2020. First report about toxic cyanobacterial bloom occurrence in Lake Sevan, Armenia. International Review of Hydrobiology, **105**(5–6): 131–142. https://doi.org/10.1002/iroh.202002060

Gitelson, A., Dall'Olmo, G., Moses, W., Rundquist, D., Barrow, T., Fisher, T., Gurlin, D., Holz, J. 2008. A Simple semi-analytical model for remote estimation of chlorophyll-a in turbid waters: Validation. Remote Sensing of Environment **112**: 3582-3593.

Gurlin, D., Gitelson, A.A., Moses, W.J. 2011. Remote estimation of chl-a concentration in turbid productive waters — Return to a simple two-band NIR-red model? Remote sensing of environment. **115**: 3479-3490.

Glibert, P.M., Seitzinger, S.Y.B.I.L., Heil, C.A., Burkholder, J.M., Parrow, M.W., Codispoti, L.A. and Kelly, V.I.N.C.E., 2005. Eutrophication. Oceanography, **18**(2), p.198.

Han, L. 1997. Spectral reflectance with varying suspended sediment concentrations in clear and algae-laden waters. Photogrammetric engineering and remote sensing **63**: 701-705.

Han, L., Jordan, K.J. 2005. Estimating and mapping chlorophyll-a concentration in Pensacola Bay, Florida using Landsat ETM+ data. International Journal of Remote Sensing **26**: 5245-5254.

Harper, D. 1992. What is eutrophication?. In: Eutrophication of Freshwaters. Springer, Dordrecht. https://doi.org/10.1007/978-94-011-3082-0_1

Heblinski, J., K. Schmieder, T. Heege, T. K. Agyemang, H. Sayadyan, and L. Vardanyan. 2010. Mapping of water constituents in high mountainous Lake Sevan (Armenia). SIL Proceedings, 1922-2010 **30:** 1453–1455.

Hovhanissian, R., & Gabrielyan, B. 2000. Ecological problems associated with the biological resource use of Lake Sevan, Armenia. Ecological Engineering, **16(**1): 175–180. https://doi.org/10.1016/S0925-8574(00)00102-6

Hovsepyan, A. A., & Gevorgyan, G. A. 2017. Changes in phytoplankton community and ecological state of Lake Sevan (Armenia) due to its water level rise: a review. Electronic Journal of Natural Sciences, **29**(2): 34–39.

Ihlen, V. 2019. Landsat 8 (L8) Data Users Handbook. Version 5.0. Department of the Interior, U.S. Geological Survey. Sioux Falls, South Dakota. [https://www.usgs.gov/media/files/landsat-8-data-users-handbook]

Kachvoryan, E. A., Pepoyan, A. Z., Harutyunova, M. v, & Manvelyan, A. M. 2008. Ecosystems of Lake Sevan Basin' s Rivers in Armenia. World Academy of Science, Engineering and Technology, **44**(April): 543–547.

Kazanjian, G., Asatryan V. 2022. Report on the needs assessment for the establishment of regular hydrobiological monitoring in The Lake Sevan Basin. EU4Sevan Report. GIZ Armenia.

Kirk, J.T.O. 1994. Light and photosynthesis in aquatic ecosystems. Cambridge university press.

Krylov, A. v., Gerasimov, Y. v., Gabrielyan, B. K., Borisenko, E. S., Hakobyan, S. A., Nikogosyan, A. A., Malin, M. I., & Ovsepyan, A. A. 2013. Zooplankton in Lake Sevan during the period of high water level and low fish density. Inland Water Biology, **6**(3): 203–210. https://doi.org/10.1134/S1995082913030085

Krylov, A. v., Hayrapetyan, A. O., Tsvetkov, A. I., Gerasimov, Y. v., Malin, M. I., & Gabrielyan, B. K. 2019. Interannual Changes in the Quantitative Parameters and Structure of Invertebrates in the Littoral and Pelagic Zones of Lake Sevan (Armenia) with Fluctuations in Meteorological Conditions and Fish Biomass. I. Summer Zooplankton. Inland Water Biology, **12**(3): 298–305. https://doi.org/10.1134/S1995082919030088

Kuhn, C., A. de Matos Valerio, N. Ward, L. Loken, H. O. Sawakuchi, M. Kampel, J. Richey, P. Stadler, J. Crawford, R. Striegl, E. Vermote, N. Pahlevan, and D. Butman. 2019. Performance of Landsat-8 and Sentinel-2 surface reflectance products for river remote sensing retrievals of chlorophyll-a and turbidity. Remote Sensing of Environment **224**: 104–118.

Liu, G., Li, L., Song, K., Li, Y., Lyu, H., Wen, Z., Fang, C., Bi, S., Sun, X., Wang, Z., Cao, Z., Shang, Y., Yu, G., Zheng, Z., Huang, C., Xu, Y., Shi, K. 2020. An OLCI-based algorithm for semi-empirically partitioning absorption coefficient and estimating chlorophyll a concentration in various turbid case-2 waters. Remote Sensing of Environment **239**: 111648.

Mesropyan, E. 2022. Development plan of the residential drainage sector of the Republic of Armenia. Report. EU4Sevan. GIZ Armenia [*in Armenian*].

Minasyan, A., & Karrasch, B. 2015. Relationship between quantitative characteristics of viruses to picocyanobacteria and heterotrophic nanoflagellates in Lake Sevan waters (Armenia). Electronic Journal of Natural Sciences of NASRA, **2**(25): 24–29.

Nusch, E. A. 1980. Comparison of different methods for chlorophyll and phaeopigment determination. Archiv für Hydrobiologie—BeiheftErgebnisse der Limnologie, **14**: 14–36.

O'Reilly, J.E., Maritorena, S., Mitchell, B.G., Siegel, D.A., Carder, K.L., Garver, S.A., Kahru, M., McClain, C. 1998. Ocean color chlorophyll algorithms for SeaWiFS. Journal of Geophysical Research: Oceans **103**: 24937-24953.

Ovsepyan, A.A. and Khachikyan, T.G. 2016. Pelagial phytoplankton of the Sevan Lake, in Ozero Sevan. Ekologicheskoe sostoyanie v period izmeneniya urovnya vody (Lake Sevan: Ecological State during Water Level Dynamics), Yaroslavl: Filigran' pp. 39–60.

Pahlevan, N., B. Smith, J. Schalles, C. Binding, Z. Cao, R. Ma, K. Alikas, K. Kangro, D. Gurlin, N. Hà, B. Matsushita, W. Moses, S. Greb, M. K. Lehmann, M. Ondrusek, N. Oppelt, and R. Stumpf. 2020. Seamless retrievals of chlorophyll-a from Sentinel-2 (MSI) and Sentinel-3 (OLCI) in inland and coastal waters: A machine-learning approach. Remote Sensing of Environment **240**: 111604.

Palmer, S.C.J., Kutser, T., Hunter, P.D. 2015. Remote sensing of inland waters: Challenges, progress and future directions. Elsevier.

Parparov, A. S. 1990. Some characteristics of the community of autotrophs of Lake Sevan in connection with its eutrophication. Hydrobiologia, **191**(1): 15–21. https://doi.org/10.1007/BF00026034

Paerl, H. W., & Huisman, J. 2008. Blooms Like It Hot. Science, **320**(5872):, 57–58. https://doi.org/10.1126/science.1155398

Sakharova, E. G., Krylov, A. v., Sabitova, R. Z., Tsvetkov, A. I., Gambaryan, L. R., Mamyan, A. S., Gabrielyan, B. K., Hayrapetyan, A. H., & Khachikyan, T. G. 2020. Horizontal and Vertical Distribution of Phytoplankton in the Alpine Lake Sevan (Armenia) during the Summer Cyanoprokaryota Bloom. Contemporary Problems of Ecology, **13**(1): 60–70. https://doi.org/10.1134/S1995425520010072

Schalles, J.F., 2006. Optical remote sensing techniques to estimate chlorophyll-a concentrations in coastal waters with varying suspended matter and CDOM concentrations, in: Richardson, L.L., LeDrew, E.F. (Eds.), Remote sensing of aquatic coastal ecosystem processes. Springer Netherlands, Dordrecht, pp. 27-79.

Shikhani, M., Mi, C., Gevorgyan, A., Gevorgyan, G., Misakyan, A., Azizyan, L.V., Barfuss, K., Schulze, M., Shatwell, T., & Rinke, K. 2021. Simulating thermal dynamics of the largest lake in the Caucasus region: The mountain Lake Sevan. Journal of Limnology. doi: 10.4081/jlimnol.2021.2024

Smith, V.H. 2003. Eutrophication of freshwater and marine ecosystems: a global problem. Environ. Sci. Pollut. Res. Int. **10**: 126–139.

Smith, V. H., and D. W. Schindler. 2009. Eutrophication science: where do we go from here? Trends Ecol. Evol. **24**: 201–207.

Stadelmann TH, Brezonik PL, Kloiber S. 2001. Seasonal patterns of chlorophyll a and Secchi disk transparency in lakes of East-Central Minnesota: Implications for design of ground-and satellite-based monitoring programs. J Lake Reservoir Manage **17**: 299-314.

Toming, K., Kutser, T., Laas, A., Sepp, M., Paavel, B., Nõges, T. 2016. First Experiences in Mapping Lake Water Quality Parameters with Sentinel-2 MSI Imagery. **8**: 640.

Willén, E. 2000. Phytoplankton in water quality assessment - An indicator concept, p 57-80. In: P Heinonen, Z Giuliano, and A Van der Beken, Eds, Hydrological and Limnological Aspects of Lake Monitoring. Wiley and Sons, Ltd, West Sussex, England.

Yew-Hoong Gin, K., Teck Koh, S., Lin, I.I., Soon Chan, E. 2002. Application of Spectral Signatures and Colour Ratios to Estimate Chlorophyll in Singapore's Coastal Waters. Estuarine, Coastal and Shelf Science **55**: 719-728.